THERMO-E-SKIN: FUNCTIONAL BIONIC ENGINEERING TO ACHIEVE THERMOREGULATION AND THERMOSENSATION

ZHANG PENGXIANG

PhD

The Hong Kong Polytechnic University

2024

The Hong Kong Polytechnic University

School of Fashion and Textiles

Thermo-e-skin: Functional Bionic Engineering to Achieve Thermoregulation and Thermosensation

Zhang Pengxiang

A thesis submitted in partial fulfillment of the requirements

for the degree of Doctor of Philosophy

October 2023

CERTIFICATE OF ORIGINALITY

I hereby declare that this thesis is my own work and that, to the best of my knowledge and belief, it reproduces no material previously published or written, nor material that has been accepted for the award of any other degree or diploma, except where due acknowledgment has been made in the text.

_________________________ (Signed)

ZHANG Pengxiang (Name of student)

ABSTRACT

Electronic skin (e-skin) has broad application scenarios, including wearable technology, human-computer interfaces, smart prosthetics, and medical diagnosis, due to its ability to mimic human skin and offer versatile sensing capabilities. However, the state-of-art thermosensation is insufficient for comprehensive environmental perception. Furthermore, traditional e-skins cannot regulate temperature, like the human body with the isothermal function. This thesis conducts a systematic investigation of thermo-e-skin with both thermoregulation and thermosensation functions.

Two types of thermoregulation have been proposed, i.e. single-mode thermoregulation e-skin (S-thermo-e-skin) and dual-mode thermoregulation e-skin (D-thermo-e-skin). The S-thermo-e-skin involved a flexible thermoelectric device and a heat sink made of a phase change material, enabling the e-skin to maintain the isothermal function in both hot and chilly environments. The S-thermo-e-skin has a good isothermal function, maintaining a surface temperature of 35 °C in a broad environment with a temperature range of 10-45 °C. The effective time in the isothermal state of 35 °C could be over 2 hours in the mild environment with 10-30 °C, while decreased to 1.5 h and 0.75 h under the ambient temperature of 40 and 45 °C, respectively. The energy cost to maintain the isothermal state is a careful measurement, showing the lowest value of 14.22 mW/cm^2 within the thermoneutral zone of 35 °C. Furthermore, the D-thermo-e-skin is functionalized with the active mode of flexible thermoelectric thermoregulation layers and the passive mode of ionic hydrogel's evaporation/regeneration layer. The ionic hydrogel mimics the function of the bionic sweat gland. The D-thermo-e-skin

significantly increased the effective time of 35 °C -isothermal-state, e.g. increased from 2h to 4.2 h under ambient temperature 40 °C. Furthermore, the e-skin's hygroscopic properties allowed it to return to its initial state within 4 hours when exposed to 90% humidity, enabling reusability. Both the S-thermo-e-skin and D-thermo-e-skin have a quick response as the e-skin as the environment changes.

A new heat-source-identification sensor was designed by using the capacitance response behavior of the methoxy poly (ethylene glycol) acrylate ionic gel. The ionic-gel sensor exhibits an impressive ultra-wide temperature range of -20 °C to 180 °C and displays a highly linear response to temperature stimuli ($R^2 = 0.993$), and a temperature measurement accuracy of better than 0.005 °C. Moreover, the ionic-gel sensor has temperature-sensitive ion relaxation time and pressure-sensitive capacitance, which provides an effective to decouple the temperature and pressure signals. Furthermore, the ionic-gel sensor also shows proximity sense with a negative capacitance response. It was experimentally verified that the ionic sensor could identify the heat exchange modes, encompassing thermal radiation, thermal convection, and thermal conduction, by using the ion relaxation time and capacitance response. The heat-source-identification well mimics the thermosensation of human skin. Moreover, the integration of thermoregulation and thermosensation was conducted. The integrated thermo-e-skin successfully combines thermosensation, heat-source-identification, signal feedback, and thermoregulation, demonstrating a bionic thermo-sensory capability. This thesis provides a systematic solution to mimic the thermoregulation and thermosensation of human skin, which would has significant impact on the field of thermo-e-skin.

LIST OF PUBLICATIONS

Published papers:

1. **Pengxiang Zhang**, Zhiqian Li, Yupeng Wang, Wenting Sun, Kang Zhu, Qikai Li, Bo Li, Zeru Wang, Ke Wang, Zijian Zheng*, Weishu Liu*. Electronic skin with biomimetic structures realizes excellent isothermal regulation. **Nano Energy**, 2023, 121: 109189.

2. **Pengxiang Zhang**, Biao Deng, Kang Zhu, Qing Zhou, Shuangmeng Zhang, Wenting Sun, Zijian Zheng, Weishu Liu*. Wide-temperature range thermoregulating e-skin design through a hybrid structure of flexible thermoelectric devices and phase change materials heat sink. **EcoMat**, 2022, 4(6): e12253.

3. **Pengxiang Zhang**, Biao Deng, Wenting Sun, Zijian Zheng*, Weishu Liu*. Fiber-based thermoelectric materials and devices for wearable electronics. **Micromachines**, 2021, 12(8): 869.

4. Bo Li*, Chuanyang Cai, Yang Liu, Fang Wang, Bin Yang, Qikai Li, **Pengxiang Zhang**, Biao Deng, Pengfei Hou*, Weishu Liu*. Ultrasensitive mechanical/thermal response of a P (VDF-TrFE) sensor with a tailored network interconnection interface. **Nature Communications**, 2023, 14(1): 4000.

5. Xinzhi Wu, Yangjian Lin, Zhijia Han, Huan Li, Chengyan Liu, Yupeng Wang, **Pengxiang Zhang**, Kang Zhu, Feng Jiang, Jian Huang, Haohan Fan, Feng Cheng, Binghui Ge*, Weishu Liu*. Interface and Surface Engineering Realized High Efficiency of 13% and Improved Thermal Stability in $Mg_3Sb_{1.5}Bi_{0.5}$-Based Thermoelectric Generation Devices. **Advanced Energy Materials**, 2022, 12(48): 2203039.

6. Qian Xu*, Biao Deng, Lenan Zhang, Shaoting Lin, Zhijia Han, Qing Zhou, Jun Li, Yongbin Zhu, Feng Jiang, Qikai Li, **Pengxiang Zhang**, Xinbo Zhang, Gang Chen*, and Weishu Liu*. High-performance, flexible thermoelectric generator based on bulk materials. **Cell Reports Physical Science**, 2022, 3(3):100780.

ACKNOWLEDGEMENTS

This project is in process under the supervision of Prof. Zijian Zheng and Prof. Weishu Liu. Firstly, I acknowledge my supervisors, Prof. Zheng and Prof. Liu for their instructive advice. Prof. Zheng and Prof. Liu's meticulous attitude towards academics and rigorous treatment made me more strict with myself and made great progress in three years.

Secondly, I would like to thank the other members of the subject group. I received help from them when I encountered problems in the experiment or in life. I want to express my appreciation to Dr. Qiyao Huang, Ms. Qiuna Zhuang, Ms. Leni Zhong, Mr. Wancheng Yu, Mr. Zijian Chen, Mr. Fan Chen, Mr. Zhenyao Wei in PolyU and Prof. Bo Li, Dr. Qin Zhou, Dr. Jiajia Zhang, Dr. Kang Zhu, Dr. Qikai Li, Dr. Feng Jiang, Dr. Zhijia Han, Mr. Biao Deng, Mr. Xinbo Zhang, Mr. Shuangmeng Zhang, Mr. Jizhen Hu, Mr. Xinzhi Wu, Mr. Yupeng Wang, Mr. Shuaihua Wang, Mr. Huan Li, Ms. Wenting Sun, Mr. Bin Yang in SUSTech for their help.

Thirdly, I would like to thank all the technicians who helped me with school affairs and instrument characterization. I would also like to thank the Southern University of Science and Technology and the Hong Kong Polytechnic University for their financial support.

Finally, I am grateful to my family. I thank them for their continued support and encouragement throughout my years of study.

TABLE OF CONTENTS

LIST OF FIGURES

LIST OF TABLES

LIST OF ABBREVIATIONS

E-skin	electronic skin
TE	thermoelectric
S-thermo-e-skin	single-mode thermoregulating e-skin
PCM	phase change material
D-thermo-e-skin	dual-mode thermoregulating e-skin
PID	proportional-integral-derivative
TRP	transient receptor potential
ADP	adenosine diphosphate
ATP	adenosine triphosphate
PVDF	poly(vinylidene fluoride)
PEDOT:PSS	poly(3,4-ethylenedioxythiophene):poly(styrenesulfonate)
CNT	carbon nanotube
ZT	thermoelectric figure of merit
LM	liquid metal
PDMS	polydimethylsiloxane
PNIPAM	Poly(N-isopropyl acrylamide)
Li-PAAm	lithium- and bromine-enriched polyacrylamide
LCST	lower critical solution temperature
MPEG-DA	methoxy poly(ethylene glycol) acrylate
Li-PFSI	lithium bis(pentafluoroethylsulfonyl) imino-ammonium
Li-O	lithium-oxygen

C_{EDL}	constant phase angle element
R_B	bulk resistance
C_B	bulk capacitance
τ	ion relaxation time
$\Delta C/C_0$	normalized capacitance

CHAPTER 1 INTRODUCTION

1.1 Background and Challenges

Skin is the largest organ of the human body, showing remarkable physical and chemical attributes including extensibility, mechanical robustness, and regenerative capacity. In addition to its intrinsic properties, the skin holds a pivotal role as a receptive site for vital biological cues emanating from both the internal organs and external environment.[1] Various sensory nerve receptors embedded within the skin's layers enable individuals to perceive and interpret environmental factors like pressure, temperature, and humidity.[2] These external stimuli provoke vibrations or deformations in the skin, instigating the generation of action potentials in the skin receptors. Ultimately, these electrical signals propagate through neural tissues, reaching the brain and subsequently evoking corresponding sensory experiences.

Electronic skin (e-skin) has gained significant attention as it mimics the properties of human skin.[3-6] E-skin is as soft and thin as skin, which can be molded into various shapes and attached to the surface of human or robotic body like a garment, and can also sense various external stimuli such as strain, pressure, temperature and humidity (**Figure 1.1**). Consequently, e-skin finds promising applications in wearable technology, human-machine interfaces, smart prosthetics, medical diagnosis, and other fields.[7-9] Recently, researchers have particularly focused on achieving a high level of biomimicry in e-skin, aiming to replicate realistic sensations such as touch and thermo-sensory.

Remarkable developments have been made by extensively investigating materials, device structures, and signal transmission, resulting in e-skin that is comparable to or even surpasses, human skin in terms of functionality.[9-11]

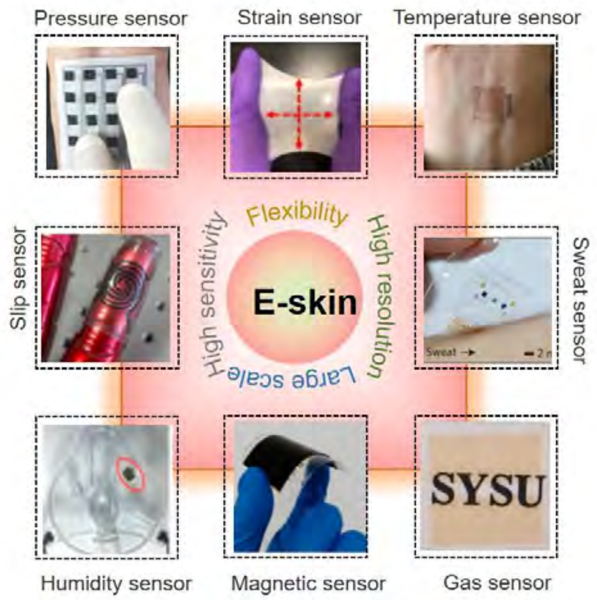

Figure 1.1 Characteristics of e-skin and its application in many fields. [12-19]

Temperature plays a crucial role in maintaining a stable internal environment and normal physiological functions in mammals, including humans. The human body possesses a comprehensive thermo-sensory system that involves perceiving and regulating temperature. This system not only reacts to temperature stimuli from the surroundings or internal factors but also maintains a constant body temperature by balancing heat generation and dissipation in response to the actual temperature (**Figure 1.2**). [20-22] However, current e-skin technology has only achieved basic thermosensation capabilities, lacking the ability to sense the external environment comprehensively.[10, 11, 23-28] Furthermore, traditional e-skin is limited in terms of material and structure, preventing it from regulating temperature and exhibiting isothermal properties like the human body. An isothermal skin temperature plays a critical role in achieving the comfort and emotional interaction between the human body and e-skin, rendering it unfavorable for practical use in prosthetics and robotics. Therefore, to enhance the bionic nature of prosthetics and robots, it is essential to mimic the thermo-sensory system of organisms, such as the human body, and design an e-skin that can detect temperature and adjust to ambient temperature conditions.

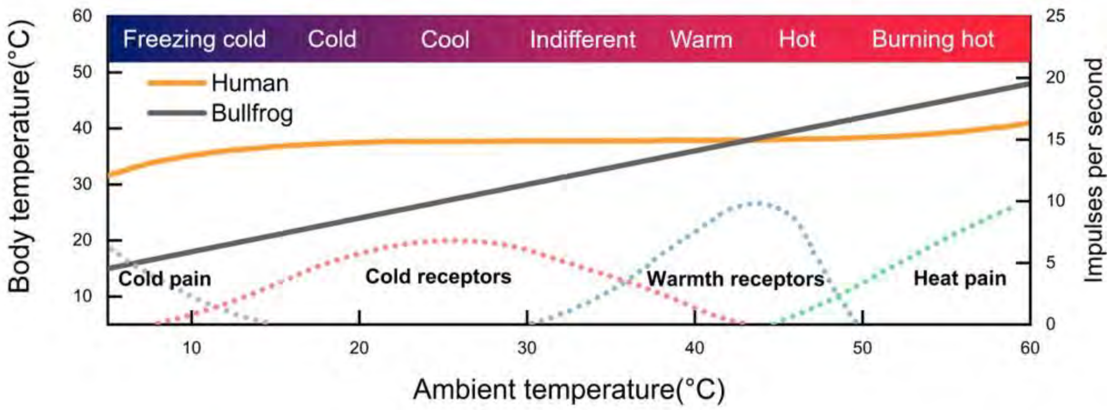

Figure 1.2 The human body can sense temperature and perform isothermal regulation.

1.2 Research Objectives

To address the above challenges, this thesis aims to develop the thermo-e-skin with thermoregulation capability and heat-source identification function. The thermoelectric (TE) technology and other thermal management strategy will be employed to realize the thermoregulation mechanism of human body. A multimodal temperature sensor capable of heat-source-identification is also developed to realize deep thermosensation based on the ion relaxation phenomenon. Finally, the thermoregulating e-skin, multimodal temperature sensor, and control system are integrated to form a thermo-sensory system to provide a closed-loop bionic thermoregulatory for the e-skin. The following are the objectives of the project:

1) Single-mode thermoregulating e-skin (S-thermo-e-skin) with flexible TE device and phase change material (PCM) heat sink

a) To fabricate the TE device with good flexibility and thermoregulation performance

b) To fabricate the PCM heat sink with good thermal storage capacity

c) To fabricate and characterize the thermoregulating e-skin with thermoregulation properties

2) Dual-mode thermoregulating e-skin (D-thermo-e-skin) with active and passive regulation layers

a) To fabricate the active regulation layer consisting of a flexible TE device

b) To fabricate the passive regulation layer consisting of hygroscopic hydrogel and silicone foam

c) To fabricate and characterize the dual-mode thermoregulating e-skin

3) Multimodal temperature sensor with heat-source-identification

a) To fabricate the multimodal temperature sensor

b) To characterize the basic thermosensation capability

c) To decouple pressure and temperature signals for heat-source-identification

4) E-skin with bionic thermo-sensory system

a) To integrate thermoregulating e-skin, multimodal temperature sensor, and control systems into a bionic thermo-sensory system

b) To characterize the bionic thermo-sensory system under different stimulus

1.3 Research Significance and Values

This research project focused on developing a bionic thermo-sensory system and three corresponding devices to implement thermo-sensory capabilities in e-skins. The three devices include a S-thermo-e-skin equipped with a flexible TE device and a PCM heat sink, a D-thermo-e-skin with both active and passive regulation layers, and a multimodal temperature sensor featuring heat-source-identification functionality. Through this investigation, we systematically examined the performance of the e-skin in terms of thermoregulation and thermosensation, successfully achieving thermo-sensory mimicry in the e-skin. These e-skin prototypes demonstrate human-like thermo-sensory capabilities, offering valuable insights into imitating human thermoregulation and providing potential solutions for integrating thermo-sensory capabilities into robotic systems.

Firstly, the S-thermo-e-skin, designed with a flexible TE device and a PCM heat sink, exhibits remarkable temperature adaptation similar to that of the human body. It effectively heats up in low-temperature environments and cools down in high-temperature environments, enabling exceptional thermoregulation. The e-skin maintains a surface temperature of 35 °C, regardless of ambient temperature variations within the range of 10 to 45 °C. This isothermal regulation feature ensures that the surface of the prosthesis remains at a constant temperature, offering thermostability. Consequently, the prosthetic user experiences heightened sensory feedback, fostering emotional interaction between human and machine, and enhancing the user's acceptance and affinity towards the prosthetic device.

Secondly, this study incorporates a simulation of the human body's thermoregulation mechanism and combines it with the bionic sweat gland structure within the D-thermo-e-skin, resulting in its dual-mode thermoregulation capabilities. The active regulation layer, comprised of a flexible TE device, serves as a heat generation structure, actively regulating the e-skin's surface temperature even in complex environmental conditions. Conversely, the passive regulation layer, consisting of hygroscopic hydrogel and silicone foam, acts as a heat dissipation structure, significantly extending the e-skin's effective thermoregulation duration within high-temperature environments. The D-thermo-e-skin presents a technological pathway for designing thermosensitive skin with a bionic structure through the seamless integration of heat generation and dissipation. Moreover, it provides fresh insights into the development of e-skins with heightened environmental sensitivity.

Thirdly, our multimodal temperature sensor, developed utilizing the ion relaxation phenomenon, not only enables the fundamental thermosensation but also simultaneous detection of force. The sensor successfully identifies three distinct heat sources: thermal conduction, thermal convection, and thermal radiation through the decoupling of temperature and pressure signals. This research offers a significant contribution to the understanding of temperature perception and broadens the scope of thermosensation investigations. Furthermore, it holds immense practical value in achieving a heightened level of robot-environment interaction, enhancing the field of robotics.

Finally, we successfully integrate the thermoregulating e-skin, multimodal temperature sensor, and proportional-integral-derivative (PID) control system into a cohesive bionic thermo-sensory system. This advanced system encompasses thermosensation, heat-source-identification, signal feedback, and isothermal regulation, imparting a closed-loop bionic thermo-sensory experience akin to that of humans onto the e-skin. This research proposes an innovative approach for future designs of comprehensive bionic thermo-sensory systems for e-skin applications by merging thermosensation and regulation capabilities.

1.4 Outline of the thesis

This thesis is organized as follows:

Chapter 1: Introduction. In this chapter, a brief background of e-skin is presented, followed by the current challenges and necessity in preparing e-skin with human-like thermo-sensory functions. Then the objectives and originality of this study are described.

Chapter 2: Review of thermosensation and thermoregulation. In this chapter, a comprehensive overview of the human thermo-sensory system and current techniques for implementing e-skin thermo-sensory is presented, and a comparison of these techniques in terms of materials, methods, and application scenarios is discussed.

Chapter 3: Single-mode thermoregulating e-skin. This chapter shows the preparation of a flexible TE device and phase change heat sink and the encapsulation of thermoregulating e-skin. Then, the heating/cooling performance, thermostability, and actual thermoregulation performance of the thermoregulating e-skin under simulated environmental changes are systematically discussed.

Chapter 4: Dual-mode thermoregulating e-skin. This chapter shows the preparation of the dual-mode thermoregulating e-skin. Then, the isothermal regulation performance, moisture circulation performance, and transient thermoregulation capability of the dual-mode thermoregulating e-skin are thoroughly tested.

Chapter 5: Heat-source-identification of temperature sensor. This chapter shows the sensing principle and preparation method of multimodal temperature sensor and then characterizes the basic thermosensation performance, temperature/pressure decoupling, heat-source-identification performance, and practical applications of multimodal temperature sensor.

Chapter 6: Integration of thermoregulation and thermosensation. In this chapter, thermoregulating e-skin, multimodal temperature sensor, and the PID control system are integrated to form a bionic thermo-sensory system. The response of this bionic thermo-sensory system to different environmental stimuli is measured.

Chapter 7: Conclusions and suggestions for future research. In this chapter, the results of the whole thesis are summarized and the prospects of bionic temperature-sensitive e-skin are given.

CHAPTER 2 REVIEW OF THERMOSENSATION AND THERMOREGULATION

This chapter provides an overview of the human thermo-sensory system and the progress of the temperature sensors, which is divided into three main sections. Firstly, a comprehensive introduction to the human thermo-sensory system, encompassing thermosensation and thermoregulation, will be presented. Secondly, a detailed examination of flexible temperature sensors utilized in e-skin will be provided, highlighting their sensing properties and underlying mechanisms. Special attention will be given to their basic principles and classification. Lastly, thermal management techniques employed for thermoregulation in e-skin will be explored. This section will include an analysis of their advantages and limitations.

2.1 Thermosensation and thermoregulation of human skin

Thermosensation and thermoregulation represent integral components of the human thermo-sensory system.[29] Temperature receptors in the human skin elicit diverse bioelectrical signals that are subsequently relayed to the thermoregulatory center through the detection of thermal gradients within internal and external environments. The thermoregulatory center then integrates the resultant temperature information at different temperatures and sends command signals to activities such as skeletal muscles, endocrine glands, and vascular changes in the skin to enable the body's ability to produce heat and cool down to maintain a relatively stable body temperature.

2.1.1 Thermosensation of human skin

Temperature receptors in the human body are responsible for detecting fluctuations in both internal and external environmental temperatures.[30] The process of thermosensation within the skin not only provides vital input signals for regulating body temperature but also serves to identify potential damage caused by extreme temperature stimuli. These incoming impulses enable the sense of touch to discern the temperature of diverse objects and materials, such as metals and wood, by perceiving their temperature properties. Remarkably, temperature receptors possess distinct structures that allow them to sense temperature variations across different regions of the body, typically encompassing the temperature range of -10 °C to 60 °C.[31] On the surface of the skin, specialized receptors for cold pain, cold, heat, and thermal pain exist. Each type of temperature receptor specifically responds to particular stimuli, leading to sensations of cold, heat, pain, and other related perceptions.

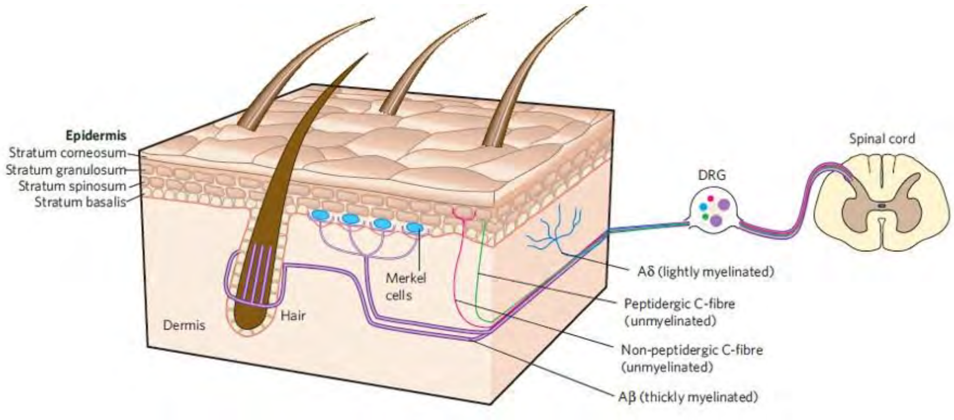

Figure 2.1 Diversity of somatosensory neurons in the skin.[32]

Thermosensation relies on temperature-activated ion channels, predominantly belonging to the transient receptor potential (TRP) channel family, as depicted in

Figure 2.1.[33] TRP channels exhibit diverse biophysical and physiological characteristics, playing critical roles in sensory transduction.[34] TRPV3/4 and TRPM8 genes encode heat and cold sensations, while TRPV1/2 and TRPA1 genes facilitate the transduction of thermal and cold pain stimuli, respectively. In mammals, heat-sensitive TRPs are primarily expressed in cutaneous sensory neurons or other cell types, finely tuned to specific temperature ranges. These cutaneous sensory afferent neurons encode thermo-sensory information, wherein heat and cold sensations are conveyed through dedicated afferent fibers known as heat fibers and cold fibers, respectively. In contrast, heat and cold pain stimuli are detected by A_δ and C fibers.

2.1.2 Thermoregulation of the human body

The human body faces a complex and fluctuating external environment, but it possesses a remarkable regulatory mechanism to maintain a constant body temperature.[35] The concept of body heat balance arises from the intricate interplay between heat generation and heat dissipation. Approximately 50% of the chemical energy derived from nutritional metabolism is utilized to sustain the isothermal body.[36] The surplus energy is eventually transformed into heat energy after undergoing energy conversion and utilization. The body maintains an isothermal state by effectively balancing the processes of heat generation and heat dissipation through the meticulous control exerted by the thermoregulatory mechanisms. In a comfortable environment, our body dissipates the heat to the environment through convection, conduction, and radiation. In other words, the human body is a thermodynamic desperation system.

Heat generation by the human body

In addition to the mechanical work performed by muscles, the energy released through the catabolism of substances within the body is ultimately converted into thermal energy, crucial for maintaining body temperature.[37] The majority of body heat stems from the fundamental metabolic processes, while there are other contributing factors to heat production. Heat generation is a result of metabolic activities occurring in all cells. Essential physiological organs such as the viscera and brain contribute significantly to heat production in the resting state, accounting for over 70% of the basal organism's heat generation. The liver and brain exhibit heightened metabolic rates, resulting in increased heat production, with temperatures reaching approximately 38 °C.

Basal metabolism is responsible for generating the necessary heat energy to maintain the body temperature within the thermoneutral zone. Mitochondria, consuming approximately 90% of the oxygen, play a significant role in this process.[38] Energy derived from adenosine diphosphate (ADP) conversion to adenosine triphosphate (ATP) is produced through mitochondrial oxidative phosphorylation. However, this chemical reaction is typically only 50% efficient, with the remaining energy resulting in heat production. The production of ATP enables various cellular functions, such as active ion pump transport, synthesis of biological macromolecules, and muscular contraction. Consequently, biological tasks generate heat, which contributes to regulating body temperature within a comfortable range and facilitating normal physiological functions.

Heat dissipation of the human body

In the absence of an efficient cooling mechanism that preserves the equilibrium of normal body temperature, the continuous production of heat energy through metabolism and the absorption of external heat will lead to a progressive increase in body temperature. The human metabolism employs two main processes to dissipate heat during daily activities: internal heat transfer and body surface heat dissipation. Internal heat transfer primarily relies on heat conduction and blood circulation to reach the skin, facilitating the subsequent transfer of heat from the skin to the external environment. Heat is conveyed to the body surface through various cooling modes, including radiation, conduction, convection, and water evaporation. In addition to excretion and breathing to take away some of the heat, the skin is the most important way for the body to lose heat.[39] Governed by the body's thermoregulation mechanism, skin heat dissipation plays a vital role in maintaining body temperature stability (**Figure 2.2**).

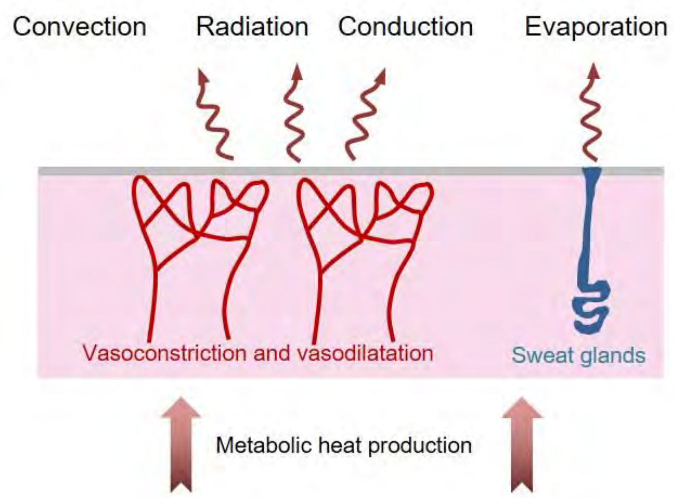

Figure 2.2 The form of heat exchange between the body and the environment.

It emits heat in the form of thermal radiation when an object's temperature surpasses absolute zero. The process of radiation is influenced by various parameters such as the temperature disparity between the skin and the object's surface, the surface area involved in radiation, and the object's color. There is a corresponding increase in radiant heat loss as the temperature difference increases, while a decrease in temperature difference leads to a decrease in radiant heat loss. The sun's energy is absorbed and transformed into heat. The body receives heat from the radiating object when the ambient temperature exceeds the body surface temperature. Some skin surfaces interact with other skin surface areas during the exchange of radiative heat in the environment. The effective radiation area of the human body is approximately 75% of the total radiation area when a person stands with their arms by their sides.[40] However, the effective radiation area can reach 85% of the total area when the arms and legs are extended. At normal temperatures, and in a calm state, radiation accounts for approximately 60% of body heat emission.

Conduction is a heat transfer mechanism wherein thermal energy is transmitted directly from a hotter body to a cooler body.[41] It involves the molecular interaction between two objects in contact, without any material transfer. The direction of heat flow is determined by the temperature gradient between the bodies. When the skin comes into contact with a colder object, heat is conducted and dissipated to the cooler object. The effectiveness of conduction heat dissipation is influenced by factors such as the temperature difference between the skin and the contact surface, the thermal conductivity of the objects, and the contact area. In static conditions, solid conduction plays a minimal role in heat dissipation, and clothing creates a layer of stagnant air that acts as insulation by reducing heat exchange. Conduction occurs when the body's surface interacts with substances of varying temperatures, such as air or water, resulting in heat absorption or loss.

Convection refers to the process by which heat is transferred through a gas or liquid medium. This occurs when the gas or liquid in contact with the body's surface gains heat through conduction, leading to increased movement and allowing cold gas or liquid to replace it. As a result, the body dissipates heat through the convection process facilitated by the exchange of hot and cold air.[42] The natural convection of air, influenced by outdoor wind speed, plays a significant role in heat dissipation. Generally, higher wind speeds enhance heat loss, while lower speeds reduce it. The convective heat transfer and its characteristics are affected by the medium between hot and cold objects, as well as the rate of exchange of heat between their surfaces. Natural convection takes place when warm air rises from the skin and enters a cooler environment, while forced convection employs an electric fan to cool the skin. Before convecting through the skin, heat must first pass through a thin layer of air that is tightly bonded to the skin's surface. This air layer's thickness is determined by the skin temperature and the rate at which air flows over the surface.

Evaporation serves as a mechanism to absorb body heat through the vaporization of water from the body's surface.[43] Body heat loss occurs through two distinct channels: sensible heat and latent heat. Sensible heat encompasses the transfer of heat through convection, conduction, and radiation, while latent heat involves the transfer of heat through the mass transport of sweat evaporation and exhalation from the skin's surface. Sensible perspiration refers to the increase in latent heat of evaporation resulting from active perspiration during instances where the ambient temperature is high and sensible heat exchange is inadequate to maintain the body's thermal equilibrium. This represents the primary means by which the human body dissipates heat in a thermal environment. Evaporative heat dissipation is influenced by various factors such as environmental temperature, wind speed, and air humidity. Evaporative cooling can occur at any temperature experienced by humans due to the higher humidity of a moist surface relative to the surrounding air. Particularly when the ambient temperature is equal to or surpasses the skin temperature, radiation, and conduction no longer contribute significantly to heat dissipation, making evaporative heat dissipation the sole pathway for the human body to dissipate heat.

2.1.3 Temperature comfort zone and energy expenditure

Humans instinctively seek out the optimal ambient temperature, known as the comfortable temperature, to ensure proper physiological functioning.[44] Maintaining a stable metabolic rate necessitates a suitable environmental temperature, while the body temperature must remain within a predefined range, as illustrated in **Figure 2.3**.[45] Any sudden increase or decrease in body core temperature beyond the physiological limit can jeopardize life. Choosing an appropriate temperature in cold environments involves a complex behavioral process that aims to minimize the temperature difference between the body and the environment, thereby reducing heat dissipation and conserving body heat. Conversely, in thermal environments, it is desirable for the body to facilitate heat dissipation and prevent excessive body temperature, thereby increasing the temperature gradient between the body and the environment when selecting the optimal temperature.

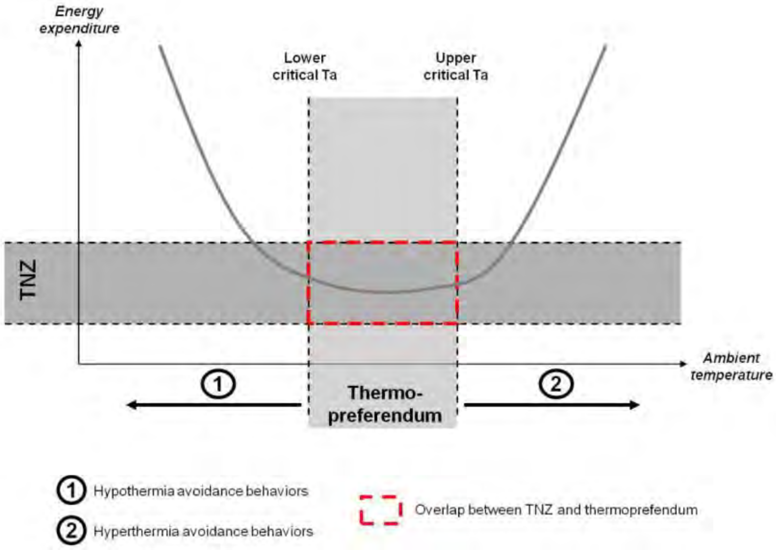

Figure 2.3 The relationship between body temperature and energy.[45]

This physiological process enables the body to sustain an isothermal temperature while minimizing energy expenditure. The optimal range of ambient temperatures aligns with the state of minimal energy consumption, known as the thermoneutral temperature comfort zone. Deviation from this zone, either falling below the lower critical ambient temperature or exceeding the upper critical ambient temperature, leads to a significant rise in energy expenditure and triggers vigorous bodily responses to counteract overheating or cooling. Behavioral thermoregulation measures are employed to prevent hypothermia or hyperthermia and mitigate the impact on the body.

2.2 Electronic thermosensation

The conventional electronic thermosensation usually involves a temperature measurement.[46-50] According to the zeroth law of thermodynamics, any physical quantity of the temperature measuring element can indicate the temperature value of the object under examination as thermal equilibrium is reached between the two objects. The flexible temperature sensor consists of a sensitive element integrated into a flexible substrate, enabling its application in intricate curved environments. Based on the sensing mechanism of the sensitive element, electronic temperature sensors are usually categorized into three groups: resistance sensing, voltage sensing, and capacitive sensing. Although these sensors exhibit remarkable performance in temperature measurement for flexible e-skin, they are not without their limitations.

2.2.1 Resistance-responsive sensor

Resistance-response temperature sensation material includes precious metals (platinum, gold, copper), carbon materials (carbon nanotubes (CNTs), graphite, graphene), and conductive polymers (poly(3-butylthiophene), polyaniline, poly(3,4-ethylenedioxythiophene):poly(styrenesulfonate)(PEDOT:PSS)).[28, 50-52] These conductors exhibit a change in resistance as a function of temperature (**Figure 2.4**). The relationship between resistance and temperature is defined by the resistance's rate of change per degree Celsius. Resistance thermometers demonstrate exceptional accuracy, operate effectively across a wide temperature range, and exhibit the most stable resistance-temperature correlation within this range, with errors as negligible as one part in ten-thousandths of a degree. Consequently, they are employed in diverse configurations as highly reliable flexible temperature sensors.

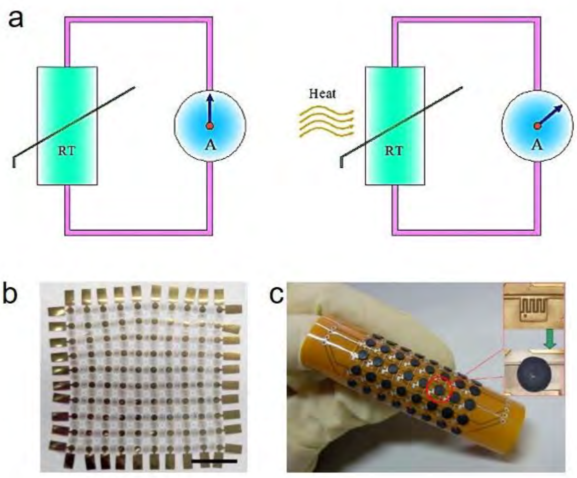

Figure 2.4 Resistance-responsive temperature sensors. a) Working mechanism of resistance temperature sensor. b) Resistive temperature sensor matrix network.[53] c) Carbon nanotube-based temperature sensor.[54]

In 2013, Rogers' group achieved the development of a snake-like temperature sensor array using Cr/Au on polyimide thin film through photolithography and metal deposition techniques.[55] This innovative approach capitalizes on the thermal resistance effect of metals to enable thermosensation. The resulting temperature sensor array exhibits exceptional conformity to human skin, enduring mechanical integrity post-bending and twisting. Moreover, it demonstrates a comparable level of accuracy to infrared temperature sensors, facilitating non-invasive real-time temperature measurements that hold significant implications for human health monitoring. Wang et al. conducted a study in 2018 to explore an integrated matrix network with exceptional stretchability, thereby expanding the capabilities of e-skin sensing.[53] This matrix network enabled signal sensing across various domains including temperature, strain within the plane, humidity, light, magnetic field, pressure, and proximity. Employing

Pt as the material for the thermosensation array, the resultant sensor not only exhibited remarkable flexibility but also demonstrated linear resistance alterations relative to temperature within the range of 0 °C to 70 °C. The accuracy achieved by this sensor was found to be similar to that of commercially available products.

The advantages of resistance thermometer are that is more sensitive, has high accuracy, easy processing, and stability, from the point of view of the use of performance. Although the resistance thermometer has a good linear relationship with temperature, but also by the pressure of the impact, is not suitable for the measurement of temperature in complex environments. Resistance thermometers need to undergo specific patterning to achieve the flexibility of the device when applied to curved environments, which is challenging for achieving large-area use.

2.2.2 Voltage-responsive sensor

Voltage-responsive temperature sensor materials comprise two main kinds of thermoelectric type and pyroelectric type, possessing the remarkable ability to convert external stimuli into voltage signal.[56-60] Thermoelectric sensor utilizes an element called a thermocouple, composed of two dissimilar metals or semiconductors interconnected to form a closed loop. An electric potential is generated within the loop when there is a temperature difference at the two junctions of the thermocouple. On the other hand, the pyroelectric effect is a charge release phenomenon exhibited by the change in polarization intensity with temperature, macroscopically the change in temperature causes a voltage or current to appear at the two ends of the material. **Figure 2.5** demonstrates the wide utilization of voltage-sensing mechanisms in temperature measurement. Flexible voltage temperature sensors possess several advantages, such as compact size, rapid response time, cost-effectiveness, versatile design options, and adaptable materials.

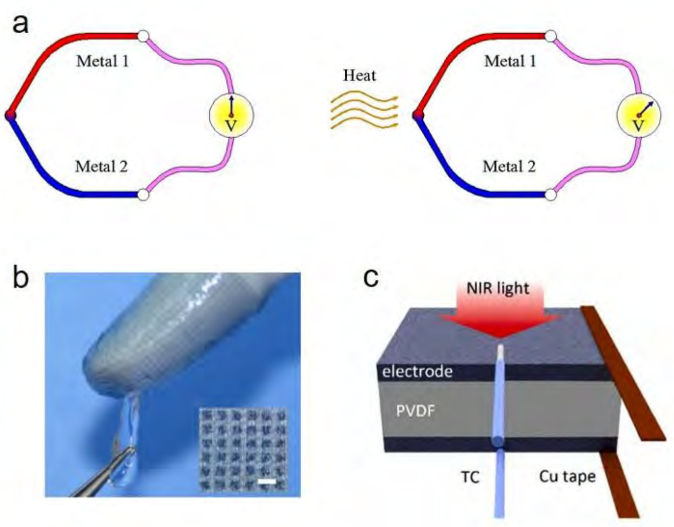

Figure 2.5 Voltage-responsive temperature sensors. a) Working mechanism of voltage temperature sensor. b) Microstructure-frame-supported organic TE device.[61] c) poly(vinylidene fluoride) (PVDF) pyroelectric generator.[62]

In 2018, Aniello et al. prepared a planar translucent thin-film thermocouple from silver nanowires and PEDOT:PSS on a flexible substrate by spray deposition method.[63] The thermocouple has a Seebeck coefficient of up to 54 μV/K, possesses a linear response of voltage and temperature, and is ideal for self-supplied thermosensation as it is capable of not only thermosensation but also energy harvesting. In 2022, Kang et al. expanded the applicability of tosylate-doped poly(3,4-ethylenedioxythiophene) as an effective electrode material for PVDF-based pyroelectric devices and electronic sensors operated by thermal radiation sources used as an effective electrode material for PVDF-based pyroelectric devices.[62] This electrode material enables stronger absorption of thermal radiation and converts electrical energy more than an order of magnitude more efficiently than other metals. This pyroelectric device is highly sensitive to thermal radiation, generates high voltages to thermal energy, and is used to charge commercial capacitors to demonstrate thermal energy harvesting capabilities.

The flexible temperature sensor employing voltage response for real-time, rapid, and dynamic temperature detection offers distinct advantages such as two-dimensional characteristics, low heat capacity, and swift response, which are unmatched by other types of temperature sensors. Furthermore, its ability to be processed into an ultra-thin profile, endure bending and flexing, and compatibility with straightforward manufacturing methods contribute to its widespread application in e-skin surface thermosensation. However, it is important to note that thermocouples exhibit low sensitivity, thereby complicating the measurement process. Similarly, pyroelectric temperature sensors only allow for transient temperature measurements and are susceptible to pressure, rendering them inadequate for continuous temperature measurement in complex environments.

2.2.2 Capacitance-responsive sensor

In capacitive temperature sensors, fluctuations in temperature induce modifications in the active material's geometric volume or internal structure, leading to alterations in capacitance (**Figure 2.6**).[64-68] Concurrently, temperature variations impact the transport capacity of material carriers, causing shifts in the relative dielectric constant and capacitance. The critical aspect in the design of capacitive temperature sensors lies in the sensitivity of sensors equipped with parallel plate electrode structures to conductive area alterations. As a result, these sensors convert changes in area due to temperature stimuli into capacitive signals. Additionally, the utilization of micro-structuring techniques in the conductive layer allows for the amplification of relative area changes in response to temperature stimuli.

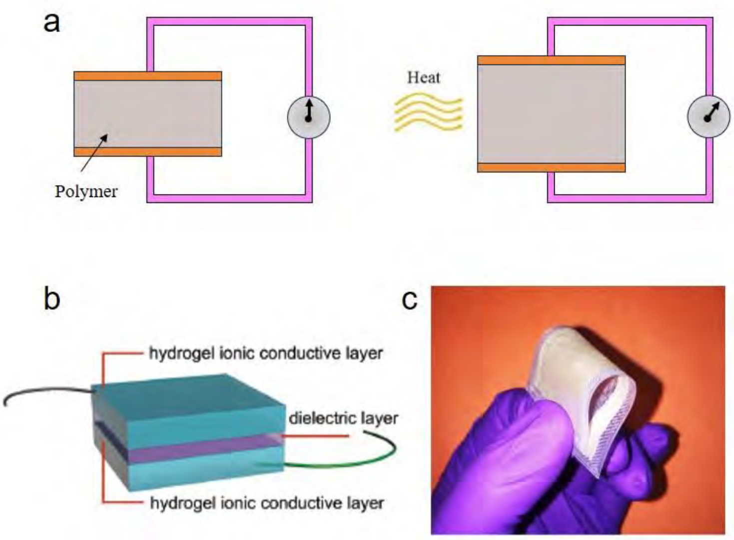

Figure 2.6 Capacitance-responsive temperature sensors. a) Working mechanism of capacitive temperature sensor. b) Flexible hydrogel-based capacitive sensor device.[69] c) Flexible PVDF-based capacitive temperature sensor.[70]

A thermally sensitive hydrogel with a dual network for a temperature sensor for e-skin was created in 2017 by Wu.[69] At a high temperature, the hydrogel in this sensor can go through a phase change that causes physical cross-linking to unravel, lowering the viscosity of the microstructure in the sensor. Additionally, the change in geometric area intensifies the expansion behavior at high temperatures, resulting in a change in capacitance. The resultant skin-like hydrogel sensors demonstrate remarkable sensitivity to temperature or pressure stimuli as a result of this logical design. In 2020, Pan et al. used chitosan to produce a capacitive response to temperature stimulation.[64] High temperatures improve the degree of ionic aggregate dissociation and redissociation, resulting in an increase in molecular spacing, which in turn increases the amount and mobility of free ions. Chitosan materials can provide steady resolution of temperature-stimulated signals via capacitance changes because of the proton conductivity's temperature sensitivity and the material's high dielectric constant. The capacitance increases with temperature in the temperature interval of 25-50 °C with a linear sensitivity of ~2.56 pF/°C.

Capacitive temperature sensors demonstrate remarkable sensitivity and linearity, rendering them suitable for temperature measurement across a wide array of surfaces. Nonetheless, meticulous consideration must be given to shielding electromagnetic interference, as this is crucial in minimizing signal noise. Additionally, it is important to address the temperature hysteresis and sluggish response speed that arise due to the inherent measurement principle of capacitive temperature sensors, particularly during transient measurements.

2.3 Artificial thermoregulation

Currently, artificial thermoregulation in a single scenario is reported in the literature, which could classified into two types, i.e. active and passive modes. For the active move mode, both the TE cooling devices and joule heating devices have been investigated. On the contrary, passive thermoregulation impacts the amount and direction of heat movement through the qualities of its material and structure. Heat conduction and insulation materials, for example, can alter the temperature of an item by speeding up or slowing down heat dissipation. These systems' thermoregulation mechanisms will be discussed in depth further down.

2.3.1 Active heating and cooling

The active mode of thermoregulation by connecting external energy, its heat change can make a significant change in the temperature of the target object. Active thermoregulation mainly includes joule heating, TE cooling, and so on.

Joule heating

The utilization of the Joule effect to induce temperature changes in objects represents a widely adopted mechanism for thermoregulation (**Figure 2.7**).[71-79] The underlying principle of this approach lies in the generation of heat on a conductor when an electric current passes through it, arising from the Joule effect resulting from resistance. Conventional electric heaters typically employ bulky metal components or wires as functional elements, facilitating rapid heat generation. However, the usage of metals for thermal management in e-skin can introduce challenges in terms of weight, hardness, and tactile properties, thereby impeding practical application. Consequently, alternative materials like conductive polymers, graphene, or metal nanowires have emerged as successful substitutes for thermoregulation in e-skin. These substitutes exhibit commendable flexibility and exceptional heating performance, constituting effective strategies for bionic thermoregulation in e-skin.

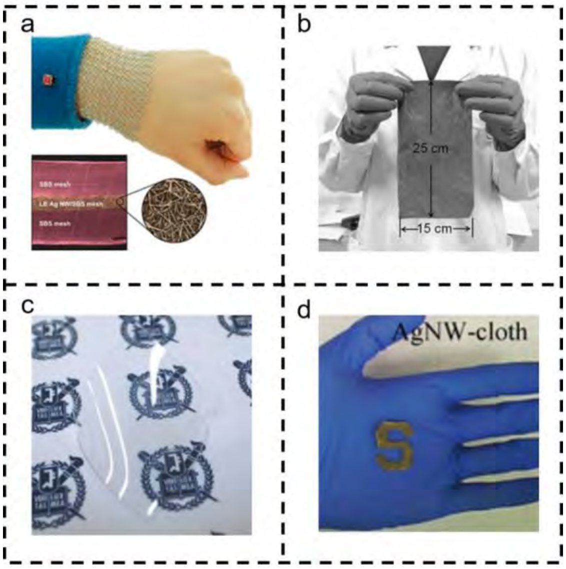

Figure 2.7 Different types of flexible heaters based on the Joule effect. a) Stretchable heater using ligand-exchanged silver nanowire nanocomposite.[71] b) Ultrathin, washable, and large-area graphene papers.[79] c) Highly stretchable and transparent metal nanowire heater.[72] d) metallic nanowire-coated textile.[77]

In 2015, Kim's group prepared a stretchable heater using silver nanowires and SBS elastomers.[71] Due to its soft properties, the conductive elastomer is well conformal to the skin, providing long-term, continuous thermal treatment for human joints. In 2017, Wang et al. prepared a large areas of graphene paper.[79] The graphene paper has good flexibility and conductivity, realizing the function of active heating. The surface temperature of graphene paper can be raised from 18 °C to around 37 °C when the current voltage is 2.5V. Although the preparation of joule heaters is simple and thermoregulation is convenient, these heaters only have the function of one-way heating and have great limitations. The temperature of the human living environment is complex and changeable, so the heater does not have the application in a high-temperature environment.

TE cooling

Thermoregulation based on the Peltier effect is one of the most widely used directions in the field of TE.[80-84] It has the advantages of small volume, adjustable cooling power, and no noise, but the TE system has many rigid structures due to its traditional configuration.[85-88] The Peltier effect was first discovered by French scientist Jean C. A. Peltier in 1834 and is a type of TE effect. This phenomenon manifests when an electric current traverses a circuit composed of dissimilar conductors, resulting in the absorption or release of heat at the interface of conductors. Fundamentally, the Peltier effect is rooted in the disparities in Fermi energy levels among charge carriers within distinct materials. As these carriers traverse from a material of high energy level to one of low energy level, they liberate excess energy. Conversely, when carriers migrate from a low-energy-level material to a high-energy-level one, they absorb heat from the surroundings. The occurrence of heat absorption at the junction undergoes a thermodynamic transformation from endothermic to exothermic when the material type or the current direction is altered.

The effective dissipation of heat generated at the hot side into the surrounding environment is of utmost significance when utilizing TE devices for thermoregulation. Wearable TE coolers operate within environments characterized by substantial thermal resistance due to the inherent poor thermal conductivity of human skin and the surrounding air. This external thermal resistance significantly influences the performance of TE materials, device design, and overall efficiency, thereby posing a fundamental challenge in achieving effective on-body applications. **Figure 2.8** illustrates various TE devices presently employed in the realm of temperature management.

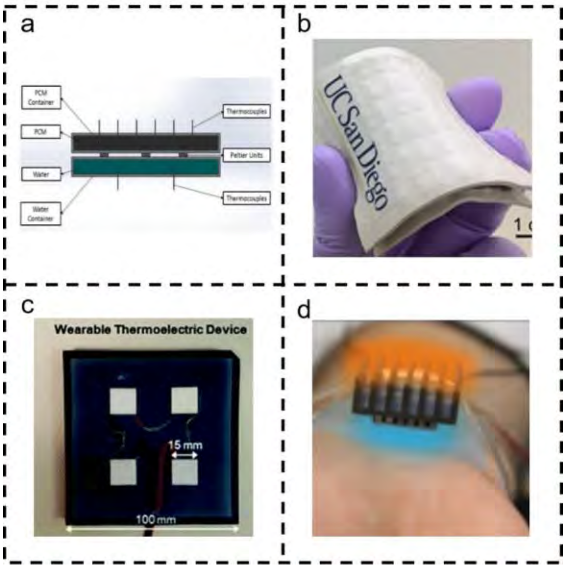

Figure 2.8 Different types of TE thermoregulation devices based on the Peltier effect. a) TE cooling device for patients.[89] b) Wearable TE device for personalized thermoregulation.[90] c) Lightweight wearable TE cooler.[91] d) Ultra-high performance wearable TE cooler.[92]

In 2014, Elsayed et al proposed to use TE devices to relieve the symptoms of multiple sclerosis patients.[89] The study developed a compact lightweight wearable upper limb cooling device that combines the heat extraction capability of TE devices with the heat storage capability of PCM to reduce skin temperature to 10 °C for a duration of 20 min. In 2019, Chen et al. designed and demonstrated the first model with long-term and flexible wearable TE devices with large active cooling effects.[90] The TE device uses an innovative design of rigid inorganic high TE value (ZT) legs sandwiching between stretchable elastomer plates to produce a huge cooling effect of over 10 °C on the skin without the use of any heat sink.

TE devices exhibit commendable refrigeration capabilities and are indeed suitable for e-skin thermoregulation. However, their widespread implementation in thermoregulation is hindered by the inherent conflicts between structure and performance. Consequently, TE devices are rarely employed at a large scale. To facilitate the practical application of e-skin, the current dominant research paradigm primarily focuses on enhancing the performance of organic TE materials through material design or improving the flexibility of inorganic TE devices via innovative structural designs.

2.3.2 Passive cooling

Heat sink

The advancement of multifunctional e-skin and integration has brought forth two major challenges: high power consumption and consequential heat dissipation. These factors severely impede the rapid progress of e-skin technology. Ineffective cooling not only hampers the performance of electronic devices but also diminishes their lifespan. Hence, there exists a pressing demand for the development of high-performance cooling solutions. Passive thermal regulation stands at the forefront of e-skin temperature control research. It primarily focuses on the exploration of flexible materials with exceptional thermal conductivity and extensibility, such as liquid metal and carbon nanotubes, employing the principles of heat transfer.[93-96] These high thermal conductivity materials, aided by specific material or structural designs, facilitate even and swift heat conduction within the e-skin (**Figure 2.9**). This process ensures that the e-skin remains within a designated temperature range, thereby safeguarding it against overheating.

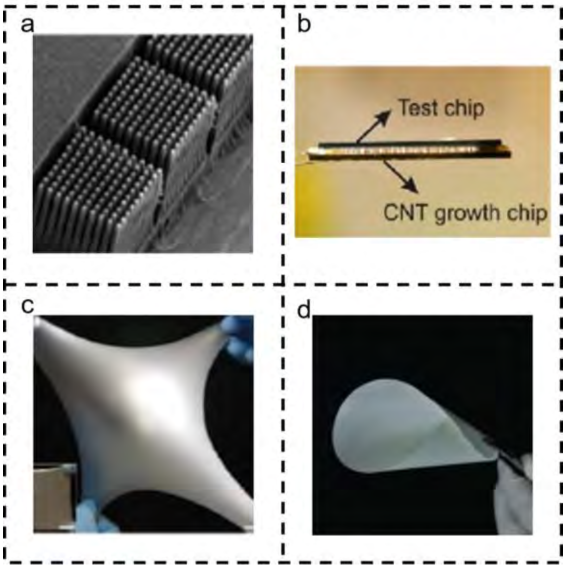

Figure 2. 9 Different types of heat sinks with high thermal conductivity. a) Chip cooling with integrated carbon nanotube microfin architectures.[95] b) A complete carbon-nanotube-based heat sink.[94] c) High thermal conductivity in soft elastomers with elongated liquid metal inclusions.[93] d) Highly thermal conductivity of cellulose nanofibrils/AlN hybrid films.[96]

In 2007, Ajyan et al. demonstrated a simple and effective cooling method.[95] In this method, a patterned carbon nanotube fin is transferred on the back of the chip by micro-nano technology for thermal management of the chip, in which flexible and high thermal conductivity carbon nanotubes are used to replace the heat dissipation components on the silicon chip. In 2016, Majidi's group designed an elastomer composite containing an elongated inclusion of liquid metal (LM) that performs heat conduction.[93] This study demonstrates the potential of liquid metal inclusions to significantly improve thermal conditions in applications requiring electrical insulation materials with rapid thermal conductivity and soft elastic functions.

Extensive research has substantiated the suitability of high thermal conductivity materials for efficient thermoregulation in e-skin, as they facilitate rapid dissipation of heat in various directions. Nevertheless, the process of fabricating heat dissipation structures using such materials is intricate and financially burdensome, impeding widespread implementation. Moreover, the primary role of high thermal conductivity materials within the e-skin is to conduct heat, primarily safeguarding against overheating in high-temperature environments.

Phase change material

The heat absorption method uses the phase change properties of materials to absorb the heat inside or outside the e-skin, to keep the e-skin within a certain temperature range, to widen the use range of the e-skin, and to improve the comfort of the e-skin. Thermal management of e-skin by means of thermal absorption of PCM is considered to be an effective way, which mainly utilizes latent heat properties of PCM.[97-101] For instance, the solid material undergoes a phase transition when the temperature reaches the melting point of the PCM, transforming into a liquid state and absorbing a significant amount of latent heat. Similarly, the PCM transitions from a liquid to a solid state when the temperature drops to the solidification point, releasing a considerable amount of stored heat. The PCM absorbs or releases substantial latent heat throughout these phase transformations, while its temperature remains nearly constant. This property holds tremendous potential for achieving efficient thermal management in electronic systems. As a passive cooling technology, PCM has been widely used in transient electronic cooling due to its advantages of large latent heat of melting, high specific heat, controllable temperature stability, and small volume change during phase transformation, as shown in **Figure 2.10**.

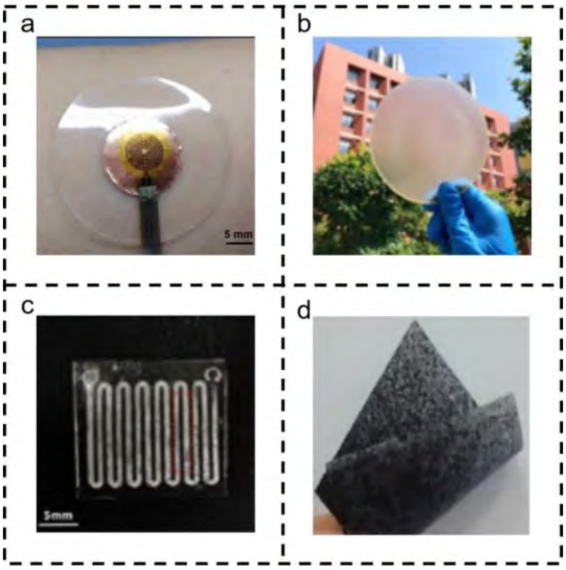

Figure 2.10 Different types of PCM devices for overheating protection. a) Functional soft composites as thermal protecting substrates.[100] b) An intrinsically flexible phase change film.[101] c) PDMS-PDMS micro channels filled with phase-change material.[99] d) Flexible PCM film.[98]

In 2018, Wang and his team reported a chip cooling scheme for a polydimethylsiloxane (PDMS) microfluidic device filled with n-octadecane.[99] Experimental results show that the temperature of a microfluidic chip with n-octadecane can be reduced by about 16 °C compared with that without n-octadecane under the same experimental conditions. In

2019, Li et al reported a functional soft composite material as a thermal protection substrate for wearable electronic devices, which has the ability to control heat flow and effectively absorb heat without compromising the flexibility of the substrate.[100] Compared with traditional substrates, thermal protection substrates can reduce skin temperature peaks by more than 85% with appropriate parameters.

Superior because of its unique characteristics of PCM have been proven its broad application prospect of thermal management in e-skin, however, PCM in the melting and solidification process of the changes in physical form will cause volume change, plus the possible balance will lead to its shape changes, the use of e-skin will produce very big effect. How to solve the deformation problem of PCM is the key to realize the large-scale application of PCM in e-skin.

Evaporative cooling

As previously mentioned, mammals regulate body temperature through perspiration in high-temperature environments, so passive biological perspiration cooling strategies are used in thermal management, such as cooling of electronic devices, cooling of buildings, or refrigeration of biological products (**Figure 2.11**).[102-106] Because the heat of vaporization of water is up to 2400 J/g, the limited mass can take away a lot of heat, so evaporative refrigeration has good cooling ability. Hydrogel contains a lot of water and is an ideal evaporative heat dissipating matrix. Thermally responsive hydrogel materials have a critical temperature, and when the ambient temperature exceeds this critical temperature, the hydrogel undergoes a process similar to phase transition, releasing water and taking heat away.

In 2019, Wang et al. demonstrated an evaporative cooling strategy through the desorption process of water inside the adsorbent.[106] The desorption agent is coated on the metal substrate, and as the temperature of the metal substrate rises, the water in the desorption agent vaporizes and evaporates, achieving a maximum cooling of 8.6 °C at 1.5 W heating power. In 2021, Lee et al. prepared a composite material with poly(N-isopropyl acrylamide) (PNIPAM) and PDMS that provided a novel cooling strategy.[104] The composite has good water evaporation switch control ability and has different evaporation rates in low-temperature environment and high-temperature environments.

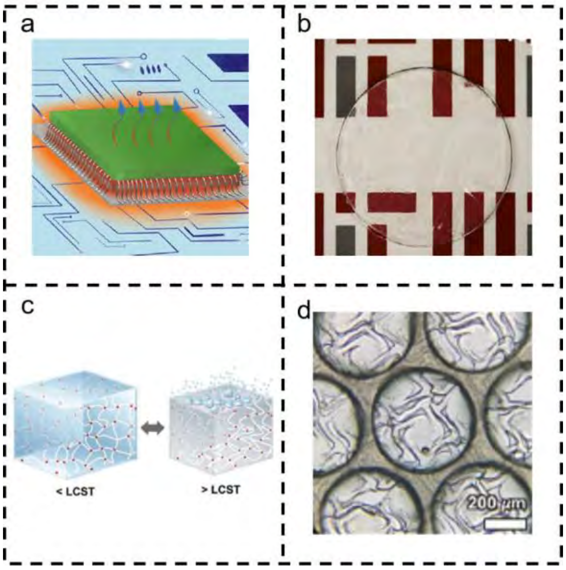

Figure 2.11 Different types of evaporation cooling devices. a) A thermal management strategy based on moisture sorption-desorption processes.[106] b) A transparent evaporation-insulation bilayer.[105] c) Evaporative cooling hydrogel packaging.[102] d) Artificial perspiration membrane.[103]

The evaporative cooling method of the simulated sweat gland has attracted wide attention because of its high efficiency and no energy consumption. It has the advantages of simple preparation and low cost and is an ideal method for e-skin thermoregulation.

2.4 Conclusions and Summary of Research Gaps

The isothermal skin is critical for the human being, enabling the sensitive response to the tiny environment change. However, the functional bionic engineering to achieve thermoregulation and thermosensation for elect is still lacking.

In the area of thermoregulation of e-skin, there have been studies to achieve the management of e-skin temperature. Its realization can be divided into active thermoregulation and passive thermoregulation. Active thermoregulation uses the Joule effect and Peltier effect to convert electrical energy into thermal energy, but there are problems such as unidirectional regulation and limited regulation time. Passive thermoregulation uses thermally related materials such as heat absorbing and heat dissipating materials to provide overheating protection for e-skin, but there are problems such as limited heat capacity and uneven heat absorption or dissipation in the process of heat absorption or heat dissipation, and passive thermal regulation only focuses on the application of e-skin in hot environment, which has certain limitations. In this work, we will improve the flexibility of the TE device through structural design and combine PCM and hygroscopic hydrogel to realize the unification of active and passive thermoregulation, which expands the application of e-skin in a low-temperature environment and high-temperature environment and has kind of significance for the promotion and application of human prosthesis and intelligent robot field of e-skin in the future.

In the context of thermosensation in e-skin, the bionic replication of thermosensation can be achieved through the utilization of temperature sensors. As previously mentioned, the temperature sensors can be further classified as resistance-responsive sensors, voltage-responsive sensors, and capacitive-responsive sensors based on their corresponding signal outputs. However, all variations of temperature sensors face certain challenges when applied in the process of thermosensation for e-skin. For instance, resistive temperature sensors are susceptible to pressure interference during temperature measurement, voltage temperature sensors exhibit lower sensitivity, and capacitive temperature sensors require increased energy consumption and present other issues. Moreover, these sensors solely provide a simplistic representation of the temperature value of an object, thus lacking the capacity to deeply analyze the thermosensation of the object. In this study, a multimodal temperature sensor will be developed based on the principles of ion relaxation time. This sensor will not only facilitate the realization of fundamental temperature responses but also enable the identification and differentiation of different heat source types such as conduction, convection, and radiation by effectively decoupling the temperature and pressure signals. This innovative approach provides a novel technical solution for achieving comprehensive and insightful thermosensation capabilities in e-skin applications.

In this thesis, we are admins to applying thermo-e-skin and multimodal temperature sensors to the bionics of e-skin, to realize the e-skin has or even exceeds the temperature sensation function of human skin.

CHAPTER 3 SINGLE-MODE THERMOREGULATING E-SKIN

3.1 Introduction

Achieving and maintaining a suitable body temperature range through thermoregulation is of utmost importance for humans. Traditional e-skin, unfortunately, faces limitations in terms of materials and structure that prevent it from maintaining a consistent temperature as the environment changes. This absence of thermoregulation not only leads to physical discomfort but also has negative psychological effects. Consequently, the integration of a thermoregulatory design in e-skin is crucial in improving comfort and enhancing the self-confidence of individuals who rely on assistive prostheses.

The primary objective of e-skin thermal management is to optimize the overall thermal environment of an object by modulating the heat transfer mechanism.[107-110] However, current thermal management practices, as discussed in Chapter 2, primarily focus on a singular purpose of either heating or cooling.[111-114] Active approaches need to be implemented to control temperatures in diverse thermal environments to achieve effective thermoregulation. For instance, harnessing the Joule effect inherent in conductors offers efficient heating capabilities.[115-117] Moreover, TE devices can be utilized to both heat and cool by creating a temperature gradient across the device using the Peltier effect.[118-120] Nevertheless, there is currently a lack of research on achieving human-like isothermal regulation in e-skin within a variable thermal environment.

To address this challenge, the chapter introduces a novel solution in the form of a single-mode thermoregulating e-skin (S-thermo-e-skin). This innovative approach utilizes a hybrid structure consisting of a flexible BiTe-based TE device and a paraffin-based PCM heat sink. Our investigation aims to comprehensively evaluate the thermoregulatory capabilities of this hybrid e-skin in both hot and cold environments, while also considering the energy consumption required to maintain a comfortable temperature within the e-skin. Remarkably, our proposed design successfully achieves a consistent surface temperature of 35°C across a broad temperature range spanning from 10°C to 45°C.

3.2 Concept design

It is crucial for the e-skin to have the ability to heat at low temperatures and cool at high temperatures in order to achieve thermoregulation capabilities comparable to the human body. A TE device was selected as the central component for the thermoregulatory system to fulfill this requirement. It is possible to establish a hot side and a cold side by connecting the TE device to an external heat source, similar to the thermoregulation mechanisms observed in the human body, allowing for heating or cooling of the e-skin. However, there are several challenges associated with using TE devices for thermoregulation. Firstly, traditional TE devices are typically rigid or semi-rigid, necessitating structural optimization for improved flexibility. Secondly, efficient dissipation of accumulated heat on the hot side of the TE device is crucial during the cooling process to prevent thermoregulation failure. Lastly, the dynamic nature of temperature environments necessitates the implementation of real-time thermostatic regulation functions.

In this chapter, a novel S-thermo-e-skin design is proposed, incorporating a flexible TE device and a PCM heat sink, as illustrated in **Figure 3.1 a**. An important characteristic of this e-skin configuration is the inclusion of a PCM layer at the bottom of the flexible TE device, providing enhanced active thermoregulation capabilities. Specifically, in a low-temperature environment, the flexible TE device utilizes the TE effect to convert electrical energy into thermal energy, thereby heating the surface. This is achieved by designating the upper side of the TE device as the hot side, resulting in an effective increase in the surface temperature of the thermoregulatory device.

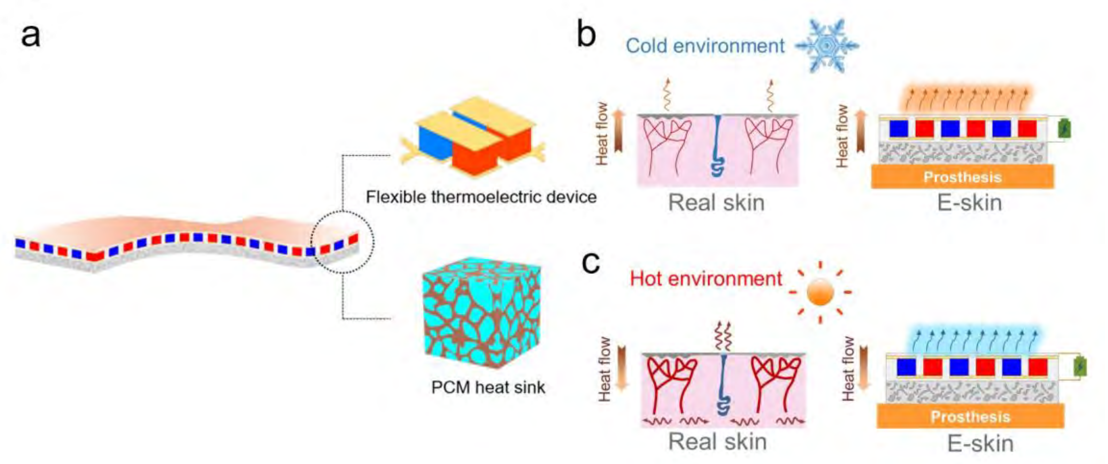

Figure 3.1 The design concept and application mechanism of S-thermo-e-skin. a) Basic structure of S-thermo-e-skin. b) The mechanism of S-thermo-e-skin in a cold environment. c) The mechanism of S-thermo-e-skin in a hot environment.

The human skin exhibits remarkable thermoregulation capabilities in complex temperature environments (**Figure 3.1 b**). This is achieved as cells generate significant heat through metabolism, maintaining the body temperature around 37 °C and supporting vital physiological processes. In cold environments, cold receptors in the skin detect temperature and transmit signals to the brain, causing the sensation of cold.[19] The brain then orchestrates various mechanisms within the skin tissue to minimize heat loss, including vasoconstriction, contraction of the arrector pili muscle, and minimal sweating. Similarly, the TE unit in the S-thermo-e-skin can be analogized to a human body cell, while the temperature sensor within the S-thermo-e-skin corresponds to a human body temperature receptor. The temperature sensor sends a signal to the control system upon detecting low ambient temperatures. Subsequently, the control system instructs a TE device connected to a power supply to convert electrical power into heat. This process, known as cold adaptation, transforms the upper surface of the TE device into the hot side, thereby elevating the surface temperature of the e-skin through the generated heat.

In a hot environment, however, the skin senses the temperature through warm receptors and relays the information to the brain, resulting in the sensation of being hot. As depicted in **Figure 3.2 c**, the brain orchestrates cooling mechanisms in the skin tissue, including vasodilation, the dilation of the arrector pili muscles, and profuse perspiration. Likewise, when the temperature sensor embedded in the thermoregulation e-skin detects an excessively high external temperature, it transmits a signal to the control system. The upper surface of the TE device functions as the cold side, actively absorbing heat and cooling the surface of the e-skin, a process referred to as thermal adaptation. Meanwhile, the lower surface of the TE device generates substantial heat, limiting the device's cooling efficiency. While human skin has the capability to radiate heat into the surrounding environment, the e-skin lacks this ability, necessitating the retention of heat in a heat reservoir beneath it to maintain the thermal adaptation effect on the surface.

3.3 Fabrication of S-thermo-e-skin

The S-thermo-e-skin consists of a flexible TE device and a PCM heat sink, so its manufacture includes the fabrication of the flexible TE device, the fabrication of the PCM heat sink, and the encapsulation of the S-thermo-e-skin.

3.3.1 Fabrication of flexible TE device

TE devices play a pivotal role in enabling the heating and cooling functionalities of S-thermo-e-skin. The basic structure of the TE device includes thermoelectric leg and copper electrode. In a series arrangement, both N-type TE legs and P-type TE legs are positioned on these electrodes. Each N-type TE leg and P-type TE leg combine to form the essential unit, known as the π type structure, within the TE device.

The fundamental operating principle of a TE device can be described as 'electric series, thermal parallel'. During the conversion of electrical energy into heat energy via the TE effect, the magnitude of heat generation and cooling is contingent upon both the material properties and the quantity of π type structures employed. However, the inherent contradiction between the performance and structure of the TE leg limits the true flexibility of bulk TE devices employed for thermoregulation. To address this, a commonly utilized approach in the design of flexible electronic devices is the 'island-bridge' structure. This involves the dispersion of rigid island structures on a flexible substrate, followed by the integration of functional devices and subsequent connection of these islands via stretchable and flexible interconnecting conductors. Implementing this method effectively reduces device deformation and enhances device reliability. A flexible TE device capable of bending is achieved by adopting this approach, thereby exhibiting a certain degree of flexibility suitable for wearable applications. The proposed design involves the arrangement of four TE legs to form two π-shaped structures, which serve as the TE cooling unit, as depicted in **Figure 3.2**.

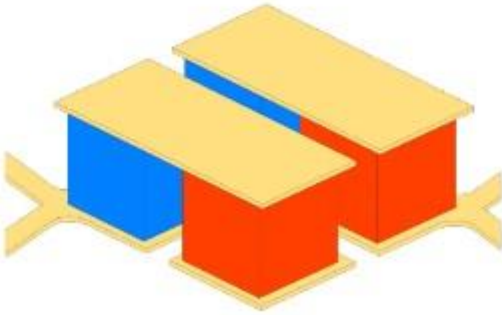

Figure 3.2 Island-bridge structure of flexible TE device.

Each TE unit is connected to each other by flexible circuits, and these flexible circuits are located on one side of the TE device, so that the device can withstand bending in multiple directions and can withstand greater bending curvature, providing sufficient heating/cooling capacity while maximizing the flexibility of the device. The flexible TE device is coated with a layer of copper of 100 μm thickness on a polyimide film of 50 μm thickness by an electroplating process, and the excess polyimide is removed from the upper and lower electrodes by laser processing to improve the flexibility of the substrate and reduce the thermal resistance of the polyimide. In this way, the upper and lower electrodes required for flexible TE device are fabricated (**Figure 3.3**).

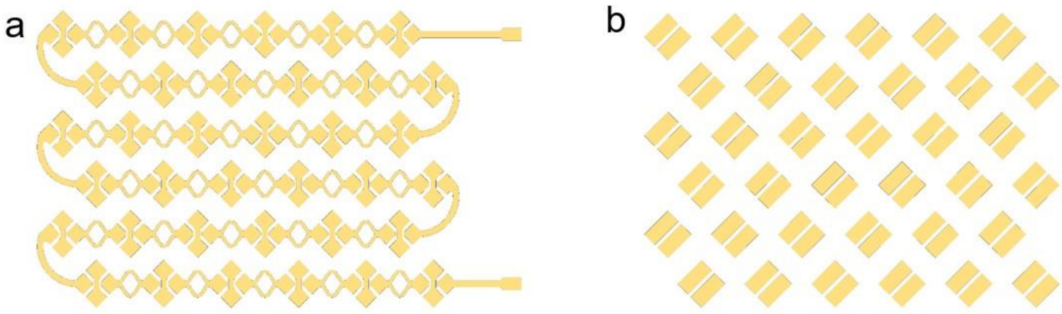

Figure 3.3 The design of flexible electrodes. a) lower electrode b) Upper electrode.

The TE leg used in the experiment was purchased from Guangdong Fuxin Electronic Technology Co., Ltd, where the N-type material is $Bi_{1.95}Te_{2.8}Se_{0.2}$and the P-type material is $Bi_{0.39}Sb_{1.61}Te_{3.03}$, whose basic properties are shown in Table 3.1 and 3.2. The upper and lower surfaces of TE leg for welding are coated with a nickel metallization layer, TE leg dimensions are 1.6 mm × 1.6 mm × 1.5 mm.

Table 3.1 Relevant properties of the $Bi_{1.95}Te_{2.8}Se_{0.2}$.

Temperature [°C]	Resistance [μΩm]	Seebeck coefficient [μV/K]	Power factor [μW/mK^2]	Thermal diffusivity [mm^2/s]	Cp [μV/K]	*κ* [W/mK]	*ZT*
30	11.14	-237.83	5079	1.13	0.16	1.38	1.11
50	12.35	-238.48	4604	1.12	0.16	1.38	1.08
100	14.70	-233.43	3706	1.17	0.16	1.45	0.95
150	16.06	-218.87	2982	1.36	0.16	1.71	0.74
200	16.44	-194.81	2308	1.66	0.17	2.13	0.51
250	15.83	-161.24	1642	1.98	0.17	2.57	0.33

Table 3.2 Relevant properties of the $Bi_{0.39}Sb_{1.61}Te_{3.03}$.

Temperature [°C]	**Resistance [μΩm]**	**Seebeck coefficient [μV/K]**	**Power factor [μW/mK^2]**	**Thermal diffusivity [mm^2/s]**	**Cp [μV/K]**	***κ* [W/mK]**	***ZT***
30	7.86	189.36	4564	1.20	0.18	1.46	0.95
50	8.86	197.37	4399	1.16	0.19	1.45	0.98
100	11.51	207.40	3736	1.11	0.18	1.38	1.01
150	14.21	202.99	2900	1.18	0.19	1.49	0.82
200	16.70	183.94	2027	1.37	0.19	1.77	0.54
250	18.74	150.05	1202	1.64	0.20	2.16	0.29

The entire flexible TE device uses 36 TE units with an overall dimension of approximately 67 mm × 48 mm, which allows enough space to facilitate the bending of the TE units while maintaining performance. The P and N TE legs were arranged alternately on the copper electrode and bonded to the electrode with solder. Finally, it was placed in a reflow machine for soldering to obtain a flexible TE device (**Figure 3.4**).

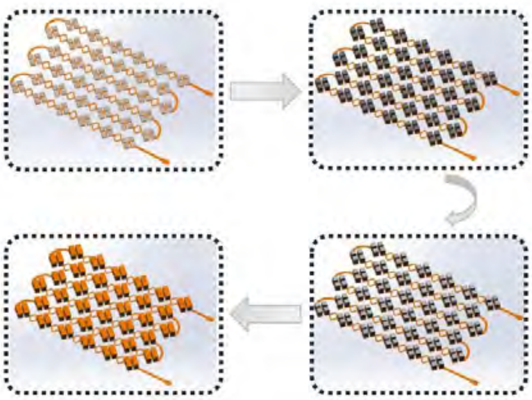

Figure 3.4 Reflow soldering process for flexible TE device.

3.3.2 Fabrication of PCM heat sink

PCM heat sink is another integral part of S-thermo-e-skin. Paraffin, a white translucent solid mixture of advanced alkanes, is employed as the PCM for overheating protection in the S-thermo-e-skin. Serving as an organic PCM, paraffin demonstrates the ability to absorb or release significant amounts of latent heat during phase change, while maintaining a relatively constant temperature. The transformative properties of paraffin come into play when the ambient temperature exceeds its own. In such instances, it acts as a medium to absorb heat from the surroundings, transitioning from a solid to a liquid state. Notably, the surface temperature remains relatively stable or shows minimal fluctuations. The specific paraffin wax utilized in the S-thermo-e-skin was purchased from Ruhr New Materials Co., Ltd.

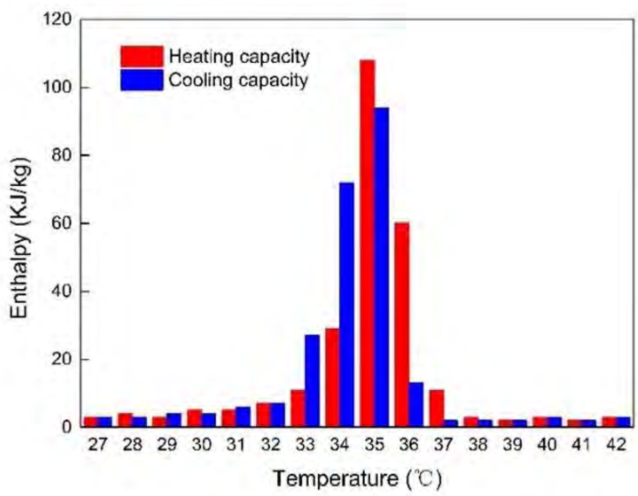

Figure 3.5 Enthalpy distribution of paraffin.

Figure 3.5 illustrates the heat storage capacity of paraffin, which measures approximately 240 kJ/kg. When undergoing heating, the enthalpy value of paraffin remains relatively low and experiences little change at temperatures below 34 °C. A significant increase in enthalpy occurs within the temperature range of 34 °C to 36 °C, peaking at 108 kJ/kg at 35 °C. Beyond 36 °C, the enthalpy value remains low and relatively constant. This change in enthalpy corresponds to the melting point. During the cooling process, the enthalpy of paraffin maintains a low and stable value until the temperature drops below 35 °C. There is a substantial rise in enthalpy as the temperature decreases from 35 °C to 33 °C, reaching a peak of 94 kJ/kg at 35 °C. Below 33 °C, the enthalpy value remains low and relatively unchanged. These findings demonstrate that paraffin, a paraffin wax material, possesses excellent heat storage capacity, with a phase change temperature close to that of the body. Consequently, it is an ideal heat storage material for thermoregulation purposes.

However, the transition of paraffin from a solid to a liquid state poses a significant concern when the temperature increases. This phase change causes the underlying layer of the S-thermo-e-skin to soften, impacting the structural integrity of the e-skin. Additionally, the solidification rate of the paraffin wax is not consistent due to uneven heat dissipation during the cooling process from a liquid to a solid state. As a result, this disparity affects the structure of the surface paraffin wax and consequently influences the performance and reusability of the S-thermo-e-skin.

Therefore, it is crucial to incorporate a porous framework capable of containing and supporting the PCM. In this study, porous foams were prepared using an inverted mold method.[121-124] The foams obtained through this method have an open-cell structure, which facilitates the infiltration of PCM and improves the thermal conductivity of the phase change modules. To create these foams, two specific materials were required: a water-soluble material to establish the pore structure and a non-water-soluble material for structural support. White sugar is the ideal porous material because of its high solubility in water and insolubility in lipids. The white sugar was mixed with a small amount of water in a beaker to form the porous foam. The resulting mixture was then poured into a mold and compacted. The molds were placed in an oven set at 80 °C for 1 hour to remove moisture and dry the foams (**Figure 3.6**).

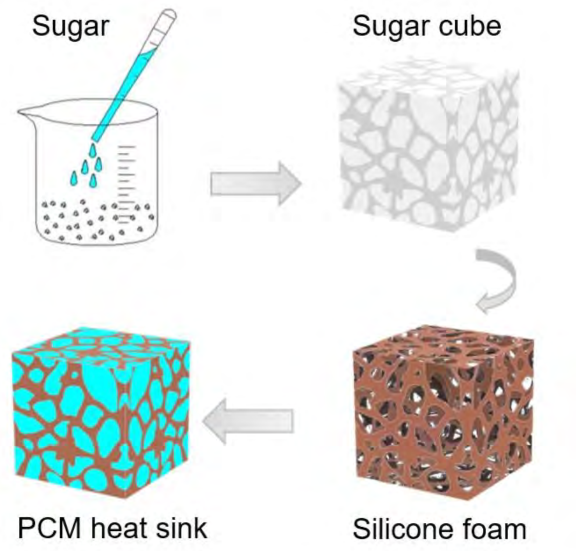

Figure 3.6 The fabrication process of the PCM heat sink.

A high thermal conductivity silicone material is utilized as the framework material to enhance the heat conduction of the S-thermo-e-skin and achieve uniform heat absorption by the PCM within the porous foam. This silicone material, obtained from Huiwei Thermal Management Co., Ltd., exhibits a remarkable thermal conductivity value of 2 W/mK. To ensure proper mixing, the silicone was blended in a 1:1 ratio and stirred thoroughly to prevent incomplete curing. Subsequently, the stirred silicone was applied onto the surface of the pre-made sugar cube using brushes, promoting capillary action for its penetration throughout the sugar cubes. The adequately coated sugar cube was then dried in an oven at 80 °C for one hour. Finally, the dried silicone-sugar cube was immersed in a beaker containing an appropriate quantity of water, resulting in the dissolution of the sugar and the formation of the desired silicone-based porous foam (**Figure 3.7**).

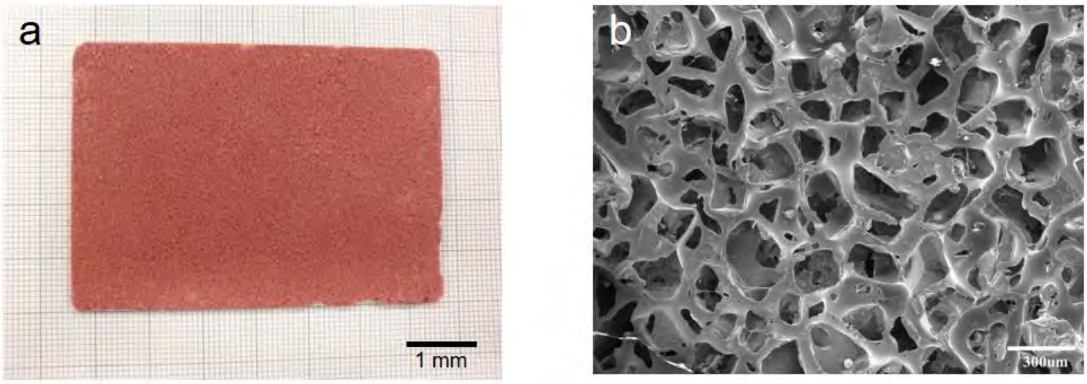

Figure 3.7 Structure of silicone foam. a) Physical photo of silicone foam. b) SEM image of silicone foam.

Finally, paraffin was melted at high temperature and filled by penetrating the silicone foam through the dropper, and after cooling, a PCM heat sink with silicone foam as the frame and paraffin wax as the filler was obtained. The silicone foam is made by the inverted mold method with a porosity of about 65%. The microstructure of the organosilicon foam was also characterized by electron microscopy. The thermally conductive adhesive foam had an open pore structure with a pore size of about 200 μm, which matches the particle size of the sugar.

3.3.3 Encapsulation of S-thermo-e-skin

Following the fabrication process, the flexible TE device and PCM heat sink underwent encapsulation (**Figure 3.8**). The flexible TE device was filled with low thermal conductivity aerogels/PDMS composites, which prevented the undesired heat transmission from the hot side to the cold side during TE device operation. To facilitate faster heat transfer, the flexible TE device and PCM heat sink were then enclosed using a high thermal conductivity potting adhesive. Once these stages were completed, the thermoregulation e-skin was successfully manufactured. The resulting S-thermo-e-skin typically measured approximately 67×48×4 mm in effective size.

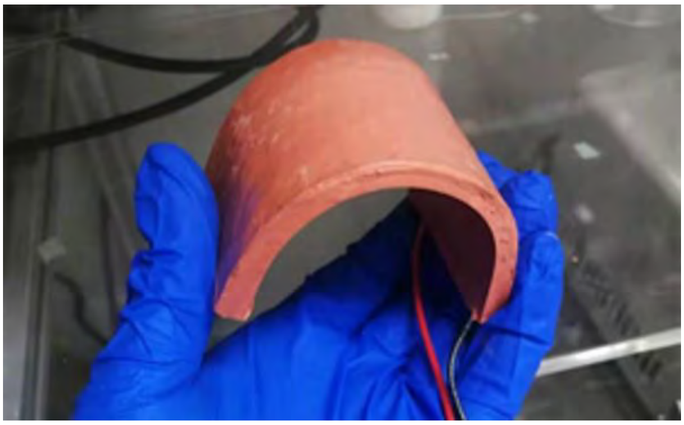

Figure 3.8 Physical photo of S-thermo-e-skin.

3.3.4 The establishment of an environment simulator

The encapsulated S-thermo-e-skin is attached to the prosthesis. It is crucial to evaluate prosthetics under realistic environmental conditions in order to investigate the practical application of the S-thermo-e-skin as human environments exhibit significant diversity.

A home-built wind channel was used to imitate the genuine environment,

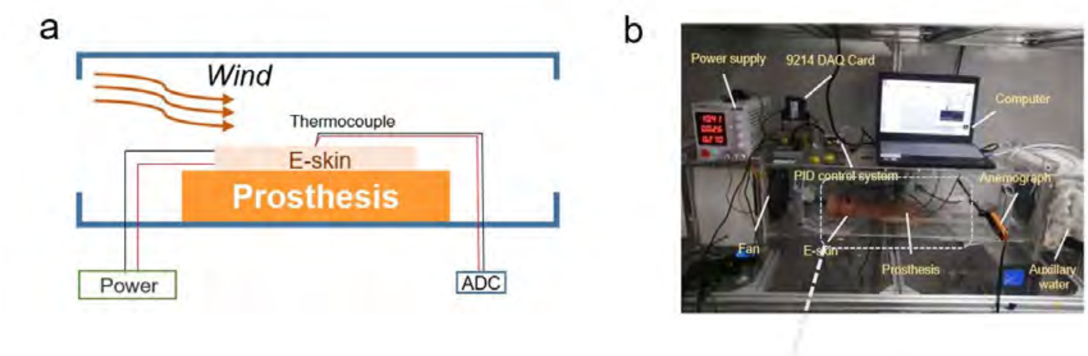

Figure 3.9 The establishment of environment simulator. a) Test schematic of wind channel. b) Photos of simulation test platform.

Figure 3.9 a and **b** are the schematic and photo of the simulation test platform respectively. The air temperature as well as the speed can be precisely controlled using the ancillary water-cooling equipment and the fan mounted at the end of the channel. Consequently, the environmental parameters can be achieved as required. The prosthesis was coupled to a S-thermo-e-skin before being put in the wind channel. Several thermocouples were inserted into the channel to monitor the temperatures of the wind, the e-skin's surface, and the silicone prosthesis. By altering the input electric power density (Power input of the power supply divided by the effective area of the S-thermo-e-skin), the S-thermo-e-skin can regulate the temperature of the e-skin's surface. The thermoregulation capacity of the e-skin was investigated by varying the input power density of the TE device under various environmental conditions.

3.4 Flexibility of S-thermo-e-skin

The traditional flexible TE device and the design of flexible TE device are analyzed by the finite element method. The structure of the two flexible TE devices is shown in **Figure 3.10**, and the deformation and stress distribution of the two devices are analyzed.

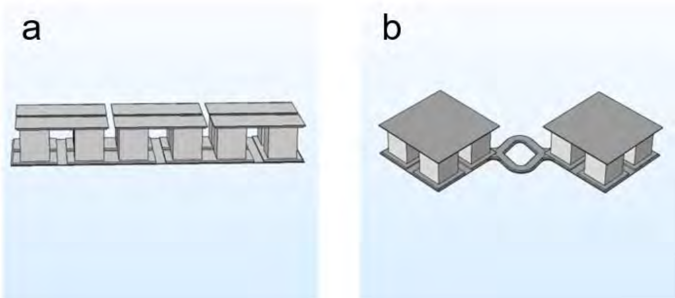

Figure 3.10 Two different configurations of flexible TE devices.. a) Traditional flexible configuration; b) Island-bridge configuration.

Figure 3.11 shows the results of a simulation of the mechanical characteristics of the flexible TE device in traditional and island-bridge configurations. The equivalent stress peak of the traditional and island-bridge configurations was 210 MPa and 152 MPa, respectively, when a negative z-axis displacement of 0.5 mm was applied to the right side of the device. The stress peak of the island-bridge configuration was 85 MPa after eliminating the local stress concentration locations, which was around 60% lower than the traditional configuration. The traditional flexible device bent in the x-z plane when a negative z-axis force of 0.02 N is applied to the right side of the device, with a maximum displacement of around 74 μm. The maximum displacement of the island-bridge configuration under the same force was 0.89 mm, which was an order of magnitude greater than the traditional configuration, suggesting that the island-bridge arrangement's overall flexibility was substantially superior to the traditional configuration.

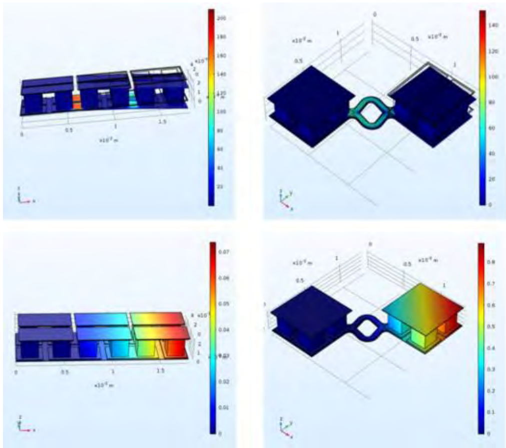

Figure 3.11 Mechanical simulation results of flexible TE devices.

The mechanical flexibility and durability of the thermoregulation e-skin were also put to the test, as these were the most important requirements for real-world applications. For cyclic bending and resistance testing, the e-skin was fastened on a stretcher. The results reveal that the e-skin was highly reliable, with resistance barely changing after 200 bending cycles (**Figure 3.12**).

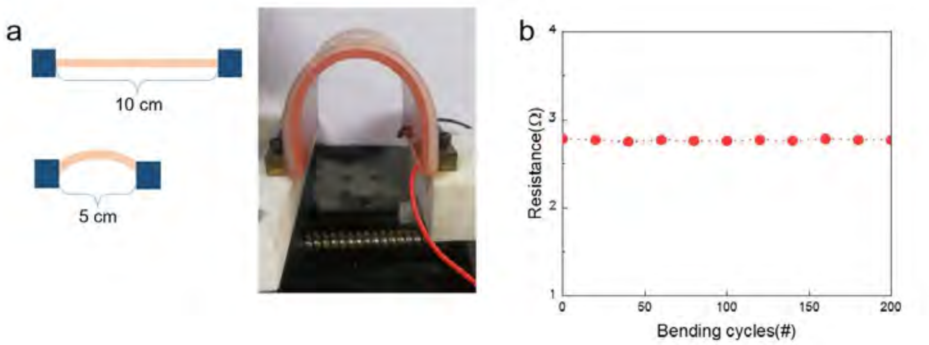

Figure 3.12 Mechanical properties testing of S-thermo-e-skin. a) Bending test; b) Resistance changes after cyclic bending.

3.5 Thermoregulation performance of S-thermo-e-skin

3.5.1 Cold adaptation of the S-thermo-e-skin

Figure 3.13 shows the performance of the S-thermo-e-skin for cold adaptation in a cold environment. Under the ambient temperature of 20 °C and the wind speed of 0.5 m/s, the input power density of S-Thermoe-Skin directly affects the surface temperature (**Figure 3.13 a**). It is evident from the graph that with an input power density of 7.8 mW/cm^2, the S-thermo-e-skin 's surface temperature initially rose rapidly and then gradually increased over time to reach 24.8 °C after 600 s. The S-thermo-e-skin 's cold adaptation ability steadily strengthened with higher input power density, causing a gradual rise in surface temperature to reach 33.2 °C at a power density of 31.2 mW/cm^2. The augmentation of input power enhanced the S-thermo-e-skin's heat generation, thereby elevating its surface temperature. **Figures 3.13 b** and **c** depict the measurement of S-thermo-e-skin's surface temperature under different wind speeds and ambient temperatures, respectively. When the wind speed was low (0.25 m/s), the final surface temperature of the S-thermo-e-skin was 28.7 °C compared to a temperature of 25.3 °C at a high wind speed of 1 m/s. Elevated wind speed intensified the convective heat exchange between the S-thermo-e-skin's surface and the surroundings when subjected to the same input power density, resulting in a decline in temperature rise on the S-thermo-e-skin's surface. Modifying the air temperature in the wind channel impacted the cold adaptation of the S-thermo-e-skin. By maintaining a constant input power density and wind speed, the S-thermo-e-skin's surface temperature fluctuated by 8.2 °C between wind temperatures of 10 °C and 25 °C. Lower temperatures facilitated better heat convection between the S-thermo-e-skin's surface and the surroundings, augmenting heat dissipation from the S-thermo-e-skin's surface and impairing its cold adaptation capabilities.

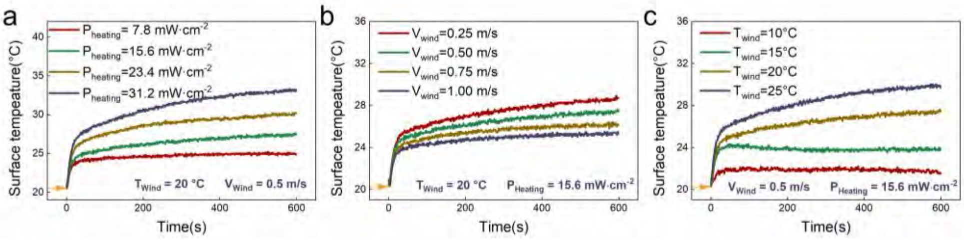

Figure 3.13 Cold adaptation of S-thermo-e-skin. a) The surface temperature of the S-thermo-e-skin under different input power densities. b) The surface temperature of the S-thermo-e-skin under different wind speeds. c) The surface temperature of the S-thermo-e-skin under different wind temperatures.

The power density requirements of S-thermo-e-skin, concerning the change in surface temperature per degree Celsius (energy cost) across various environmental conditions, are examined in **Figure 3.14**. The cold adaptation efficiency per unit of power diminishes when the input power density was increased. For an input power density of 31.2 mW/cm^2, the power necessary to elevate the surface temperature by 1 °C amounts to approximately 2.5 mW/(cm^2·°C). However, at an input power density of 7.8 mW/cm^2, the power required was only about 60% of the aforementioned scenario. Additionally, the energy cost gradually escalated due to enhanced heat transfer as wind speed amplifies or ambient temperature decreases. The e-skin's ability to raise the surface temperature by 1 °C was 1.5 times greater than at a wind speed of 0.25 m/s at a wind speed of 1 m/s. Similarly, the energy cost of the e-skin was 8.5 mW/(cm^2·°C) at a wind temperature of 10 °C, which was five times higher than at a wind temperature of 25 °C. Consequently, greater energy was demanded to sustain the surface temperature at a steady level when desiring a higher e-skin temperature.

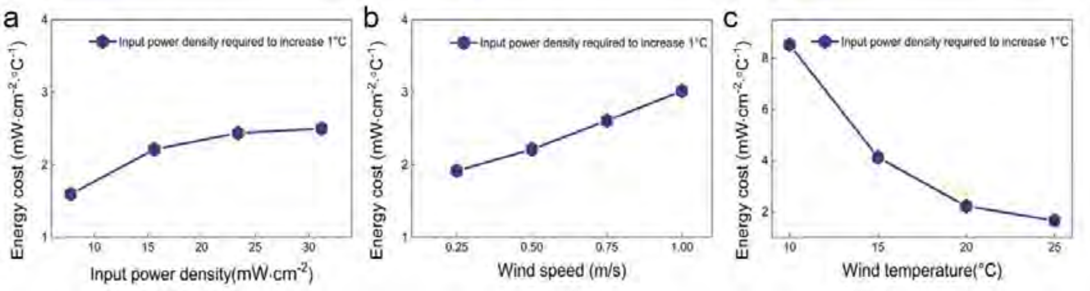

Figure 3.14 Energy cost of S-thermo-e-skin for cold adaptation. a) Energy cost under different input power densities. b) Energy cost under different wind speeds. c) Energy cost under different wind temperature conditions.

In general, S-thermo-e-skin adapted well to cold temperatures and was affected by both internal and external heat transfer. In mild environments, similar to the human body, the S-thermo-e-skin efficiently attained surface temperature cold adaptation with minimal energy cost. However, the effectiveness of cold adaptation diminished, and energy cost increased when heat generation was restricted and heat exchange became intensified. This situation can be modified by manipulating the input power density of the S-thermo-e-skin.

3.5.2 Thermal adaptation of the S-thermo-e-skin

Figure 3.15 shows the performance of the S-thermo-e-skin for thermal adaptation in a hot environment. The effect of input power density on the surface temperature of S-thermo-e-skin at an ambient temperature of 35 °C and wind speed of 0.5 m/s was depicted in **Figure 3.15 a**. The surface temperature of the S-thermo-e-skin decreased over time with an input power density of 7.8 mW/cm^2, reaching a final temperature of

32 °C. The surface temperature of the S-thermo-e-skin gradually decreased as the input power density increased. At an input power density of 31.2 mW/cm^2, the surface temperature reached 29 °C. However, over time, the heat generation surpassed the capacity of the PCM to store heat, leading to a progressive increase in surface temperature. **Figure 3.15 b** and **c** illustrate the surface temperature of the S-thermo-e-skin at different ambient temperatures and wind speeds, respectively. When the ambient temperature was 35 °C and the wind speed is 0.25 m/s, an input power density of 15.6 mW/cm^2 can rapidly decrease the S-thermo-e-skin's surface temperature from 35 °C to 30 °C and maintained it within this range consistently. Similarly, the S-thermo-e-skin can decrease from an initial temperature of 35 °C to 30 °C and effectively maintain this temperature when exposed to a wind temperature of 30 °C at the same wind speed and power density. The thermal adaptation function of the S-thermo-e-skin, similar to cold adaptation, was influenced by heat transfer. High ambient temperatures and fast wind speeds enhanced heat transfer between the S-thermo-e-skin and the environment, thereby limiting the thermal adaptation effect of the S-thermo-e-skin.

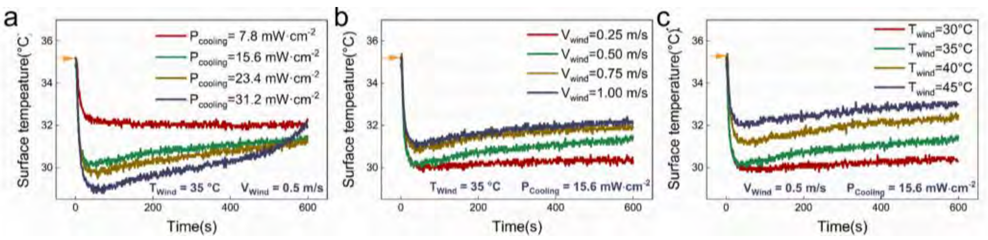

Figure 3.15 Thermal adaptation of S-thermo-e-skin. a) The surface temperature of the S-thermo-e-skin under different input power densities. b) The surface temperature of the S-thermo-e-skin under different wind speeds. c) The surface temperature of the S-thermo-e-skin under different wind temperatures.

The energy cost trend aligns with that of cold adaptation at low temperatures, as depicted in **Figure 3.16**. Increasing input power density leads to a decrease in energy efficiency, as demonstrated in **Figure 3.16 a**. For an input power density of 7.8 mW/cm^2, the energy cost amounted to 2.6 mW/(cm^2·°C). However, when the input power density reached 31.2 mW/cm^2, the energy cost became 2.7 times higher than the previous condition. Changes in wind speed also impacted the energy cost of e-skin's thermal adaptation, as shown in **Figure 3.19 b**. The energy cost for e-skin's thermal adaptation was 3.3 mW/(cm^2·°C) at a wind speed of 0.25 m/s. Conversely, when the wind speed increased to 1 m/s, the energy cost rose to 5.2 mW/(cm^2·°C). Rising ambient temperatures hindered the thermal regulation of e-skin, as depicted in **Figure 3.16 c**. Under the same conditions, higher temperatures required more energy for thermal regulation. The energy cost for thermal regulation was 7.3 mW/(cm^2·°C) at a wind temperature of 45 °C, which was twice the energy cost at a wind temperature of 30 °C. The energy cost was determined by the extent of heat transmission between the e-skin's surface and the environment, with greater heat transfer necessitating higher energy cost.

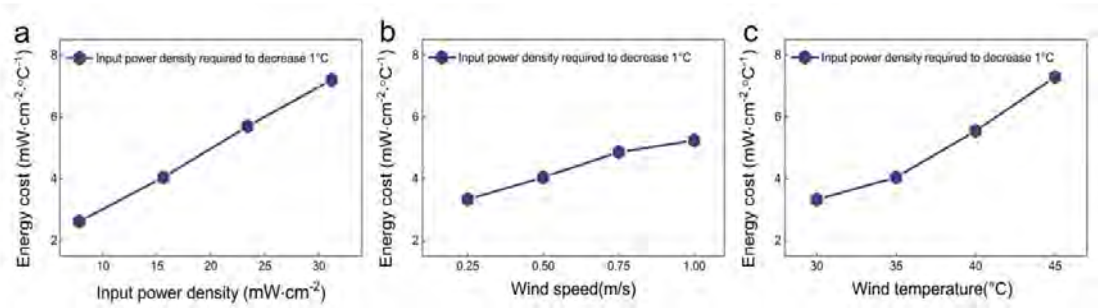

Figure 3.16 Energy cost of S-thermo-e-skin for thermal adaptation. a) Energy cost under different input power densities. b) Energy cost under different wind speeds. c) Energy cost under different wind temperature conditions.

The efficacy of S-thermo-e-skin cooling was influenced by heat transfer mechanisms. Elevated wind speeds and higher temperatures intensified the transmission of heat between the e-skin and its environment, thereby diminishing the cooling impact of the e-skin. The quantity of heat transferred between the S-thermo-e-skin surface and the surroundings governed the associated energy cost, which escalated with higher rates of heat transfer. In summary, the S-thermo-e-skin exhibits commendable thermal adaptability across diverse conditions by effectively reducing surface temperatures in high-temperature environments.

3.5.3 Isothermal regulation of S-thermo-e-skin

The S-thermo-e-skin has been shown to provide thermoregulation in various cold and hot environments but at the cost of energy consumption. To achieve feedback thermoregulation, we implemented a PID control system to automate the control of the e-skin surface temperature. The desirable skin temperature for humans typically falls between 31.5 to 35.5 °C, although this can vary depending on the season and surroundings.[125, 126] For this study, we selected a target temperature of 35 °C for the S-thermo-e-skin. However, humans and organisms in general have limited energy resources and tend to seek an optimal environment based on their preferred temperature. This behavior aims to minimize the temperature gradient between the individual and the environment, reducing the energy required to maintain body temperature. Similarly, its energy storage capacity for thermoregulation support is limited when the S-thermo-e-skin is applied to a prosthetic limb or robot.

In this study, we define the isothermal regulation capacity of the e-skin as the maximum effective time it can maintain a surface temperature of 35 °C with a limited power supply. This capacity is influenced by the energy cost and the effective time of the e-skin. At low temperatures, the effective time can be indefinite. However, the e-skin requires more energy to regulate temperature as the temperature decreases, resulting in a shorter period of thermoregulation when energy is limited. Consequently, the temperature adaptability of the S-thermo-e-skin gradually declines as the temperature drops below the target temperature. On the other hand, in high-temperature environments, the S-thermo-e-skin's temperature adaptability is restricted by the heat storage capacity of the PCM, leading to a reduction in the effective period of thermoregulation as the ambient temperature rises. Hence, the S-thermo-e-skin exhibits weaker temperature adaptability at higher ambient temperatures.

Figure 3.17 shows the S-thermo-e-skin's capability to adapt to different temperature conditions, ranging from 10 to 45 °C. Initially, the e-skin temperature was set at 20 °C, accompanied by a wind speed of 0.5 m/s. After five minutes, the PID control system and auxiliary water were activated simultaneously to modify the air temperature. The PID control system was deactivated once the e-skin surface temperature exceeded the desired setpoint. Specifically, **Figure 3.17 a-c** visually represent the isothermal regulation process of the S-thermo-e-skin in response to wind temperatures of 10, 25, and 40 °C, respectively.

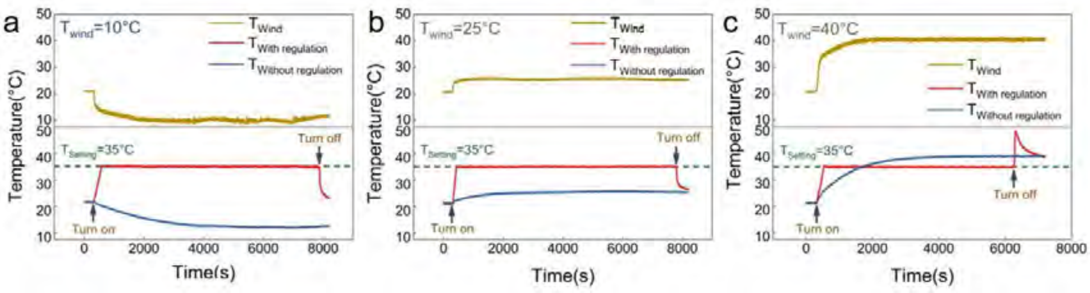

Figure 3.17 Isothermal regulation of the S-thermo-e-skin. a) Isothermal regulation of e-skin at 10 °C wind temperature. b) Isothermal regulation of e-skin at 25 °C wind temperature. c) Isothermal regulation of e-skin at 40 °C wind temperature.

The S-thermo-e-skin surface temperature rapidly increased to the preferred body temperature of 35 °C when the ambient temperature was 10 °C, and it remained stable for a significant period of time. However, with changing ambient temperatures, the surface temperature of the prosthesis gradually decreased and eventually dropped below the desired range, reaching a low of 12.5 °C. Similarly, the surface temperature of the prosthesis only reached 25 °C when the wind temperature was 25 °C, while the e-skin maintained the desired temperature. In a hot environment of 40 °C, the e-skin endured both heating and cooling processes. Initially, the surface temperature of the e-skin rose quickly, but once the overall temperature reached 35 °C, surface cooling began to maintain the desired temperature. If the amount of heat generated by the hot side exceeded the capacity of the PCM to handle, the isothermal regulation would eventually fail. Conversely, the surface temperature of the prosthesis rapidly rose and exceeded 35 °C by the 28^{th} minute when the ambient temperature increased (**Figure 3.17 c**).

Figure 3.18 illustrates the isothermal regulation performance and effect time of the e-skin with regulation. The S-thermo-e-skin demonstrated isothermal regulation performance comparable to that of humans, maintaining a surface temperature of 35 °C within the experimental temperature range of 10-45 °C When powered on (**Figure 3.18 a**). However, without power, the prosthesis exhibited inadequate isothermal regulation capability, with a surface temperature response similar to that of the surrounding environment. Additionally, inset images in Figure 3.18 a) show two infrared photographs of the S-thermo-e-skin in the powered-on mode at temperatures of 20 °C and 40 °C. This ability of isothermal regulation gives the S-thermo-e-skin human-like temperature properties and provides emotional support to the user when interacting with the outside world.

Figure 3.18 b presents the effective time of isothermal regulation of the S-thermo-e-skin at varying temperatures. The S-thermo-e-skin functions solely for heating purposes when the ambient temperature is equal to or lower than the target temperature and excess heat can be dissipated without affecting the thermoregulation of the e-skin. Throughout the 2-hour experimental duration, the e-skin consistently maintained an isothermal surface temperature of 35 °C, even in low temperatures. However, the heat generated by the S-thermo-e-skin's cooling mechanism hinders its ability to adapt to temperature fluctuations when the ambient temperature exceeds the desired level. Nonetheless, the S-thermo-e-skin effectively remained under control for 1.5 hours at a wind temperature of 40 °C, demonstrating its commendable adaptability in maintaining surface temperature.

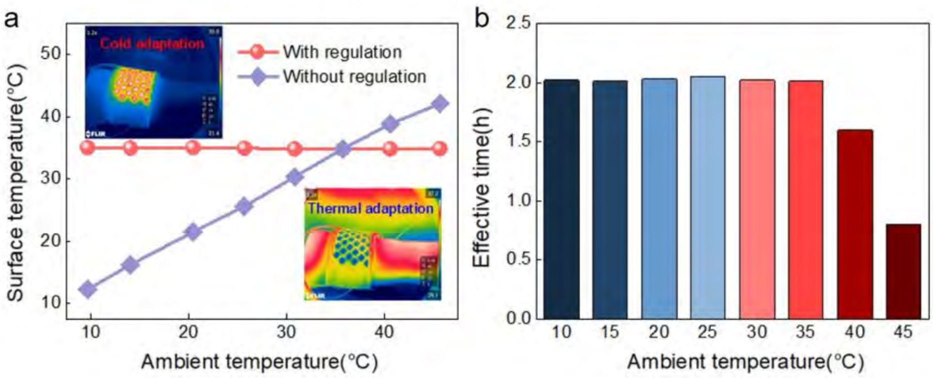

Figure 3.18 Isothermal regulation performance of S-thermo-e-skin and its effective time. a) Effects of isothermal regulation on S-thermo-e-skin. b) The effective time of isothermal regulation under different ambient temperatures.

Figure 3.19 shows the energy cost of the S-thermo-e-skin to maintain a surface temperature of 35 °C in the presence of varying wind temperatures. The average power density of the e-skin over a ten-minute period was used to calculate power cost once the surface temperature reached 35 °C and stabilized. At an ambient temperature of 10°C, the e-skin consumed 71.32 mW/cm^2 of energy. The energy cost progressively decreased as the ambient temperature increased, reaching a minimum of 14.22 mW/cm^2 at 35 °C. However, as the external temperature continued to rise, the e-skin began to cool, resulting in a gradual increase in energy cost to 36.91 mW/cm^2 at 45°C. This pattern resembles the energy expenditure required by humans to regulate their body temperatures in different environments.[45] Homeotherms have a thermoneutral zone, a range of ambient temperatures where the oxygen consumption is least affected. Keeping a steady temperature becomes more costly as the ambient temperature deviates further from this thermoneutral zone. For the S-thermo-e-skin, this thermoneutral zone is approximately 35 °C.

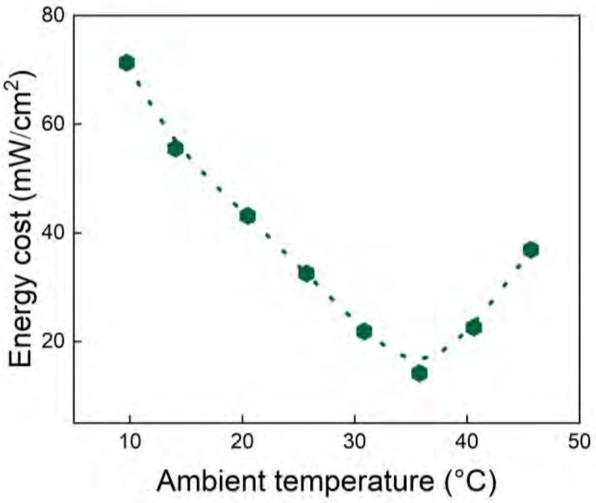

Figure 3.19 The energy cost of S-thermo-e-skin under different temperatures.

The isothermal regulation of e-skin in a windless environment with temperature of 20°C and 45°C is shown in **Figure 3.20**. Isothermal regulation capability was increased since the e-skin's heat exchange with the environment is weaker in a windless environment than it is in a windy one. It took less energy to sustain 35 °C in a room temperature environment (33.31 mW/cm^2), but it took more time (70 minutes) to do it in a high-temperature environment.

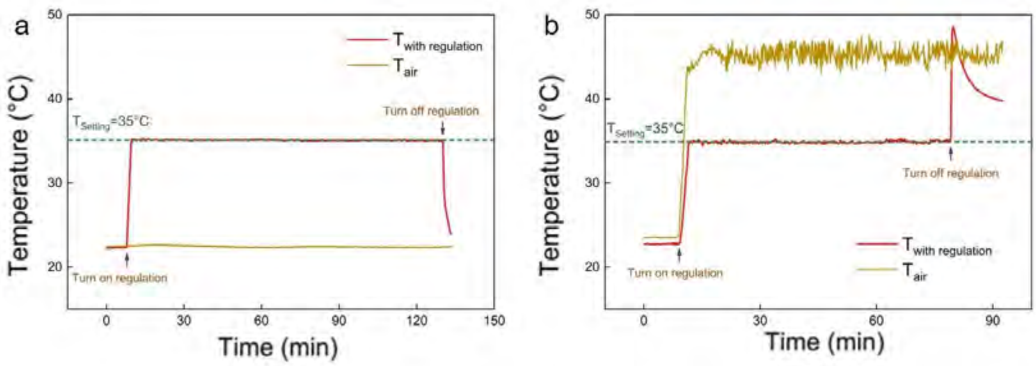

Figure 3.20 The isothermal regulation performance of e-skin in a windless environment. a) Isothermal regulation of e-skin at 20 °C. b) Isothermal regulation of e-skin at 45°C.

In order to assess the effectiveness of the S-thermo-e-skin in regulating temperature, a simulation was conducted to replicate the rapid temperature changes experienced by individuals moving between indoor and outdoor environments on a hot summer day. The experimental setup is depicted in **Figure 3.21**. Initially, the e-skin was kept at room temperature (22 °C) for one hour. Subsequently, a hot air flow was used to elevate the ambient temperature to the outdoor level (42 °C). Using the PID feedback circuit, the e-skin swiftly transitioned from regulating a cool environment to regulating a hot environment in under one minute. The surface temperature of the e-skin remained stable at 35 °C throughout the process. After spending one hour in the outdoor temperature (42 °C), a cold air flow was employed to return to the indoor temperature (22 °C). Remarkably, the S-thermo-e-skin demonstrated exceptional performance in the reverse scenario as well, adapting to the new temperature in less than a minute. These findings suggest that the S-thermo-e-skin, which incorporates a hybrid flexible TE device and a PCM heat sink, has promising potential for replicating the isothermal regulation capability of human skin.

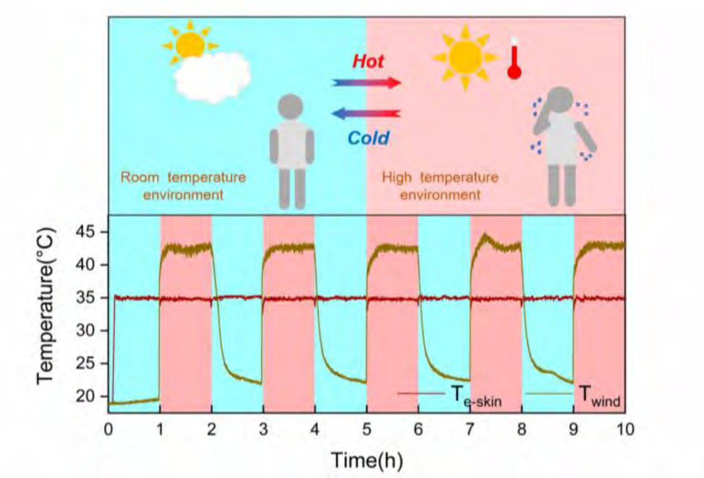

Figure 3.21 The S-thermo-e-skin maintained agile isothermal regulation in a test of cycling low- and high-temperature environments.

3.6 Heat dissipation challenges

As mentioned in the previous section, insufficient heat dissipation in high-temper environments can lead to temperature regulation failure of the thermoelectric device, thereby significantly reduce the effective time for isothermal regulation.

Heat dissipation involves the transport of heat, which can only be dissipated to the environment or stored in a timely manner by means of thermal management. Highly thermally conductive materials such as carbon are often used as heat sinks for passive cooling of e-skin.[127, 128] However, under prolonged natural cooling conditions, an accumulation of insufficiently dissipated heat can occur, leading to cooling failure. In addition, due to the superior heat transfer properties of water, it is widely used in the cooling of electronic systems. Flow water cooling can transfer heat from the hot side to other places by means of water circulation and has been used in some large electronic systems.[129, 130] However, the complex structure is what limits its miniaturization for e-skin applications. The microfluidic approach is a potential means of applying water cooling to e-skin. Another way to address the lack of heat dissipation is to perform thermal storage.[91, 131] Paraffin is a flexible thermal storage material and has demonstrated excellent temperature regulation properties in this chapter. In general, increasing the amount of phase change material can enhance heat dissipation. However, too thick a phase change material heat sink can reduce the flexibility of the e-skin.

In conclusion, there is a need to strike a balance between heat dissipation and the flexibility of the electronic skin. In recent years, the use of hydrogels for device cooling has gradually attracted attention.[132-134] The natural flexibility of hydrogels coupled with the high latent heat of the water evaporation process makes them ideal for application in thermal management of e-skins, however, how to harmonize the structure and properties of e-skins and hydrogels is the key to make them widely applicable.

3.7 Summary

This chapter introduces the concept of S-thermo-e-skin, which is designed to mimic bionic thermoregulation. The main focus of this study is to design a flexible TE device and investigate the mechanical and thermoregulatory properties of the assembled e-skin. The results demonstrate that the S-thermo-e-skin exhibits remarkable flexibility and can easily conform to curved surfaces. Additionally, the incorporation of a paraffin-based PCM heat sink enhances the heat absorption capability of the BiTe-based TE device, thereby extending the operational time for thermoregulation. By harnessing the Peltier effect, the S-thermo-e-skin is able to generate heat in low-temperature environments and provide cooling in high-temperature environments. These unique features enable the S-thermo-e-skin to maintain a constant temperature within the range of 10-45°C, effectively replicating the isothermal regulation properties of human skin.

The energy utilization of the e-skin device exhibited similarities to the energy usage of the human body in specific scenarios. The energy consumption reached a minimum level within the thermoneutral zone (measuring 14.22 mW/cm^2 at an ambient temperature of 35 °C) and increased when the environmental temperature deviated from this range (reaching 71.32 mW/cm^2 at an ambient temperature of 10 °C). When the target temperature exceeded the surrounding temperature, the e-skin successfully maintained its surface temperature at the desired level for a duration of two hours. However, the heat capacity of the PCM limited the duration of this effect when the ambient temperature was higher than the target temperature. Nevertheless, even in a temperature of 40 °C, the e-skin was able to sustain a surface temperature of 35 °C for approximately 1.5 hours, and for a duration of 0.75 hours even when the temperature reached 45 °C. Furthermore, when subjected to a simulation of swift transitions between indoor and outdoor temperatures (22 °C and 42 °C, respectively) on a hot summer day, the S-thermo-e-skin device exhibited prompt response. The e-skin's remarkable thermoregulation capability provides a promising option for the next generation of intelligent prosthetic temperature simulation, which plays a crucial role in improving amputees' quality of life and advancing research on bionics in robotics.

CHAPTER 4 DUAL-MODE THERMOREGULATING E-SKIN

4.1 Introduction

In Chapter 3, a successful implementation of surface thermoregulation was achieved using the S-thermo-e-skin. However, the current thermoregulation capability of the S-thermo-e-skin is limited in high-temperature environments due to the heat storage capacity of flexible paraffin heat sink. To broaden the potential applications of thermoregulating e-skin, it is crucial to enhance and optimize the thermoregulatory functionality of the e-skin through further refinement.

Evaporation of sweat is an effective form of cooling in the human body.[43, 135-137] Inspired by the human perspiration mechanism, the liquid-to-vapor phase transition of water serves as an appealing option for thermal management in e-skin due to its high latent heat.[138-140] Consequently, hygroscopic hydrogels have garnered considerable attention owing to their exceptional water-recycling properties.[141-146] These hydrogels exploit the alteration in saturated vapor pressure within their network of salt solution to facilitate water exchange with the environment. In high-temperature conditions, water is released, while in low-temperature conditions, water is absorbed. This water loss process significantly lowers the object's temperature. However, despite their demonstrated efficacy in cooling, hygroscopic hydrogels are passive in nature, rendering them ineffective for situations requiring active thermoregulation.

The thermoregulation mechanism of the human body is dependent on the integration of heat production and dissipation processes. Inspired by this mechanism, e-skin can achieve similar temperature modulation effects by incorporating bionic structures. A flexible TE device has the potential to generate heat in low-temperature environments and cool in high-temperature environments, resembling the heat production mechanism of the human body and allowing for thermoregulation in various conditions. On the other hand, a hygroscopic hydrogel can consistently evaporate moisture over an extended period, simulating the cooling function of human sweat glands in high-temperature settings. Therefore, a dual-mode thermoregulating e-skin (D-thermo-e-skin) can effectively and optimally regulate temperature over a long-term period by combining a flexible TE device with an active regulating functionality and a hygroscopic hydrogel with a passive regulating functionality.

4.2 Concept design

Figure 4.1 a shows the D-thermo-e-skin, comprised of both an active thermoelectric regulation layer and a passive ionic-hydrogel regulation layer. The D-thermo-e-skin encompasses a breathable encapsulation layer featuring the sweathole structure, a flexible TE device, a silicone/CNT foam, and a lithium- and bromine-enriched polyacrylamide (Li-PAAm) hydrogel endowed with hygroscopic characteristics. Among these, the active regulation layer, consisting of the flexible TE device, operating on the principles of the Peltier effect to establish cold and hot regions at opposite sides of the device, faithfully replicates the heat generation structure within the human body while effectively governing the surface temperature. Conversely, positioned beneath the active regulation layer, the passive regulation layer consisting of silicone/CNT foam and Li-PAAm hydrogel mimics the architecture of human sweat glands, evaporating water in high-temperature environments and regenerating water in low-temperature surroundings, thus emulating of perspiration behavior to cool the active regulation layer. Among them, the addition of CNT can improve the hydrophobicity of silicone foam and reduce the thermal resistance between hydrogel and silicone foam.

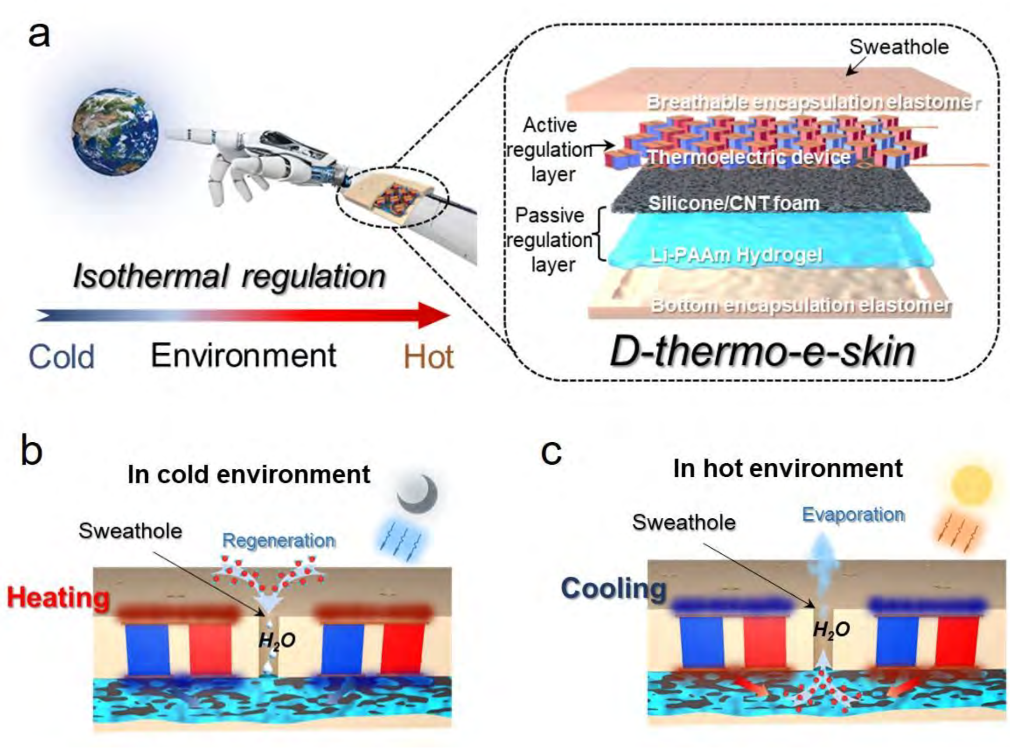

Figure 4.1 The design concept and application mechanism of D-thermo-e-skin. a) Basic structure of D-thermo-e-skin. b) The mechanism of D-thermo-e-skin in cold environments. c) The mechanism of D-thermo-e-skin in hot environments.

The isothermal regulation of D-thermo-e-skin is achieved through the combined efforts of active and passive regulation layers. In low-temperature environments, the active regulation layer generates surface heat, while the hydrogel in the passive regulation layer efficiently absorbs moisture from the surroundings through the sweatholes (**Figure 4.1 b**). On the other hand, in high-temperature conditions, the active regulation layer facilitates surface cooling by transferring heat from the lower layers to the hydrogel via the silicone/CNT foam (**Figure 4.1 c**). This induces water evaporation, which is then discharged through the sweatholes. By incorporating both active and passive regulation layers, the D-thermo-e-skin achieves a balanced combination of heat generation and dissipation. This closely resembles the behavior of human skin and enables effective isothermal regulation in complex environments.

4.3 Fabrication of D-thermo-e-skin

The fabrication of the D-thermo-e-skin includes the fabrication of a flexible TE device, the fabrication of silicone/CNT foam, and the encapsulation of the D-thermo-e-skin (**Figure 4.2**).

4.3.1 Fabrication of active TE regulation layer

The flexible TE device was prepared as in previous literature. The 1.5 × 1.5 × 1.6 mm size P-type $Bi_{0.39}Sb_{1.61}Te_{3.03}$ TE leg and the same size N-type $Bi_{1.95}Te_{2.8}Se_{0.2}$ TE leg (Guangdong Fuxin Technology Co., Ltd.) were soldered together with the prefabricated flexible circuit by reflow soldering. In this case, two pairs of P-type and N-type TE legs were alternately soldered to copper electrodes to form a TE unit, which is then connected to the flexible circuit.

4.3.2 Fabrication of the Silicone/CNT foam

An inverted mold of white sugar was used to create a foam structure from the silicone, which resulted in a foam structure with high thermal conductivity and porosity up to 65 %. CNT ink dispersions were prepared by dispersing CNT (200 mg, Shenzhen Guosen Pilot Technology Co., Ltd.) and 200 mg of sodium dodecylbenzene sulfonate as a surfactant in 200 ml of deionized water. The silicone foam was soaked several times in the configured CNT ink and then removed and dried in an oven at a temperature of 80°C to obtain the CNT/silicone foam.

4.3.3 Encapsulation of D-thermo-e-skin

PDMS was filled between the TE units and cured into shape. Subsequently, the CNT/silicone foam is bonded to the flexible TE device composite by silicone. A well-mixed solution (10 % acrylamide monomer, 0.05 % N,N′-methylenebisacrylamide, 0.05 % ammonium persulfate, 0.0002 % tetramethylethylenediamine, and 90% deionized water) was poured into the Silicone/CNT foam for free radical polymerization cross-linking to obtain the PAAm hydrogel e-skin. The PAAm hydrogel e-skin was completely swollen in deionized water and then dried in air at 70 °C until the hydrogel was dehydrated. Subsequently, the dehydrated hydrogels were immersed in LiBr solution (35 wt.%) to obtain Li-PAAm hydrogel e-skin. The hydrogel was encapsulated into the e-skin with silicone, and finally, perspiration holes of 1 mm size were prepared between the TE legs for water evaporation.

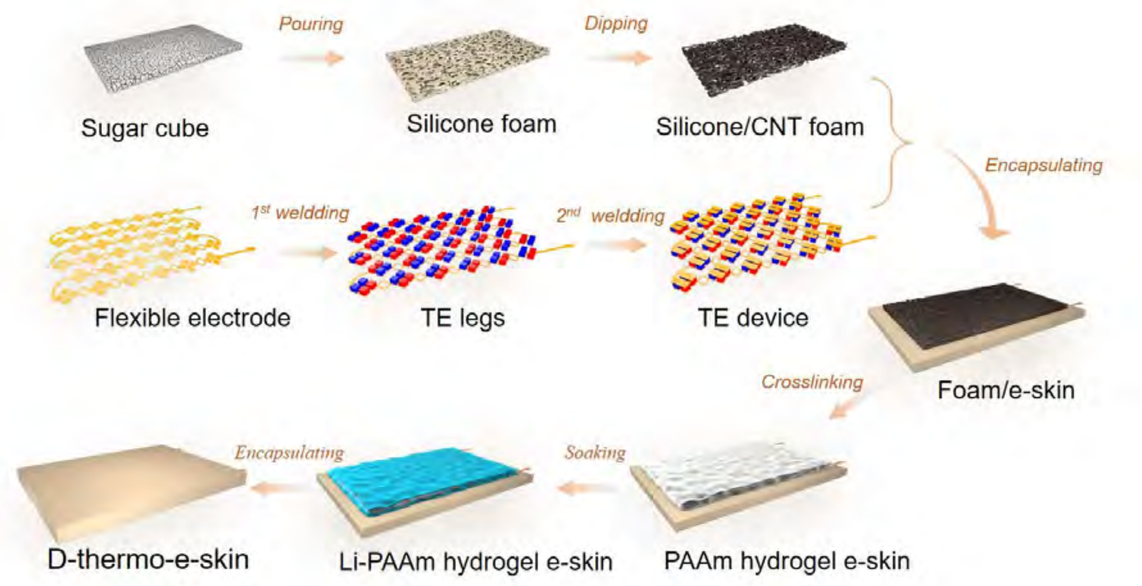

Figure 4.2 The fabrication process of D-thermo-e-skin.

4.4 D-thermo-e-skin with excellent flexibility

Figure 4.3 presents a physical photograph of the D-thermo-e-skin, measuring approximately 86 mm x 55 mm x 3.5 mm in dimensions. The figure illustrates that the sweathole structure is uniformly distributed on the surface of the D-thermo-e-skin, providing a pathway for moisture exchange between the Li-PAAm hydrogel and the external environment. The joining between the active regulation layer and the passive regulation layer is ensured by utilizing high thermal conductivity silicone. Additionally, the integration of the Li-PAAm hydrogel within the pores of the silicone/CNT foam in the passive layer promotes efficient and homogeneous heat transfer from the active layer to the hydrogel, facilitating evaporation.

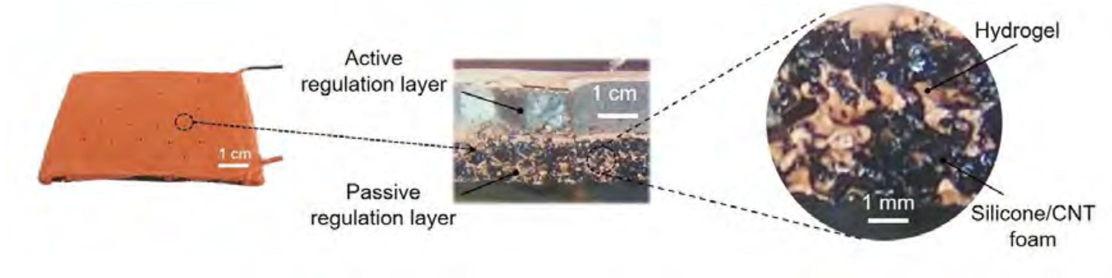

Figure 4.3 D-thermo-e-skin consisting of active and passive regulation layers.

The mechanical characteristics of the D-thermo-e-skin are vital for assessing its suitability for practical applications. Previous studies in Chapter 3 have highlighted the impressive flexibility of the TE device used in the D-thermo-e-skin. Similarly, the silicone/CNT foam and Li-PAAm hydrogel in the passive regulation layer also possess inherent flexibility. Furthermore, the e-skin demonstrated excellent mechanical stability, as evidenced by its consistent internal resistance even after undergoing 200 cycles of bending (**Figure 4.4**).

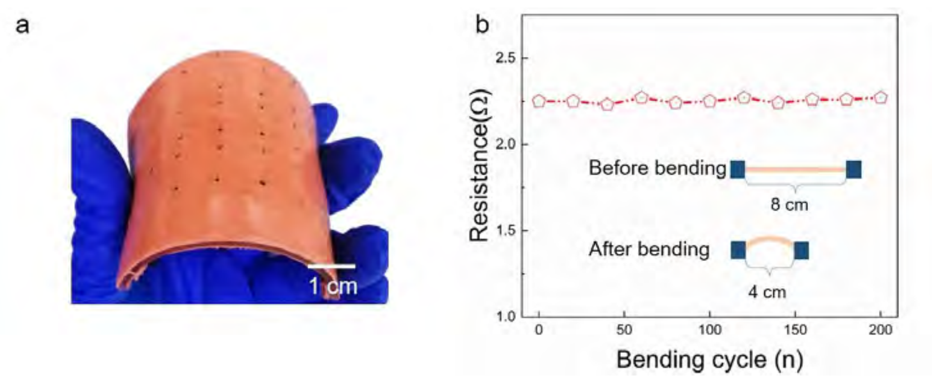

Figure 4.4 Mechanical properties of D-thermo-e-skin. a) D-thermo-e-skin has good flexibility. b) The resistance of the e-skin hardly changes after cyclic bending.

4.5 Thermoregulation Performance of D-thermo-e-skin

4.5.1 Thermoregulation of active regulation layer

The active regulation layer of the D-thermo-e-skin, as depicted in **Figure 4.5**, primarily comprises a flexible TE device. This device utilizes the Peltier effect to convert electrical energy into thermal energy, allowing for active temperature adjustments. The flexible TE device consists of 36 TE units that are connected to flexible circuits. Together, these TE units and circuits provide ample heating or cooling capacity to effectively regulate the temperature of the D-thermo-e-skin.

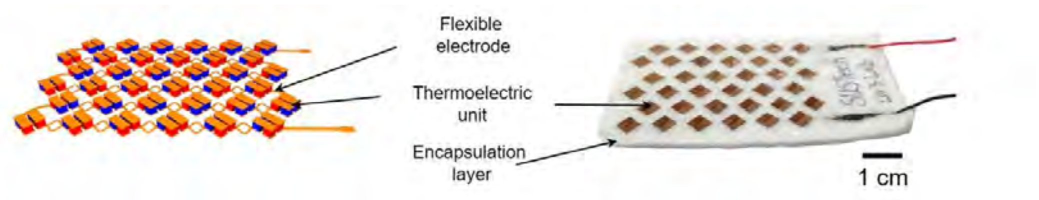

Figure 4.5 Schematic illustration of the active regulation layer.

Under heating conditions, applying an energy cost of 10 mW/cm^2 caused the surface temperature of the active regulation layer to increase from 23 °C to 26.8 °C. Increasing the energy cost further to 40 mW/cm^2 resulted in the surface temperature reaching 32 °C (**Figure 4.6 a**). Conversely, when operating in the cooling mode, applying an energy cost of 10 mW/cm^2 caused the surface temperature of the layer to decrease by 3 °C (**Figure 4.6 c**). Similarly, achieving a higher cooling capacity for the active regulation layer required a higher energy cost. For example, increasing the energy cost to 40 mW/cm^2 resulted in a surface temperature decrease of 5.7 °C. Furthermore, the inclusion of the island-bridge structure, consisting of the TE unit and flexible circuit, provides the active regulation layer with flexibility. This flexibility allows the active regulation layer to effectively conform to the curved surface of a prosthesis for heating or cooling purposes (**Figure 4.6 b** and **d**). As a result, the active regulation layer can dynamically adjust its temperature to meet specific environmental requirements, facilitating the D-thermo-e-skin in achieving isothermal regulation in different environments.

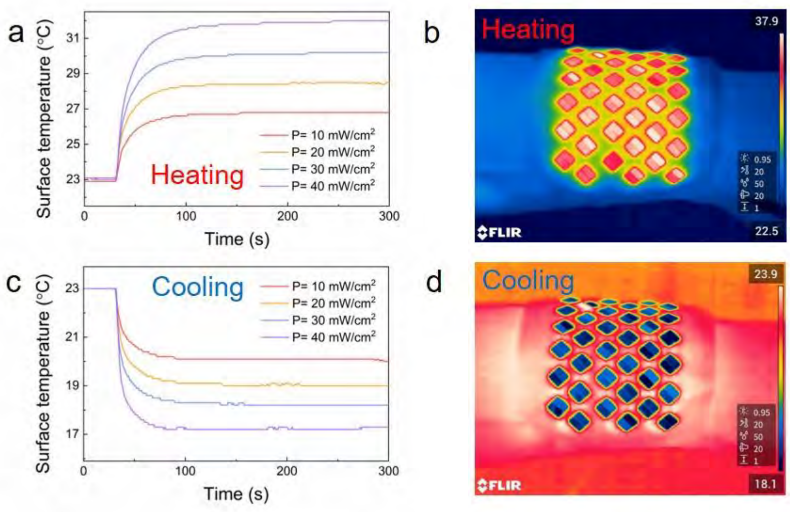

Figure 4.6 Characterization of active regulation layer. a) Heating effect of the active regulation layer. b) IR image of the active regulation layer in the heating mode. c) Cooling effect of the active regulation layer. d) IR image of the active regulation layer in the cooling mode.

4.5.2 Thermoregulation of passive regulation layer

The passive regulation layer of the D-thermo-e-skin consists of Li-PAAm hydrogel and silicone/CNT foam, mimicking the function of human sweat glands. This design enables the absorption of heat from the active regulation layer located on the topmost surface of the e-skin. As a result, water evaporation takes place at elevated temperatures, leading to passive cooling effects on the e-skin. The purpose of this mechanism is to improve the overall regulation performance of the D-thermo-e-skin, especially in high-temperature conditions (**Figure 4.7**).

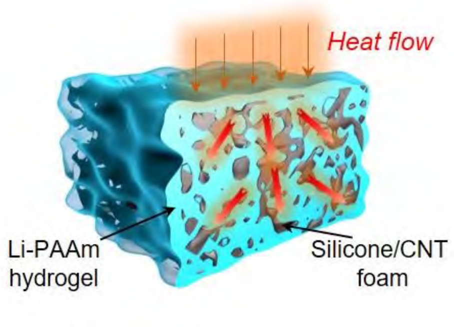

Figure 4.7 Schematic illustration of the passive regulation layer.

Water evaporation is crucial for simulating the structure of sweat glands in the passive regulation layer. Hydrogels, which are characterized by a three-dimensional network structure, have the unique ability to absorb significant amounts of water, dissolve within it, and maintain their original structure without dissolution. This makes hydrogels an ideal substrate for facilitating water evaporation. However, conventional hydrogels can only re-swell when immersed in water after losing water at high temperatures, making them unsuitable for cyclically reusing in e-skin applications. In high-temperature environments, human perspiration leads to water loss, which can be replenished by drinking water. However, D-thermo-e-skin lacks an external water source and thus relies on the unique properties of Li-PAAm hydrogel for water regeneration. Elevated temperatures disrupt the moisture equilibrium between the Li-PAAm hydrogel and the surrounding atmosphere, resulting in evaporation and contraction of the polymer network (**Figure 4.8 a**). The withdrawal of water from the Li-PAAm hydrogel at higher temperatures reduces the hydrogel's saturation vapor pressure due to an increase in the ionic concentration. In this state, the hydrogel can attract and condense water molecules on its surface at lower temperatures. Then water molecules then diffuse into the hydrogel network, facilitating water regeneration. **Figure 4.8 b** and **c** illustrate this phenomenon, showing photo images of the hydrogel before and after experiencing evaporation under heat. Remarkably, it demonstrates negligible changes in both the shape and weight of the hydrogel.

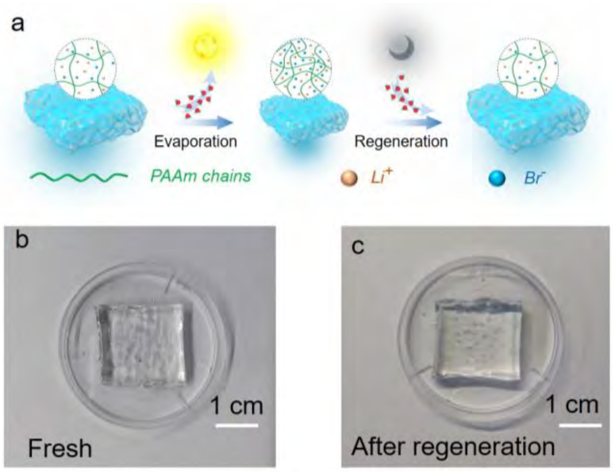

Figure 4.8 Li-PAAm hydrogel has water recycling capability. a) Water cycle processes of Li-PAAm hydrogel. b) Photograph of fresh Li-PAAm hydrogel. c) Photograph of Li-PAAm hydrogel after regeneration.

Thermogravimetric analysis was performed to evaluate the water content of the Li-PAAm hydrogel over a temperature range of 30 to 200 °C (**Figure 4.9 a**). The results showed that approximately 40 wt.% of the overall weight of the hydrogel was evaporable water. The high water content ensures an abundant supply of water available for evaporation within the D-thermo-e-skin. The stability of the Li-PAAm hydrogel is crucial for ensuring the long-term functionality and durability of the D-thermo-e-skin.

Interestingly, **Figure 4.9 b** illustrates the remarkable stability of the Li-PAAm hydrogel under ambient conditions (25 °C, 65% RH), where its weight remains constant for 8 hours. In contrast, the pure PAAm hydrogel experiences continuous water loss over time under the same test conditions.

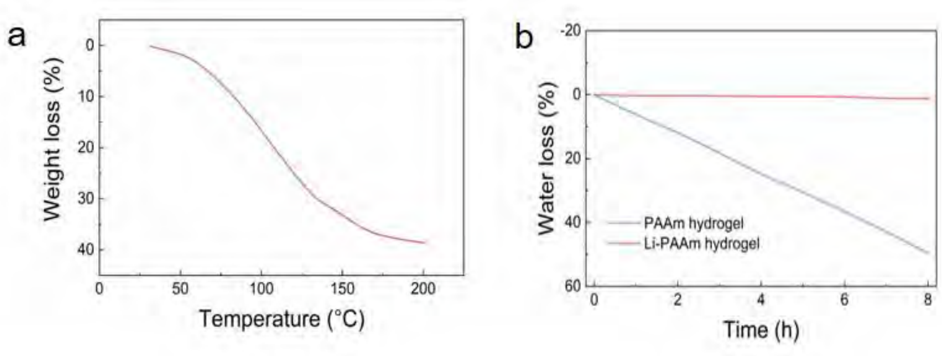

Figure 4.9 Characterization of Li-PAAm hydrogel. a) Thermogravimetric analysis of the Li-PAAm hydrogel. b) Normalized weight variation of Li-PAAm hydrogel and PAAm hydrogel in the ambient air for 8 h. The ambient temperature and relative humidity were 25 °C and 65 %, respectively.

Furthermore, the thermal conductivity of the Li-PAAm hydrogel is another important property needs to be considered. The as-fabricated Li-PAAm hydrogel has a thermal conductivity of 0.6 W/(m·K), challenging a quick response. To overcome it, a silicone/CNT porous foam frame was designed to enhance the thermal conductivity of the Li-PAAm hydrogel. As illustrated in **Figure 4.10**, the composite hydrogel exhibited a thermal conductivity of approximately 1.8 W/(m·K), which was more than three times higher than that of the pure Li-PAAm hydrogel. Additionally, the silicone material could establish effective contact with the encapsulation material of the active regulation layer, reducing the contact thermal resistance between the active and passive regulation layers.

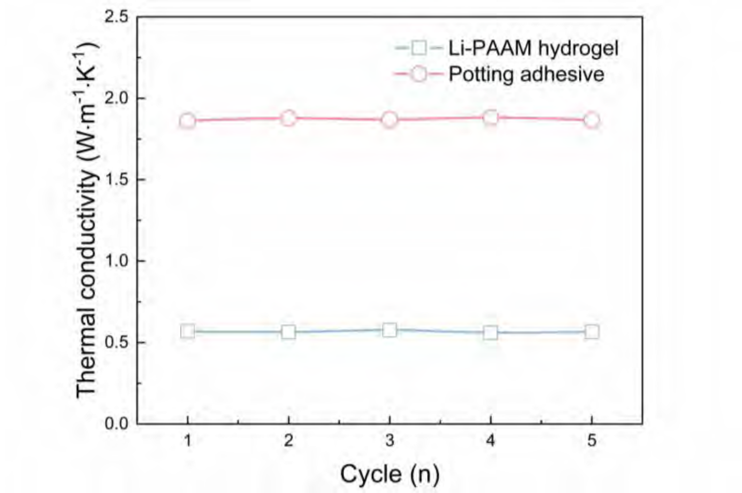

Figure 4.10 Thermal conductivity of Li-PAAm hydrogel and silicone.

It is crucial to prepare the silicone material in the form of a porous foam to accommodate the Li-PAAm hydrogel to ensure even heating. The silicone foam is designed with a pore size of approximately 500 μm and contains connective channels that allow for water exchange with the hydrogel and the surrounding environment (**Figure 4.11**). It is important to note that the hydrophilic or hydrophobic nature of the internal wall of the porous silicone influences the heat transfer between the silicone frame and the hydrogel, thus impacting the water-evaporation response. Initially, the pristine silicone displays hydrophobic behavior with a contact angle of water measurement at 110.8°, attributable to the presence of silyl groups. The large contact angle causes the hydrogel does not fill the foam smoothly, which can lead to insufficient heat dissipation from the D-thermo-e-skin. CNT, as an amphiphilic material, is ideal as a way to improve the hydrophobicity of the foam and reduce the contact thermal resistance.[123] After several immersions, the CNT were covered on the surface of the silicone foam, forming a contact surface between the hydrogel and the foam (**Figure**

4.11 b). Contact angle tests showed that water droplets could be completely absorbed by the foam, confirming the efficacy of the foam as a hydrogel cross-linking scaffold and water transport channel.

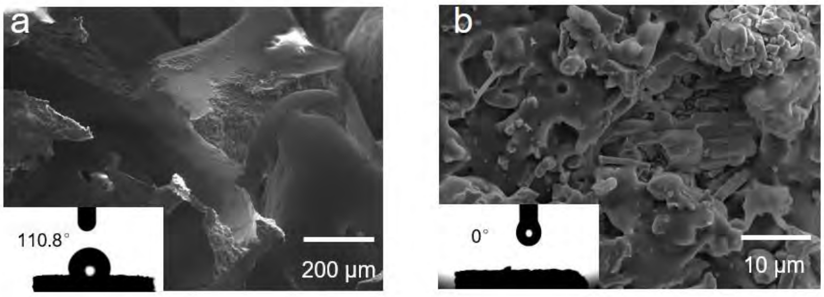

Figure 4.11 Microstructure of silicone foam. a) SEM image and water contact angle of silicone foam. b) SEM image and water contact angle of silicone/CNT foam.

The superior thermal conductivity of the Li-PAAm hydrogel/silicone composite compared to the Li-PAAm hydrogel alone is clearly evidenced by the IR image (**Figure 4.12 a**). This enhanced thermal conductivity, combined with the notable hydrophilicity of the CNT/silicone foam, leads to accelerated evaporation within the composite material. Consequently, the composite exhibits an impressive evaporation rate of 41 wt.% within a 3-hour period, and it regenerates back to its initial state within 7 hours under the same test conditions. These improved evaporation and regeneration characteristics facilitate a faster and more uniform heat transfer from the heat source, resulting in enhanced heat dissipation to the TE device (**Figure 4.12 b**).

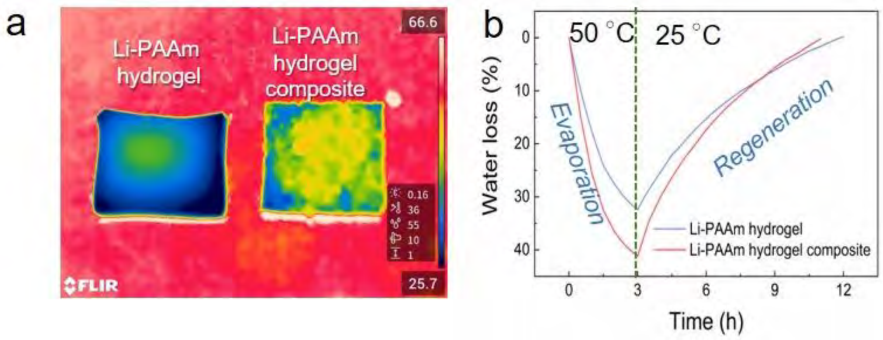

Figure 4.12 Characterization of the passive regulation layer. a) Infrared images of Li-PAAm hydrogel and Li-PAAm hydrogel/silicone composite. b) Mass change of the Li-PAAm hydrogel and Li-PAAm hydrogel composite at 50 °C and RH =50 % and subsequent mass recovery at 25 °C and RH =70 %, respectively.

4.5.3 Isothermal regulation of D-thermo-e-skin

The D-thermo-e-skin was designed to emulate the isothermal regulation capabilities of human skin, with a target temperature set at 35 °C, which falls within the comfortable temperature range for human skin.[45, 125, 126] To test the isothermal regulation abilities of the D-thermo-e-skin, it was connected to a PID control system and placed on a silicone prosthesis in a wind channel. The initial temperature of the D-thermo-e-skin was 22 °C, and the wind channel's airspeed was set to 0.5 m/s. At the 5th minute, the auxiliary water was activated to change the air temperature, while simultaneously activating the PID control system. The PID control system was turned off once the surface temperature of the D-thermo-e-skin surpassed the desired temperature. To further evaluate its performance, the D-thermo-e-skin was tested under convective conditions at three different ambient temperatures: cold (T_{amb}=10 °C), mild (T_{amb}=25 °C), and hot (T_{amb}=40 °C) temperatures (**Figure 4.13 a**).

In contrast, the reference skin, lacks isothermal regulation functionality, shows surface temperature fluctuations that mirror changes in the ambient temperature. For example, in cold temperature environments, the surface temperature can drop as low as 10.9 °C, while in mild temperature environments, it can rise to 25 °C. In hot temperature environments, the surface temperature can climb to a concerning 38.6 °C. These extreme temperature variations deviate significantly from the human body's comfort zone, making interactions with such surfaces uncomfortable and potentially harmful (**Figure 4.13 b**).

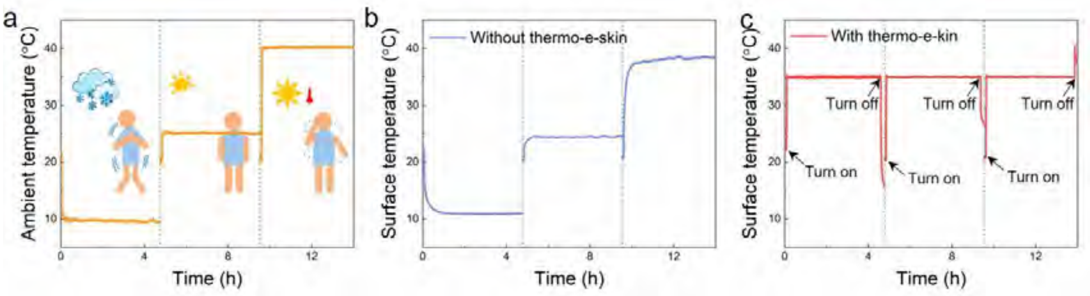

Figure 4.13 Surface temperatures of e-skin and its counterpart under the same conditions. a) Simulated environmental conditions with different temperatures. b) The surface temperature of the without D-thermo-e-skin at different environment temperatures. c) isothermal regulation of the D-thermo-e-skin at different environment temperatures.

The top layer of the active regulation section acted as a heat-producing region when exposed to a cold environment at 10 °C. Consequently, the surface temperature of the D-thermo-e-skin rapidly increased from an initial temperature of 22 °C to reach the desired temperature of 35 °C. This temperature was maintained for an extended period. Similarly, at a mild temperature of 25 °C, the D-thermo-e-skin's surface was heated to maintain a consistent temperature of 35 °C. The surface of the D-thermo-e-skin required initial heating to sustain its constant temperature as the temperature further increased to 40 °C. During this period, the top layer of the active regulation section continued as the heat source, leading to a rapid rise in surface temperature to 35 °C. Additionally, the entire surface area of the skin reached 35 °C after a certain period when testing the D-thermo-e-skin in a wind channel. At this point, the top layer of the active regulation section became the cold side and utilized surface cooling to maintain the intended temperature. Simultaneously, the passive regulation layer became operational, causing the hydrogel to perspire and remove excess heat from the hot side. This mechanism facilitated an increased duration of isothermal adaptation for the D-thermo-e-skin (**Figure 4.13 c**).

Figure 4.14 a illustrates the variations in surface temperature of the D-thermo-e-skin and its counterpart under different ambient temperatures. The D-thermo-e-skin exhibited effective isothermal regulation similar to the human body, maintaining a constant surface temperature of 35 °C within the range of 10-45 °C. In contrast, the surface temperature of the counterpart, which lacks thermoregulation, fluctuated in accordance with the ambient temperature. It is evident that the D-thermo-e-skin requires additional energy cost to maintain a constant surface temperature (**Figure 4.14 b**). Similar to the human body, the D-thermo-e-skin also achieved its minimum energy cost when the ambient temperature matches the set temperature, which was 25.9 mW/cm^2 at 35 °C. Deviating further from the thermoneutral zone, a higher energy cost was required to maintain a constant surface temperature (69.8 mW/cm^2 at 10 °C and 32.28 mW/cm^2 at 45 °C).

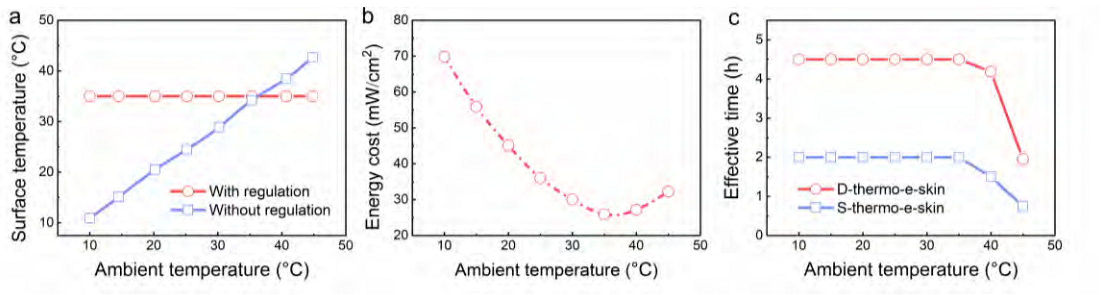

Figure 4.14 Isothermal regulation performance of the D-thermo-e-skin. a) Effects of isothermal regulation on artificial limbs. b) The energy cost of the D-thermo-e-skin to maintain the surface temperature at 35°C at different ambient temperatures. c) The effective time of isothermal regulation under different ambient temperatures.

Figure 4.14 c presents the duration for which the D-thermo-e-skin effectively maintains a surface temperature of 35 °C under varying ambient temperatures. When the ambient temperature is equal to or below 35 °C, the D-thermo-e-skin can sustain the desired temperature for an extended period as the generated heat can disperse freely into the environment (only 4.5 hours are represented in the figure). However, in situations where the ambient temperature surpasses 35 °C, the excess heat in the D-thermo-e-skin relies on the evaporation effect of the passive regulation layer. If heat dissipation is inadequate, the isothermal regulation capability of the D-thermo-e-skin will be compromised. Thanks to the design of the passive regulation layer, the effective duration of the D-thermo-e-skin in high-temperature conditions has been considerably prolonged to 4.2 hours at an ambient temperature of 40 °C (280 % of the S-thermo-e-skin) and 2 hours at an ambient temperature of 45 °C (270 % of S-thermo-e-skin).

Moreover, it was subjected to testing in a controlled environment at a temperature of 40°C with varying wind speeds to investigate the practicality of implementing the D-thermo-e-skin in real-world scenarios (**Figure 4.15**). Based on the test findings, the D-thermo-e-skin remained effective for approximately 6.3 hours when exposed to a wind speed of 0.25 m/s. However, under higher wind speed conditions of 1 m/s, the effective time of the e-skin decreased significantly to 1.6 hours. Specifically, at 0.25 m/s wind speed, the energy cost for thermoregulation by the D-thermo-e-skin was merely 21.8 mW/cm^2, in stark contrast to the increased energy cost of 37 mW/cm^2 when the wind speed escalated to 1 m/s. The intensification of wind speed augments the heat exchange between the D-thermo-e-skin and the environment, amplifying the required energy input while concurrently diminishing the operational time of the D-thermo-e-skin.

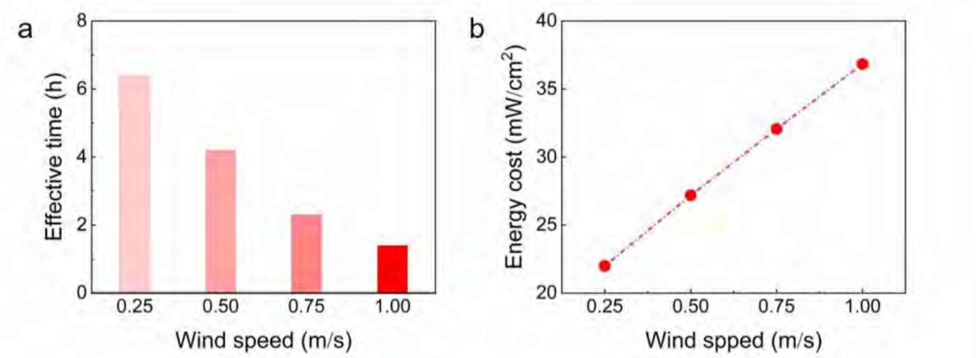

Figure 4.15 Isothermal regulation of D-thermo-e-skin at different wind speeds. a) At 40°C, the effective time of D-thermo-e-skin thermoregulation under different wind speeds. b) At 40°C, the energy cost of D-thermo-e-skin for temperature control under different wind speeds.

4.5.4 Environmental stability of D-thermo-e-skin

The passive regulation layer of the D-thermo-e-skin has demonstrated a sweat evaporation mechanism that offers significant advantages in maintaining isothermal regulation, particularly in high-temperature conditions. **Figure 4.16 a** provides a visual representation of the water loss of the D-thermo-e-skin before and after subjecting it to a surface temperature of 35 °C within an ambient temperature range of 20-45 °C. At lower temperatures, the D-thermo-e-skin generated heat with minimal sweating, resulting in only 2.2 wt.% water loss after 4.5 hours at 20 °C. The slight weight change observed can mainly be attributed to natural evaporation brought about by strong convection. As the ambient temperature increased to 40 °C, the D-thermo-e-skin underwent cycles of heating and cooling. During this phase, the D-thermo-e-skin initiated profuse sweating to maintain the isothermal regulation effect. This led to a water loss of 11.54 wt.% in 4.2 hours. As the temperature continued to rise to 45 °C, the sweating rate further increased, resulting in a water loss of 6.19 wt.% after two hours. These findings once again highlight the remarkable similarity between the thermoregulatory patterns of the D-thermo-e-skin and human skin. At low temperatures, both exhibit minimal or absent sweating, whereas at high temperatures, significant sweating occurs. The ability to replenish lost water significantly influences the self-sustaining evaporative cooling capability of the D-thermo-e-skin.

Figure 4.16 b illustrates the results of moisture regeneration in the D-thermo-e-skin under different humidity conditions after achieving isothermal regulation at 40 °C (with an ambient temperature of 25 °C). When exposed to a 60% humidity environment, the vapor pressure of the hydrogel within the D-thermo-e-skin was lower than the surrounding vapor pressure. As a result, the hydrogel absorbed moisture from the environment, gradually reducing water loss from 11.54 wt.% to 0.14 wt.%. Additionally, higher humidity levels led to a shorter regeneration time for moisture in the D-thermo-e-skin, decreasing from 11 hours to 4 hours as the humidity increased from 60% to 90%.

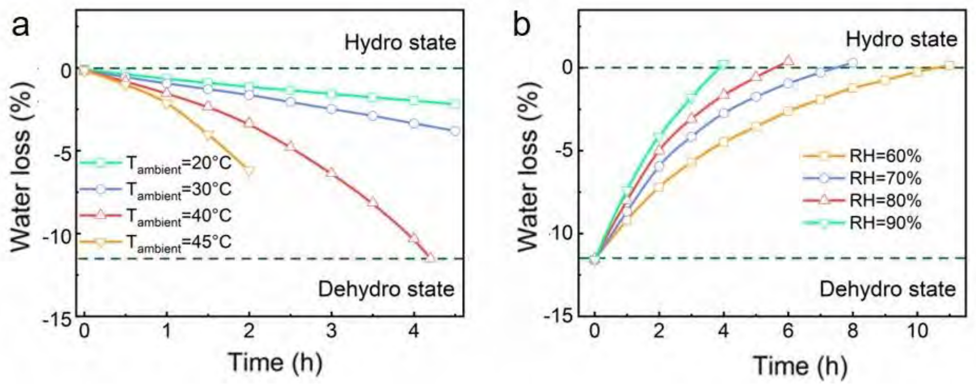

Figure 4.16 Circulatory properties of the D-thermo-e-skin. a) Water evaporation curves of the D-thermo-e-skin in the environments of different temperatures, varying from 20 to 45°C. b) The water regeneration of D-thermo-e-skin at 25 °C, and in various relative humidity from 60 % to 90 %.

In **Figure 4.17 a**, we present a visual representation of the weight variation observed in the D-thermo-e-skin during repetitive cycles of sweat evaporation and regeneration. The weight change occurred between two distinct states: the hydrated state (0 wt.%) and the dehydrated state (11.54 wt.%). Additionally, as shown in **Figure 4.17 b**, the D-thermo-e-skin consistently performed well in adapting to temperatures in a 40 °C environment across different days. Specifically, it maintained stable isothermal regulation for 4.2 hours in each instance. These findings provide evidence of the exceptional water cycling capabilities of the D-thermo-e-skin, which can be attributed to the characteristics of hygroscopic hydrogels. As a result, the D-thermo-e-skin demonstrates the necessary stability and reusability for effective isothermal regulation in real-world environments.

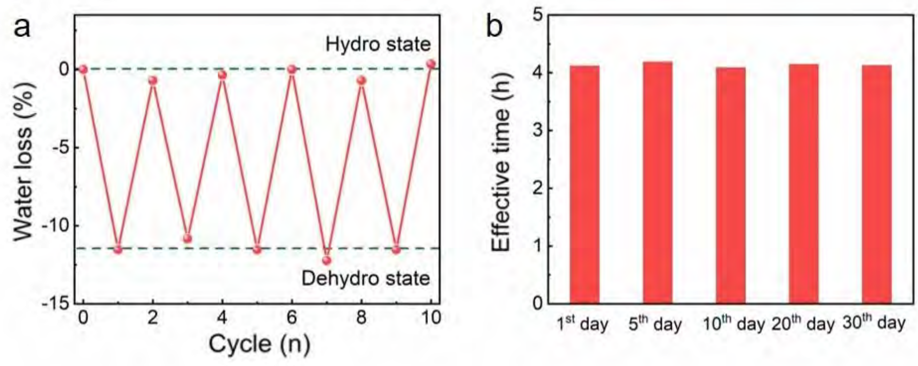

Figure 4.17 Reusability of the D-thermo-e-skin. a) Cyclic performances of water evaporation–regeneration of D-thermo-e-skin. b) Effective time of D-thermo-e-skin at 40 °C varying from 1st day to 30th day.

4.5.5 Transient thermoregulation of D-thermo-e-skin

Transient thermoregulation plays a crucial role in the temperature adaptation of the D-thermo-e-skin. The temperature receptors in their skin detect the temperature difference between their body and the object when an individual touches an object, triggering thermosensation in the nerve center. This process prompts the body to engage in transient thermoregulation. However, there is a delay in this response as it takes time for heat generation or dissipation in the core of the body to affect the surface. Prolonged contact with hot or cold objects can result in temperature fluctuations in the skin, causing discomfort or skin damage.[147] To investigate these phenomena, thermocouples were attached to both human skin and the D-thermo-e-skin. This allowed for the monitoring of temperature changes after contact with various objects, where the ambient temperature was 25 °C and both human skin and the D-thermo-e-skin were initially set at 32 °C. Additionally, an estimation was made of the energy cost required by the D-thermo-e-skin for thermoregulation, as depicted in **Figure 4.18**.

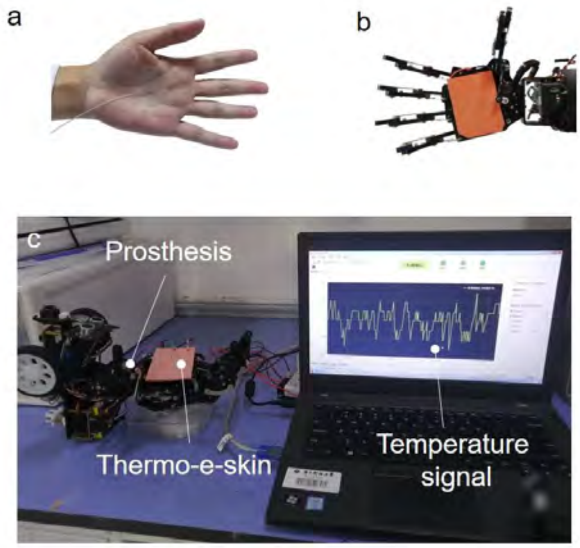

Figure 4.18 Transient thermoregulation of D-thermo-e-skin. Schematics of a) human skin touch object. b) D-thermo-e-skin touch object. c) transient thermoregulation.

The analysis focused on the temperature changes of human skin upon contact with various objects. Initially, the human skin temperature was recorded at 32 °C (**Figure 4.19 a**). When the skin came into contact with a cold-water bottle at 25 °C, the skin temperature decreased, reaching 27.9 °C, which fell below the comfortable temperature range for the human body. Subsequently, after the removal of the cold-water bottle, the skin temperature gradually increased and returned to its initial temperature within a period of five minutes. Conversely, when the skin made contact with a human hand, the skin temperature gradually increased to 34.9 °C due to reduced heat dissipation. After the hand was removed, the skin temperature slowly decreased to 32.6 °C over a span of five minutes. Similarly, when the skin was in contact with a hot-water bottle at 40 °C, the surface temperature promptly rose to 37.2 °C, deviating from the initial temperature. Following the removal of the hot-water bottle, the skin temperature gradually decreased and eventually reached 33.4 °C. These findings offer evidence of the efficient and dynamic regulation of skin temperature facilitated by the active regulation layer of the D-thermo-e-skin.

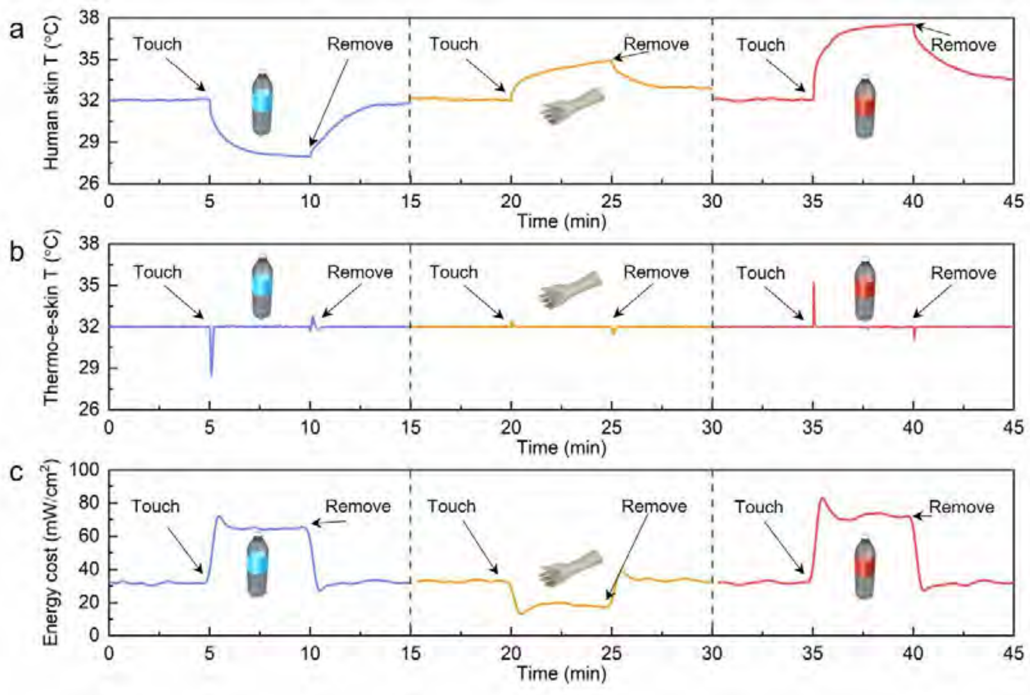

Figure 4.19 Temperature variations of human skin and D-thermo-e-skin. a) Schematic of human skin touching objects. b) Schematic of D-thermo-e-skin touch objects. c) Energy cost when the D-thermo-e-skin touches objects.

In comparison, the D-thermo-e-skin exhibited a rapid decrease in temperature upon contact with the cold-water bottle, reaching 28.7 °C. The active regulation layer then quickly heated the skin to 32 °C, which is equivalent to human skin temperature. However, upon removal of the cold-water bottle, the surface temperature initially rose due to the thermoregulation process, and then rapidly dropped. Despite these fluctuations, the surface temperature of the D-thermo-e-skin remained stable at 32 °C with minor variations during contact and removal, as it was set to align closely with the temperature of the human hand. In contrast, when in contact with the hot-water bottle, the D-thermo-e-skin experienced a swift increase in temperature, reaching 35.3 °C. The active regulation layer promptly cooled the surface, restoring the temperature to 32 °C within a few seconds. The temperature of the D-thermo-e-skin briefly decreased and then increased again once the hot-water bottle was removed, as the excess cooling capacity caused fluctuations (**Figure 4.19 b**). As a result, by interacting with various objects, D-thermo-e-skin exhibits instantaneous thermoregulation capabilities beyond those of human skin, providing faster and quicker interactions for robots.

The thermoregulation process of the D-thermo-e-skin can be evaluated through its energy cost, as shown in **Figure 4.19 c**. The energy cost of the D-thermo-e-skin increased from 32 mW/cm^2 to 65 mW/cm^2 when in contact with a cold-water bottle, indicating the need to intensify heat generation in order to maintain the desired surface temperature. Conversely, when in contact with a human hand which generates heat and has a similar temperature, the energy cost decreased from 32 mW/cm^2 to 16 mW/cm^2 as the demand for heat generation decreased. The high heat emission from a hot water bottle disrupted the surface temperature equilibrium of the D-thermo-e-skin, necessitating substantial energy consumption for cooling in order to maintain a temperature of 32 °C. Consequently, the energy cost increased from 31 mW/cm^2 to 73 mW/cm^2.

4.6 Correlation between sweathole and water evaporation

Water evaporation is a direct reflection of the heat carried away by the passive regulation layer. However, the 11.54% water evaporation at failure at high temperatures does not reach the upper limit of hydrogel evaporation. One of the reasons is that the large thermal resistance between the active and passive regulation layers results in the heat generated not being able to dissipate through water evaporation in time. Another reason is that sweatholes affect the water exchange between the e-skin and the external environment (**Figure 4.20**).

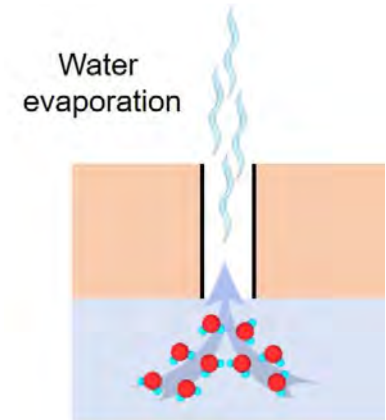

Figure 4.20 Sweatholes regulate water evaporation.

In general, sweatholes act as water exchange channels between the e-skin and the environment and serve to regulate the amount of water evaporation. Their shape and number affect the amount of water evaporation. Common sweathole materials are polymers, which are usually not hydrophilic. Selective surface modification methods are used to alter the hydrophilicity of sweatholes.[139, 148-150] The bottom of the pore is weakly hydrophilic and the top of the pore is strongly hydrophilic, resulting in a hydrophilicity gradient of the pore. This gradient wettability facilitates unidirectional water transport from the bottom to the top surface. On the other hand, thermostimuli-responsive polymers are used to fabricate smart pore switches that mimic the human body's sweat evaporation process to change the number of sweatholes.[103, 151-153] PNIPAM, a commonly used thermostimuli-responsive polymer, possesses both hydrophilic and hydrophobic transitions at a specific lower critical solution temperature (LCST) near 32°C. Below the LCST, PNIPAM becomes hydrophilic, causing the sweatholes to close. There is no channel for water exchange with the outside world, resulting in less water evaporation. Above LCST, PNIPAM becomes hydrophobic, causing the sweatholes to open. There are more channels for water exchange with the outside world, resulting in more water evaporation.

As a result, the design of sweatholes can be carried out with full consideration of the above two approaches when carrying out the moisture management of e-skin, so that the amount of water evaporation can be adjusted proactively in different environments to achieve a more bionic purpose.

4.7 Summary

In this chapter, we have successfully replicated the thermoregulation mechanism of the human body by developing a D-thermo-e-skin. This D-thermo-e-skin incorporates both active TE thermoregulation and passive water evaporation. It represents the first instance of long-lasting stable thermoregulation in a D-thermo-e-skin. We achieved this by combining a flexible TE device with a Li-PAAm hydrogel composite, which allowed us to unify heat generation and heat dissipation, thereby altering the temperature characteristics of conventional e-skin. Our developed D-thermo-e-skin is capable of maintaining a surface temperature of 35 °C across a wide temperature range of 10-45 °C. This achievement is attributed to the design of our active and passive regulation layers, which significantly enhance the effective time of the D-thermo-e-skin in different environmental conditions. For instance, at an ambient temperature of 25 °C, the D-thermo-e-skin can maintain its thermoregulation capability for 4.5 hours, while at an ambient temperature of 40 °C, it remains effective for 4.2 hours. An important feature of our D-thermo-e-skin is its hygroscopic hydrogel properties. These properties enable the D-thermo-e-skin to reabsorb water from the surrounding atmosphere during isothermal regulation. In fact, in a humidity level of 90%, the water in the D-thermo-e-skin returns to its hydro state within a mere 4 hours. Stability is another notable characteristic of our D-thermo-e-skin. We observed nearly constant effective time across multiple isothermal regulation cycles in a 40 °C environment, indicating remarkable stability. Additionally, the water evaporation-regeneration mechanism ensures that the D-thermo-e-skin can be reused. Furthermore, the D-thermo-e-skin demonstrates rapid thermoregulation capabilities that surpass those of human skin. Its surface temperature can be rapidly adjusted to approximately 32 °C within seconds by leveraging the cooling or heating function of the flexible TE device when in contact with various objects. Overall, our bionic D-thermo-e-skin exhibits practical thermoregulation abilities, providing valuable insights into mimicking human thermoregulation. This development also holds promise for implementing bionic thermal sensing in robots.

CHAPTER 5 HEAT-SOURCE-IDENTIFICATION OF TEMPERATURE SENSOR

5.1 Introduction

Chapters 3 and 4 aim to replicate the function of isothermal regulation, demonstrating the ability to maintain a consistent temperature within a wide temperature range. Conventional temperature sensors only provide a simple measurement of absolute temperature.[154-161] Conversely, the human body's perception of thermal comfort relies on various factors, such as different heat sources, energy levels, and duration. By integrating multidimensional thermal sensing capabilities, e-skin can assist humans in identifying a more comfortable temperature environment. Moreover, e-skin can adapt its thermal regulation methods to diverse heat sources, and respond by generating or dissipating heat, or avoiding extreme temperatures. This proactive approach minimizes the likelihood of performance degradation or damage caused by overheating or overcooling, thereby improving work efficiency and extending the service life of e-skin. Achieving successful heat source identification remains a significant challenge for temperature sensors.

External heat sources include three types: thermal conduction, thermal convection, and thermal radiation, based on the mode of heat exchange between the human body and the environment. We then explain the signal characteristics of these heat sources. Thermal conduction is characterized by temperature change, pressure change, and proximity effect. Thermal convection is characterized by temperature change and pressure change. Thermal radiation is characterized by temperature change only. To capitalize on these signal characteristics, we designed a multimodal temperature sensor that utilizes the ionic relaxation time as a key determining factor. This sensor has the ability to convert various environmental stimuli, such as temperature, pressure, proximity, and wind speed, into electrical signals. This capacity allows the sensor to effectively differentiate between heat sources that employ different heat exchange mechanisms.

5.2 Concept design

The decomposition of heat-source signals is essential for realizing heat-source identification. In heat exchange scenarios, the heat source and object experience additional physical responses alongside the temperature stimulus. Thermal conduction involves direct contact between the heat source and the object, resulting in proximity, pressure stimuli, and temperature. Thermal convection occurs when a fluid, such as air, interacts with an object, leading to temperature and pressure stimulation combined with wind. Thermal radiation, on the other hand, relies on the principle of blackbody radiation for heat exchange with an object. As there is no direct contact, only temperature stimulus affects the object. The unique characteristics of heat source signals allow for the implementation of heat-source identification functionality in e-skin.

Multimodal sensing is necessary to differentiate between various physical signal types emitted by a heat source. The efficacy of multimodal sensing relies on decoupling, which involves eliminating interference between different stimuli in a multi-input scenario to ensure accurate measurement of the desired input signal. However, this requirement often leads to complex fabrication processes and high costs due to the utilization of heterogeneous sensing units with varying architectures, materials, and mechanisms. To address this challenge, a promising solution entails the development of novel materials that integrate multiple sensing mechanisms within a single sensing unit, resulting in a solitary signal output. For instance, Bao's team has successfully created a multimodal e-skin featuring an electrode-electrolyte-electrode sandwich structure, utilizing the ionic conductor as the active material. This clever design exploits the principles of ionic relaxation dynamics to achieve complete decoupling of temperature and strain measurements within the sensor.[162]

In this chapter, the multimodal temperature sensor is introduced, which is a capacitive type sensor designed with a sandwich structure consisting of copper electrodes and a methoxy poly(ethylene glycol) acrylate (MPEG-DA)-based ion gel (**Figure 5.1 a**). The electrochemical properties of this sensor are primarily determined by the movement of ions near the interface of the electrode-ion gel and within the active material. Notably, the ion gel exhibits frequency-dependent ionic properties, which are essential for utilizing the ionic relaxation response in thermosensation. The ionic relaxation time, denoted as τ, is an inherent material parameter that is solely affected by temperature and remains unaffected by other signals (**Figure 5.1 b**). Meanwhile, the capacitance of the sandwich structure displays variations under the influence of external pressure, making it suitable for pressure detection. Furthermore, the capacitance can be utilized as an external variable that is insensitive to temperature, enabling the detection of strain.

Lastly, capacitive sensors are capable of proximity sensing since their surface charge distribution can be influenced by external objects.

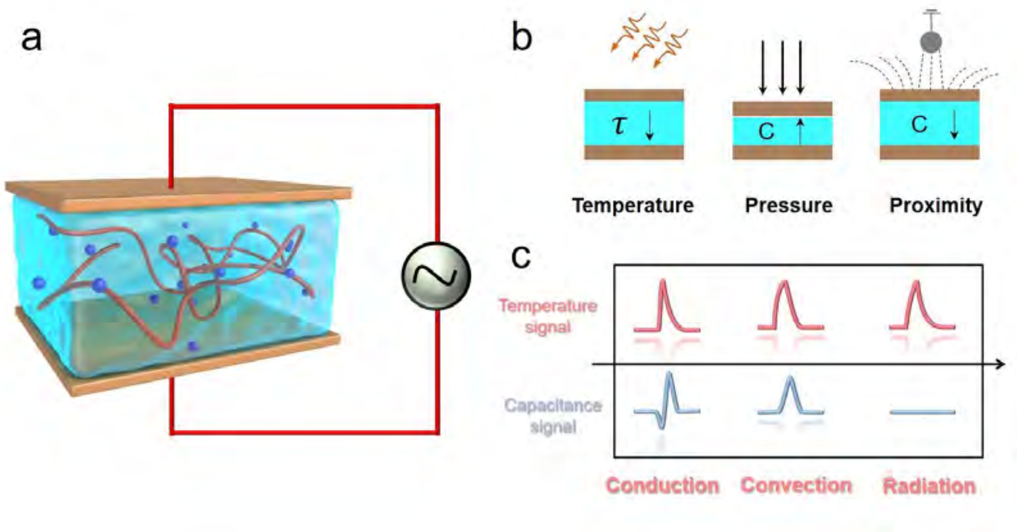

Figure 5.1 The design concept and application mechanism of multimodal temperature sensor. a) Basic structure of the multimodal temperature sensor. b) The mechanisms of multimodal sensing. c) The heat-source-identification mechanism of multimodal temperature sensor.

The above-mentioned sensing mechanisms respond differently to temperature, pressure, and proximity stimuli. When the heat source signals are decomposed, this mechanism can be effectively used for identifying heat sources of objects (**Figure 5.1 c**). In the thermal conduction model, changes in temperature-induced τ, proximity-induced negative capacitance, and pressure-induced positive capacitance reflect this process. In the thermal convection model, the signal can be decomposed into changes in temperature-induced τ and wind pressure-induced positive capacitance. However, in the thermal radiation model, only temperature-induced changes are observed. The proposed multimodal temperature sensor combines intrinsic and extrinsic variables in a single unit, providing a valuable alternative for designing multimodal thermosensation in e-skin applications.

5.3 Fabrication and characterization equipment of multimodal temperature sensor

The multimodal temperature sensor utilized a rapid photopolymerization process to create an ion gel. Methoxy poly(ethylene glycol) acrylate (MPEG-DA) was used as the monomer and lithium bis(pentafluoroethylsulfonyl) imino-ammonium (Li-PFSI) was used as the electrolyte salt at a concentration of 0.1 M. Thorough mixing was performed. In **Figure 5.2 a**, the molecular structures of the monomer (MPEG-DA), electrolyte salt (Li-PFSI), cross-linker (poly(ethylene glycol) diacrylate), and photoinitiator (UV184) are presented. **Figure 5.2 b** illustrates the mechanism of ion transport in ionic gels, where Li^+ ions form lithium-oxygen (Li-O) bonds with the oxygen atoms in the chain of the methoxy poly(ethylene glycol) acrylate, enabling their migration within the gel matrix through the formation and breakage of these Li-O bonds. Intra- or inter-chain hopping can facilitate ion transport, along with the gradual replacement of Li^+ solvating ligands and the rearrangement of chain segments, enabling long-range ion transport. **Figure 5.2 c** showcases a photograph of the fabricated multimodal temperature sensor device, featuring a sandwich structure with copper electrodes positioned at both ends and an ion gel film in the middle. **Figure 5.2 d** shows the precision impedance analyzer used to test the sensor. During testing, the upper and lower electrodes of the device were connected to the fixture of the precision impedance analyzer to access the signal acquisition system and generate electrical output signals.

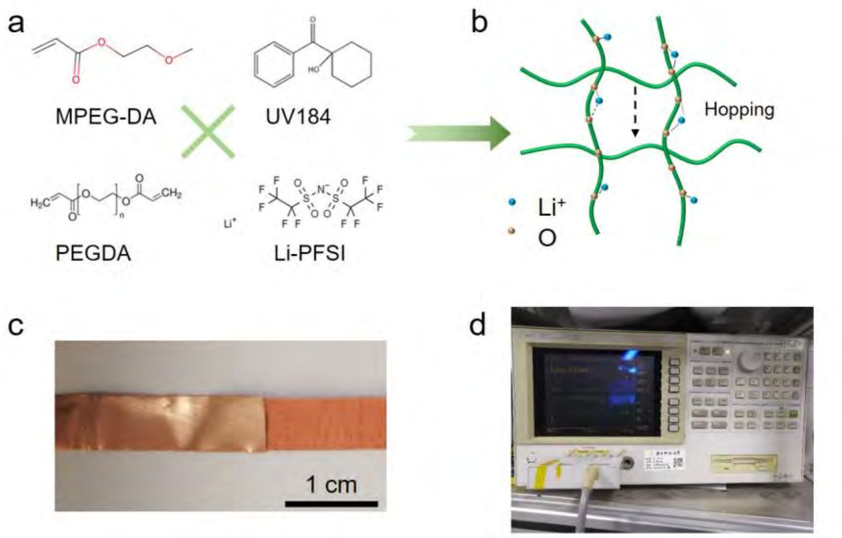

Figure 5.2 Fabrication and characterization equipment of multimodal temperature sensor. a) Molecular structure and composition of ionic gel precursors. b) Ion gel structure and ion transport mechanism. c) Image of the multimodal temperature sensor. d) Agilent 4298A Precision Impedance Analyzer.

5.4 Multimodal temperature sensor realizes basic thermosensation

The ion relaxation time of the multimodal temperature sensor is an intrinsic parameter that is temperature-sensitive. This parameter can be represented and fitted using an equivalent circuit, which serves as a measuring tool. In the case of this sensor, the impedance spectrum of the electrochemical system can be effectively captured and modeled using the equivalent circuit depicted in **Figure 5.3**. This circuit is composed of several elements, namely a constant phase angle element (C_{EDL}), a bulk resistance (ionic resistance) (R_B), a bulk capacitance (geometrical capacitance) (C_B), and an electrode resistor (R_E) resulting from the electrically-doped double layer, abbreviated as R(RQ)Q thereafter.

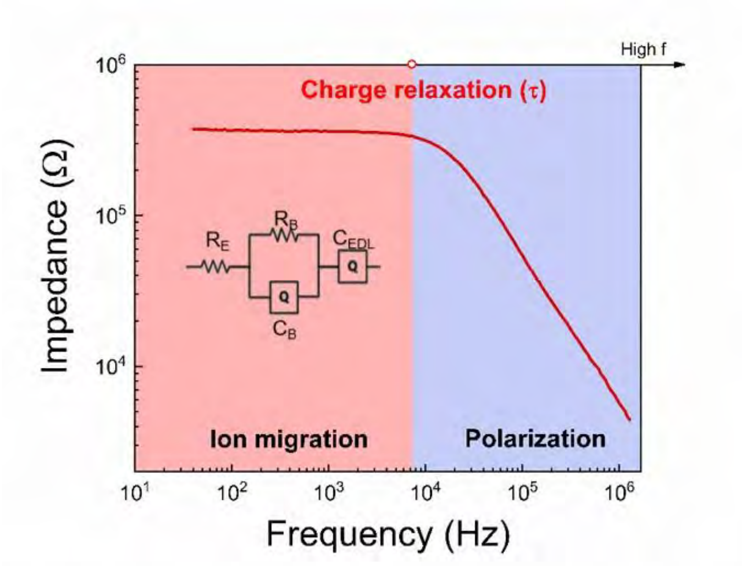

Figure 5.3 Ion relaxation time that can be used for temperature sensing

In the electrochemical system of metal electrode-ion gel-metal electrode, the impedance spectra of ion gels with ion relaxation time response provide clear characterization. The electrochemical parameters of the ion gel are predominantly influenced by ion migration at low frequencies, while molecular polarization of the polymerized chains dominates at high frequencies. Throughout the lhigh-frequencyquency range, the electrical response corresponds to the behavior of C_B due to the reduction of virtual resistance and is particularly impacted by molecular polarization at high frequencies. The discharge process in the RC parallel circuit takes place within a specific duration known as the ion relaxation time (τ), which is determined by the product of resistance and capacitance ($\tau = RC$). This duration represents the time required for ion polarization to dissipate and serves as a fundamental concept used in this chapter for implementing thermosensation. Utilizing the Porter diagram, the ion relaxation frequency (τ^{-1}) in the RC parallel circuit can be identified as the frequency at which the real impedance (plateau) intersects the imaginary impedance (diagonal). Notably, the relaxation time (τ) of ion polarization in the system corresponds to the critical frequency, which serves as an inherent parameter of ionic gels and is exclusively influenced by temperature. Higher temperatures lead to an increase in the ionic relaxation frequency, while the application of pressure has no effect on its value.

The ability of the multimodal temperature sensor to carry out thermosensation in e-skin is reliant on its thermosensation ability. The multimodal temperature sensor was connected to a heat source using electrodes and linked to a precision impedance analyzer. During this experiment, the temperature of the heat source was altered, and the impedance spectrum of the multimodal temperature sensor was measured. **Figure 5.4** provides a representation of the electrochemical parameters of the multimodal temperature sensor within the temperature range of -20 °C to 180 °C. The R_B and C_B values shown in the figure were obtained by fitting an equivalent circuit model and have a temperature interval of 10 °C. As the temperature increases from -20 °C to 180 °C, the bulk resistance of the multimodal temperature sensor gradually decreased from 11.29 MΩ ($ln(R)$ = 16.24) to 15 kΩ ($ln(R)$ = 9.64) (**Figure 5.4 a**). This decrease can be attributed to the increased movement of polymer chains at higher temperatures, allowing for easier transportation of Li^+ ions within or between the chains and resulting in higher conductivity. Figure 5.4 b) shows that the bulk capacitance initially increased and then decreased as the temperature rose from -20 °C to 180 °C, with the maximum capacitance observed at 20 °C. The change in capacitance was smaller compared to the change in bulk resistance. These findings demonstrated that the ionic gels used in the multimodal temperature sensor can reliably generate electrochemical signals over a wide temperature range, spanning from extremely low (-20 °C) to high (180 °C) temperatures.

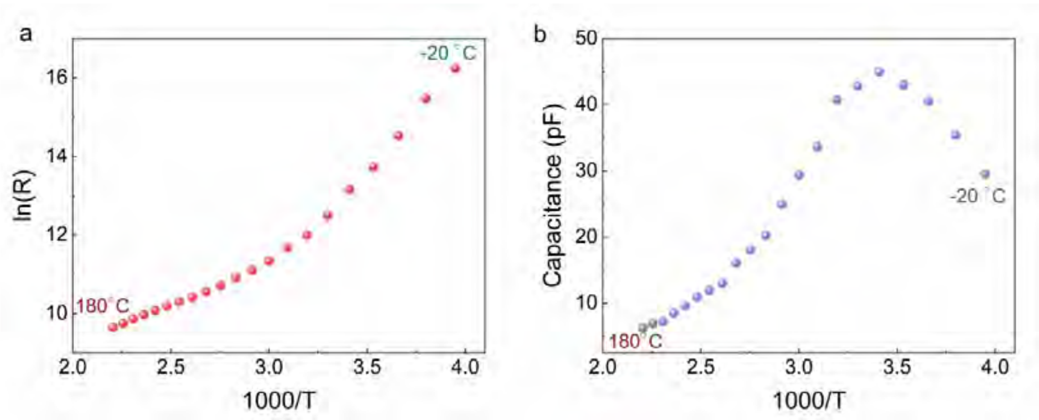

Figure 5.4 Electrochemical parameter responses of multimodal temperature sensor in the range of -20 °C to 180 °C. a) Bulk resistance R_B. b) Bulk capacitance C_B.

The accuracy of a temperature sensor depends on its linearity, which represents the relationship between the sensor's output and input values. In **Figure 5.5**, the temperature response of the multimodal temperature sensor within the range of -20 °C to 180 °C was presented based on the ionic relaxation time obtained by fitting the measured bulk resistance and bulk capacitance using an equivalent circuit ($\tau = RC$). The results demonstrated that the multimodal temperature sensor exhibited a high degree of linearity in its output response to temperature variations. The value of $ln(\tau)$ increased from 8.01 at -20 °C to 16.15 at 180 °C, resulting in a linearity coefficient of 0.993.

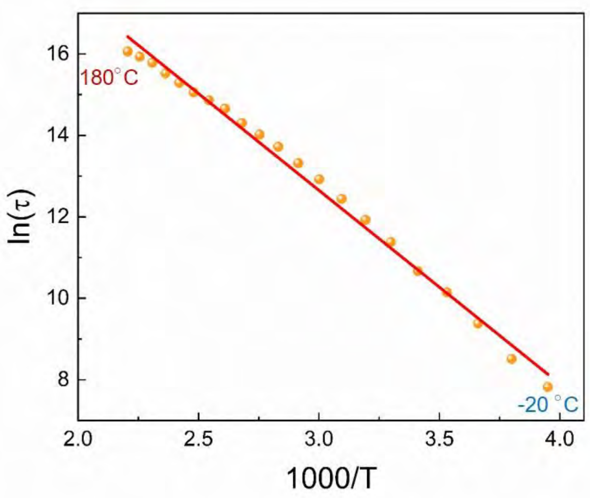

Figure 5.5 Linear response of ion relaxation time to reversed temperature in the range of -20 °C -180 °C for the multimodal temperature sensor.

The detection limit of a sensor refers to the smallest detectable physical quantity or variation, which indicates the sensor's sensitivity and accuracy. Traditional temperature sensors typically have a minimum detection limit of 0.1 °C. However, improving the minimum detection limit of temperature sensors allows for more precise sensing in challenging test environments. The temperature response of its ion relaxation time was measured to evaluate the detection limit of the multimodal temperature sensor (**Figure 5.6**). A commercial TEC device was used as the heat source and a multimodal temperature sensor was attached to the heat source and placed in a draft-free environment. The temperature of the heat source surface was controlled using a PID control system connected to a thermistor. The heat source's temperature varied between 23.750 °C and 23.755 °C (**Figure 5.6 a**). Remarkably, **Figure 5.6 b** shows that the ion relaxation time of the multimodal temperature sensor exhibits a noticeable response to a mere 0.005 °C temperature change. This result demonstrates the sensor's exceptional sensitivity to temperature fluctuations, surpassing a detection limit of 0.005 °C and confirming its ability to detect slight temperature changes in the surrounding environment.

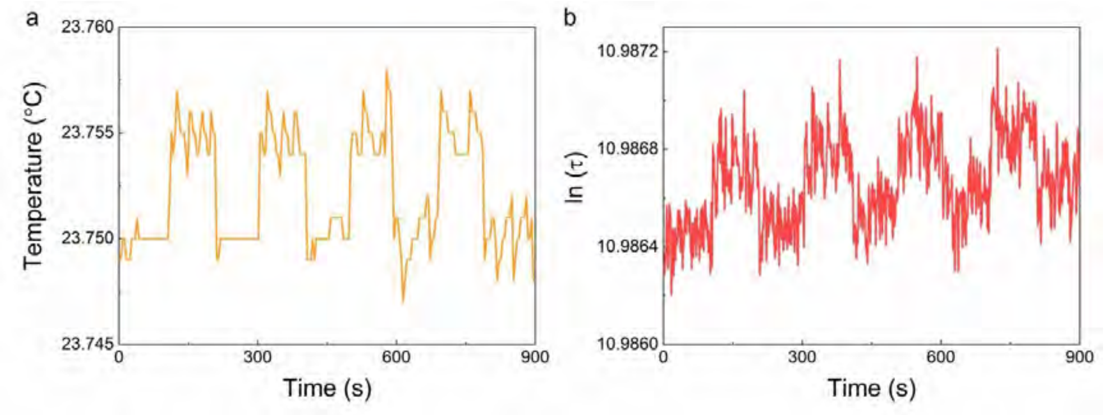

Figure 5.6 Detection limits of the multimodal temperature sensor. a) Temperature change of the heat source. b) Response of multimodal temperature sensor.

The response time of sensors is a critical performance parameter that ensures the accuracy and stability of measurement outcomes. It refers to the delay in the sensor's internal processing after signal transmission caused by the physical quantity of the actual stimulus. A prolonged response time can lead to significant hysteresis, resulting in reduced measurement accuracy and real-time monitoring efficiency, which fails to meet the requirements of real-time monitoring. In the structure of the multimodal temperature sensor, high thermal conductivity copper electrodes are present at both terminations, along with an ultra-thin (100 μm) ionic gel serving as the middle layer to facilitate rapid heat transfer. **Figure 5.7** depicts the swift response of the multimodal temperature sensor to changes in temperature, with a response time of merely 0.3 s, confirming its capability for real-time temperature measurement.

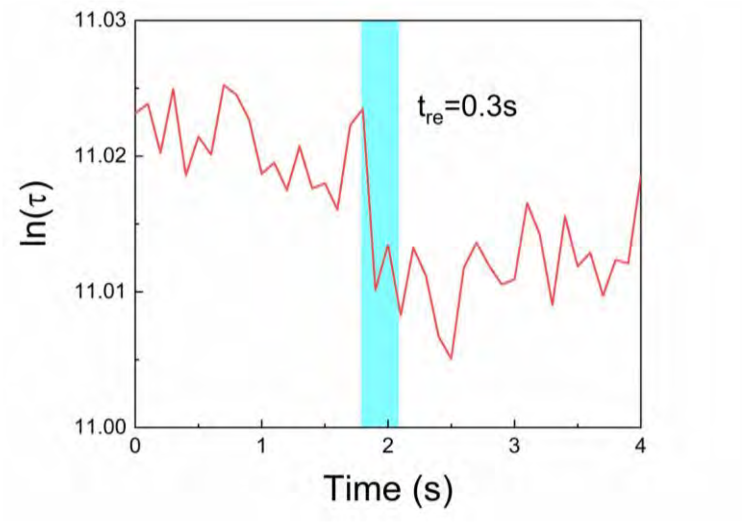

Figure 5.7 Response time of multimodal temperature sensor under a wind stimulus.

Cyclic stability is a critical factor in assessing the long-term operational stability of a sensor, as it determines the stability of the sensor's output signal under repetitive measurements. In this study, Figure 5.7 illustrates the real-time signal of the multimodal temperature sensor's ion relaxation time output when subjected to a continuous temperature stimulus. The stimulus involved periodic heating and cooling cycles of a heat source, ranging between 25 °C and 30 °C, precisely controlled using a PID system (**Figure 5.8 a**). The results indicate that the multimodal temperature sensor exhibited a consistent and uniform signal output throughout 20 temperature fluctuation cycles, with $ln(\tau)$ values ranging from 11.05 to 11.33 in response to temperature variations. This indicates the absence of signal drift during the testing process (**Figure 5.8 b**).

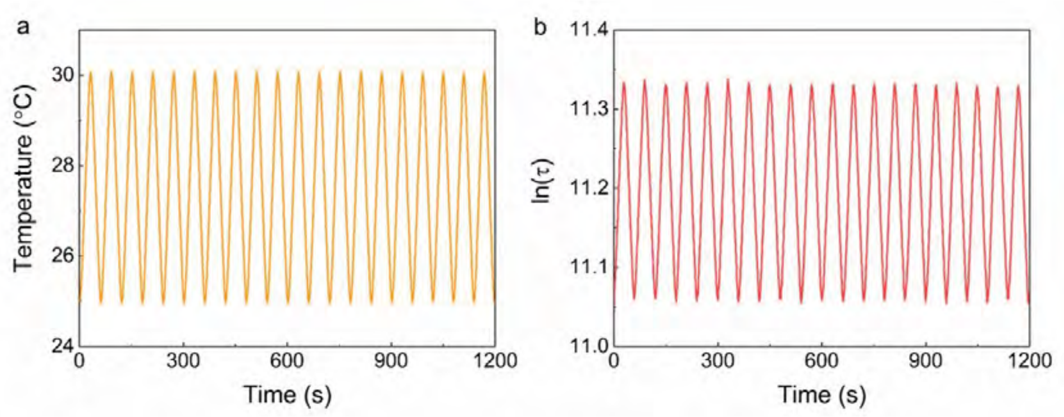

Figure 5.8 Stability of multimodal temperature sensor under temperature cycling. a) Temperature change of the heat source. b) Ion relaxation time response of multimodal temperature sensor.

5.5 Sensing mechanisms for multimodal temperature sensor

Following the comprehensive characterization tests mentioned above, the multimodal temperature sensor demonstrates exceptional performance in terms of temperature response work function, validating its fundamental thermosensation capability. However, when it comes to identifying multi-dimensional heat sources, relying solely on individual temperature detection signals falls short of achieving the desired resolution. As a result, this chapter aims to separate temperature and pressure considerations by leveraging the ion relaxation time response mechanism. The ionic relaxation time provides an ideal pressure-insensitive variable for temperature detection. Normalized capacitance, on the other hand, can effectively detect changes in capacitance due to size-independent variations caused by external forces, making it suitable for pressure sensing. Furthermore, parallel shift capacitors exhibit changes in capacitance caused by an induced charge when in close proximity to charged objects, enabling proximity induction. Combined with these mechanisms, the multimodal temperature sensor completes the identification of various excited heat sources.

5.5.1 Ion relaxation time for temperature-sensitive

The ionic relaxation time serves as a temperature-sensitive and pressure-insensitive parameter, employed in this chapter's analysis. It is represented by the product of the R_B and the C_B. While both R_B and C_B are influenced by the material's dimensions, the dimensional factor entirely cancels out when multiplying them together. As a result, it can function as a crosstalk-independent parameter for temperature measurements, completely immune to dimensional variations.

$$\tau = R_B C_B \tag{5-1}$$

Within the electrochemical system featuring an ionic gel as the electrolyte, the Bode plot showcases the ionic relaxation time reaching a critical point at both mid and high frequencies. By scrutinizing the frequency shift in this plot, it becomes possible to visualize the temperature sensitivity. **Figure 5.9** exhibits a notable downward shift in the overall sensor resistance and a corresponding shift of τ towards higher frequencies as the temperature rises. Specifically, the impedance at 1 kHz decreased from 2.3 MΩ to 112 kΩ, accompanied by an increase in the ion relaxation frequency from 3.4 kHz to 29 kHz. Additionally, under varying pressures exerted at constant temperatures, the impedance spectrum as a whole underwent a downward shift. At 1 kHz, the impedance diminished from 339 kΩ to 303 kΩ, while the ion relaxation frequency remained consistent at 5.8 kHz.

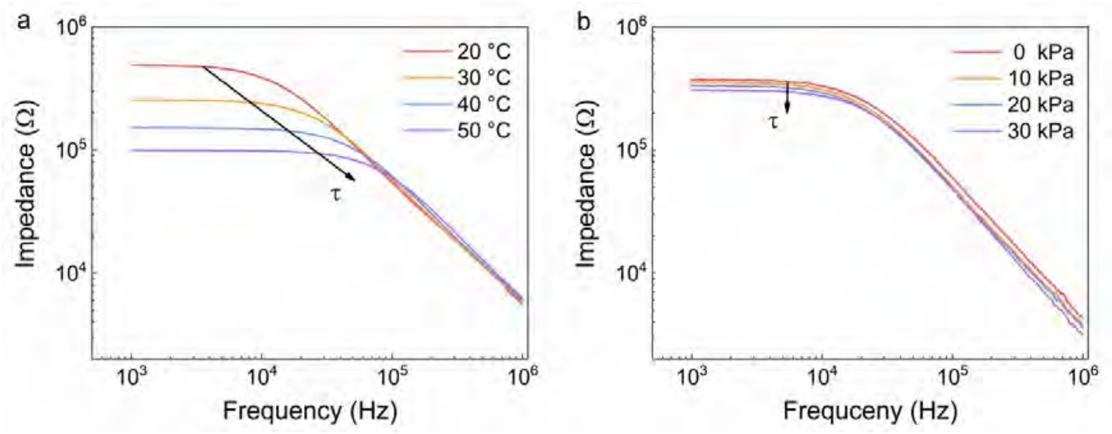

Figure 5.9 Analysis of temperature-pressure decoupling mechanism for multimodal temperature sensor. a) Response at different temperatures. b) Response at different pressures.

As shown in **Figure 5.10**, the change of τ of the device from 20 °C to 40 °C remained almost constant compared to not being subjected to pressure and maintained a good linearity when pressures of 10 kPa and 50 kPa were applied to the multimodal temperature sensor. The insensitivity of τ for thermosensation to pressure and its accuracy under large deformation were verified by testing the thermosensation linearity of the multimodal temperature sensor when subjected to pressure. Thus, *τ* responded only to temperature and not to other stimuli such as pressure and thus can be used as a reference variable to separate and decouple it from the mixed signal and achieve accurate identification in multiple stimulus signals.

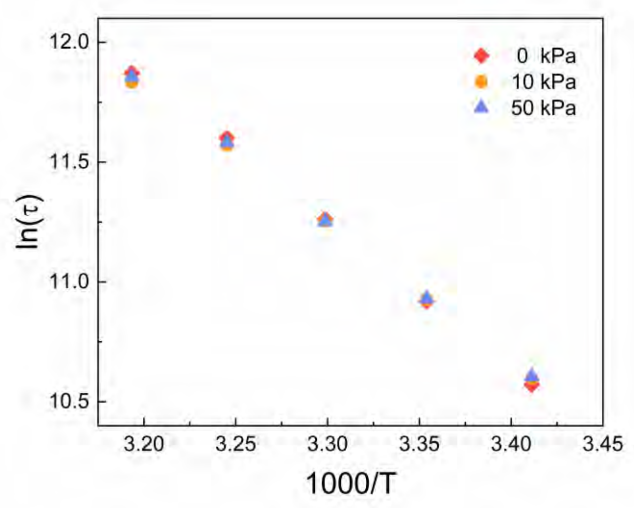

Figure 5.10 Temperature linear response of multimodal temperature sensor at constant pressure.

5.5.2 Capacitance change for pressure-sensitive

Capacitance is an external variable affected by the dimensions of the sensing region or volume. This enables its application in monitoring the forces leading to dimensional alterations. In the case of a multimodal temperature sensor subjected to pressure, the ionic gel's thickness diminishes, resulting in an increase in C_B and a decrease in R_B, while maintaining a constant value for τ. The underlying principle of capacitive pressure sensing resides in the alteration of body capacitance induced by material deformation.

$$C_B = \frac{\varepsilon A}{d} \tag{5-2}$$

The C_B represents a geometric capacitance, intimately linked to the dielectric constant (ε) and the size parameters (A, d). Illustrated in **Figure 5.11**, when subjected to external pressure, the sensor experiences a reduction in the thickness of the ionic gel, leading to a capacitance alteration. By employing an elastic material, the device can undergo deformation even under minimal pressure, consequently generating a signal output.

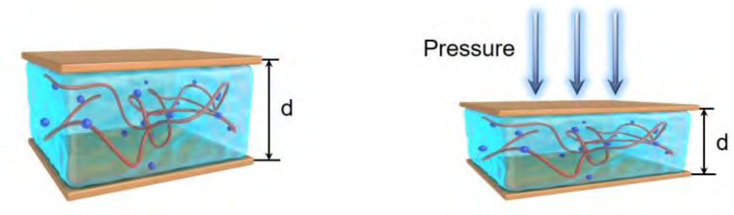

Figure 5.11 The capacitance of the multimodal temperature sensor is affected by pressure.

The downward shift of the impedance spectrum is observed as R_B experiences a decrease in impedance under compression. However, the ion relaxation time remains unaffected due to the compensatory effect of the dimensional elements. Consequently, the normalized capacitance ($\Delta C/C_0$) can be determined based on τ to eliminate any temperature-related influences. $\Delta C/C_0$ serves as a calibrated parameter by passing C_B through the pressure-insensitive τ, and it is independent of temperature. Hence, it can be employed as a pressure-sensing variable, decoupled from any temperature changes.

Figure 5.12 presents the pressure response of the multimodal temperature sensor's normalized capacitance $\Delta C/C_0$ within the range of 200 Pa to 800 Pa. The results demonstrated the multimodal temperature sensor's remarkable sensitivity to pressure variations during the cyclic pressure test at 600 Pa. The $\Delta C/C_0$ value reached 0.59%, indicating a substantial response to the applied pressure stimulus. Moreover, the multimodal temperature sensor exhibited not only a strong linear response to pressure changes but also the capability to detect pressure stimuli as low as 200 Pa.

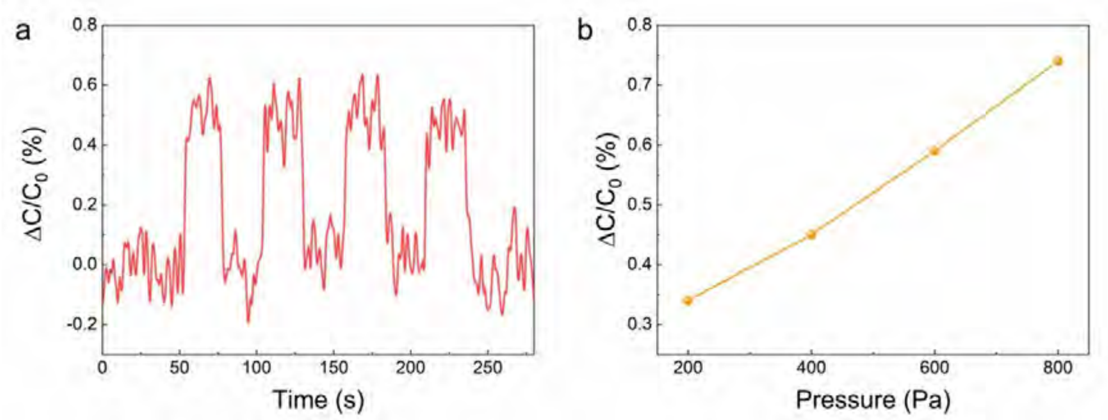

Figure 5.12 The capacitance of a multimodal temperature sensor is affected by pressure. a) $\Delta C/C_0$ at a pressure stimuli of 600 Pa. b) $\Delta C/C_0$ at different pressures.

5.5.3 Capacitance change for proximity sensing

The principle of capacitive proximity sensing, on the other hand, hinges upon alterations in capacitance caused by induced charges stemming from the conductive body's proximity to the device. As depicted in **Figure 5.13**, the conductor and the electrode generate an induced charge when an object draws near the top electrode, leading to an electric field redistribution and consequent increases in capacitance. The generation of induced charges is contingent upon the conductor's charge, proximity distance, and proximity speed.

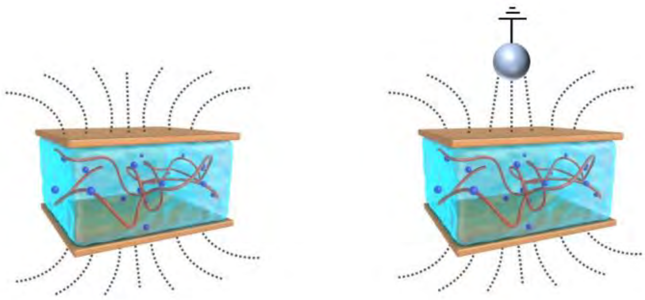

Figure 5.13 The capacitance of multimodal temperature sensor is affected by proximity.

In **Figure 5.14 a**, the multimodal temperature sensor's non-contact proximity sensing mode was demonstrated, specifically focused on object proximity detection. In this experiment, a finger moved closer to the electrodes positioned on the upper surface of the multimodal temperature sensor. As this occurs, the original electric field of the parallel-plate capacitor underwent modification, leading to the swift generation of an induced charge on the electrode surface. This charge manifested as a rapid reduction in electric potential, with a corresponding variation in $\Delta C/C_0$ of -0.45% observed at a proximity distance of 1 cm.

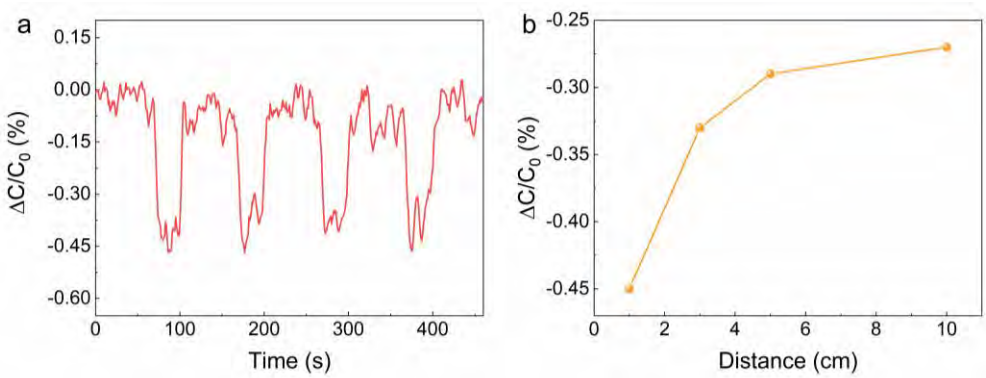

Figure 5.14 The capacitance of a multimodal temperature sensor is affected by approach. a) $\Delta C/C_0$ at an approaching excitement of 1cm. b) $\Delta C/C_0$ at different approaching distances.

Figure 5.14 b presents the graph depicting the normalized change in capacitance relative to the proximity distance for the multimodal temperature sensor when in the vicinity of a charged entity. The sensor exhibited a capacitive reaction to non-contact approaches and departures even at finger proximity distances of up to 10 cm from the electrodes, with a $\Delta C/C_0$ value of -0.27%. Diminishing the proximity to 5 cm and 3 cm led to a $\Delta C/C_0$ response of -0.29% and -0.33%, respectively. Consequently, the sensor demonstrates considerable sensitivity to object proximity and its rapid response aids in the identification of heat exchange patterns.

5.5.4 Temperature and pressure decoupling of multimodal temperature sensor

The multimodal temperature sensor effectively distinguishes external temperature and pressure stimuli by utilizing two distinct quantities: $ln(\tau)$ for temperature sensitivity and $\Delta C/C_0$ for pressure sensitivity, as described earlier. The performance of the multimodal temperature sensor was evaluated by testing its $ln(\tau)$ and $\Delta C/C_0$ response to changes in the heat source temperature, as illustrated in **Figure 5.15**. During multiple testing cycles, $ln(\tau)$ consistently increased from 11.03 to 11.36 as the heat source temperature increased from 25 °C to 30 °C. Furthermore, when the heat source temperature reached 45 °C, $ln(\tau)$ exhibited a synchronized response, reaching 12.21. Throughout the temperature shift range (25 °C - 45 °C) of the heat source, $\Delta C/C_0$, which was sensitive to pressure, remained at 0 in the absence of any pressure stimulation, indicating that it solely responded to changes in temperature.

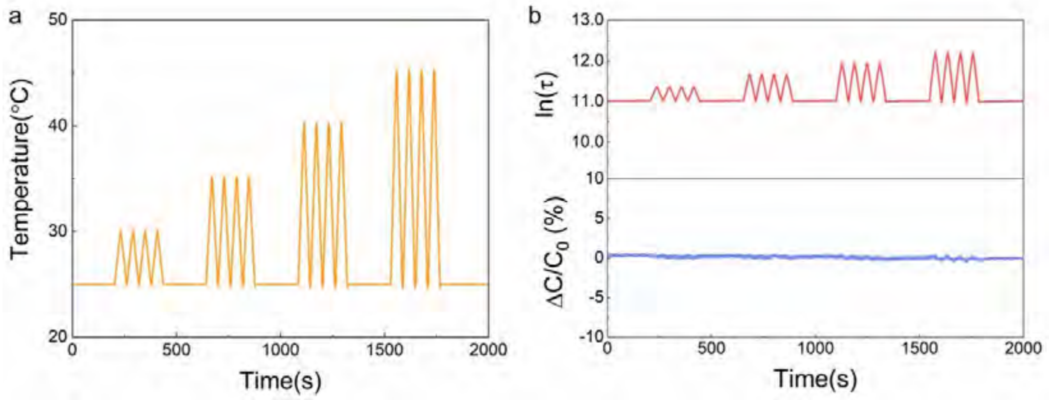

Figure 5.15 Signal response of multimodal temperature sensor under temperature stimulation. a) The temperature of the heat source. b) $ln(\tau)$ and $\Delta C/C_0$ at different temperature.

Similarly, the response of $ln(\tau)$ and $\Delta C/C_0$ of the multimodal temperature sensor under exclusive pressure stimuli was examined (**Figure 5.16**). The multimodal temperature sensor underwent cyclic pressure evaluations in a dedicated apparatus at room temperature. $\Delta C/C_0$ exhibited a rise from 0 to 1.99% and maintained stability across multiple tests as the pressure increased from 0 kPa to 5 kPa. Furthermore, $\Delta C/C_0$ climbed to 4.73% as the pressure source escalated to 20 kPa, aligning with the pressure stimulus. Notably, during the pressure transition (0 kPa - 20 kPa), $ln(\tau)$, acting as a temperature-sensitive parameter, hovered around 11.08, unaffected by the pressure stimulus and constant room temperature. The complete decoupling of temperature and pressure demonstrates that the multimodal temperature sensor has the potential to realize multimodal sensing in a single sensing unit with only a single signal output, laying the groundwork for subsequent heat-source-identification functions.

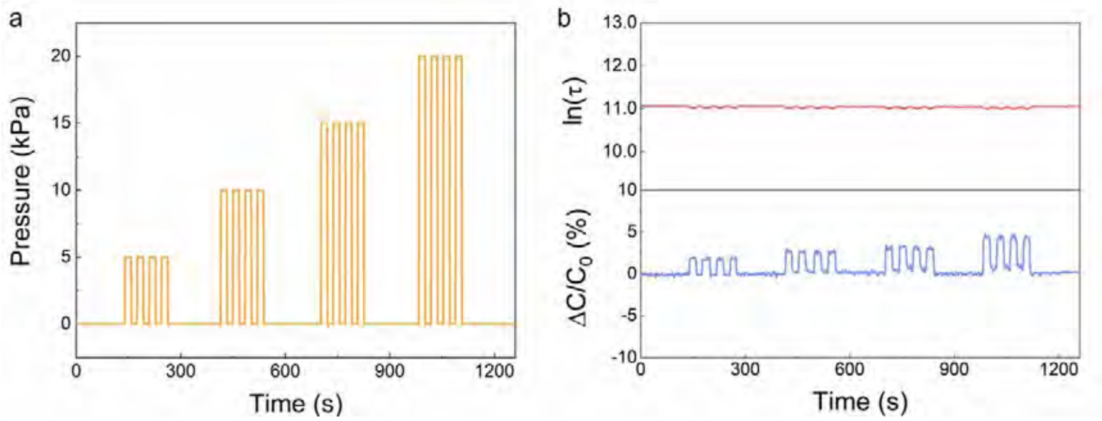

Figure 5.16 Signal response of multimodal temperature sensor under pressure stimulation. a) The pressure of the pressure source. b) $ln(\tau)$ and $\Delta C/C_0$ at different pressure.

5.6 Heat-source-identification for multimodal temperature sensor

The integumentary system of human skin plays a pivotal role in facilitating the body's interaction with the external environment, enabling the detection of various stimuli such as temperature, tactile sensations, and pain. The simultaneous integration of these diverse signals enhances an individual's overall well-being. Here, by harnessing the sensor's unique temperature, pressure, and proximity response mechanisms, it becomes feasible to accurately discern three distinct modes of heat transfer, encompassing thermal conduction, thermal convection, and thermal radiation.

5.6.1 Identification of thermal radiation

Thermal radiation is a heat transfer mode caused by the thermal motion of particles within matter, and it is one of the three modes of heat transfer. In this mode, the sensor responds solely to temperature variations originating from a heat source, without any external force stimulation or electrical charge induction. In order to evaluate the response of the multimodal temperature sensor to thermal radiation, a sunlight simulator was used as the stimulus source in the experiments conducted in this chapter. The exposure of the multimodal temperature sensor to simulated sunlight with a light intensity of 600 W/m^2 for a duration of 5 seconds is shown in **Figure 5.17**. The sensor consistently demonstrated temperature changes throughout four consecutive thermal radiation stimulations, with each radiation stimulus resulting in an approximate 0.3 °C increase in temperature ($ln(\tau)$ increased from 10.915 to 10.932). Importantly, the $\Delta C/C_0$ of the sensor remained constant during continuous thermal radiation stimulation. These consistent electrical responses provide evidence supporting the capability of the multimodal temperature sensor to detect and identify thermal radiation within the thermal sensing model.

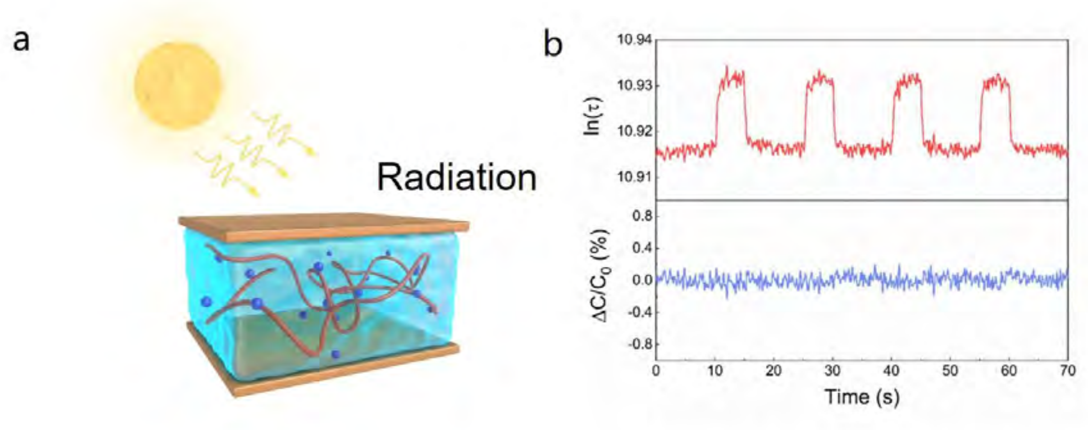

Figure 5.17 Multimodal temperature sensor stimulated by thermal radiation. a) The schematic diagram when stimulated by thermal radiation. b) $ln(\tau)$ and $\Delta C/C_0$ at a radiation intensity of 600 W/m^2.

The multimodal temperature sensor was tested for temperature response by subjecting it to a 5-second thermal radiation stimulus generated by simulated sunlight with varying intensities (**Figure 5.18**). A thermal radiation stimulus of 400 W/m^2 caused the sensor's temperature to increase by approximately 0.18 °C, while a radiation intensity of 1,000 W/m^2 resulted in a temperature increase of 0.63 °C. By measuring the temperature changes induced by different radiation intensities, it is possible to determine the radiation intensity of the thermal radiation stimulus on the sensor surface based on the amplitude of the temperature increase at a specific radiation time.

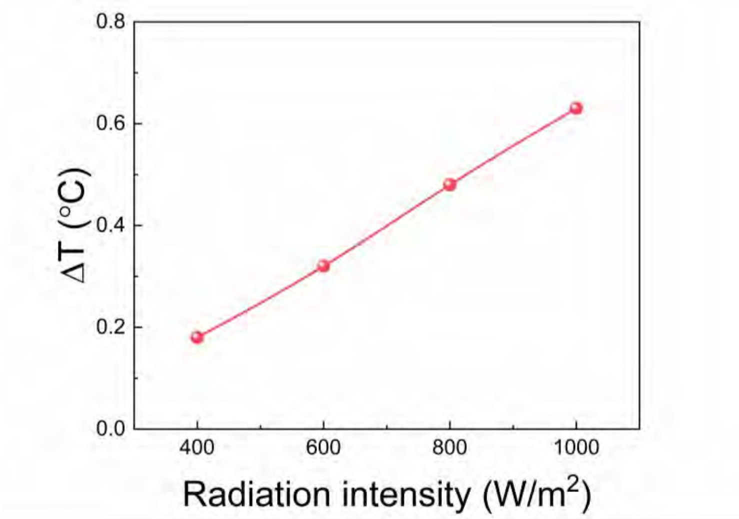

Figure 5.18 ΔT of multimodal temperature sensor stimulated by different radiation intensities.

5.6.2 Identification of thermal convection

Thermal convection is a heat transfer mechanism that involves the movement of liquids or gases. In this mode, the interaction between the sensor and the surrounding hot or cold air leads to a change in temperature. The sensor also experiences a change in capacitance due to the pressure exerted by the moving air on its surface. Thus, determining the heat source in thermal convection mode requires analyzing the variations in $ln(\tau)$ and $\Delta C/C_0$ caused by temperature and pressure stimuli. To investigate thermal convection, an air gun is attached to the upper end of the multimodal temperature sensor in this chapter. By controlling the rotational speed of the air gun and the size of the generated airspeed speed, an anemometer placed on the sensor's surface measures airspeed speed. **Figure 5.19** illustrates that subjecting the sensor to an air speed of 8 m/s for 5 seconds resulted in a rapid temperature increase of approximately 0.8 °C (leading to a shift from $ln(\tau)$ = 10.946 to $ln(\tau)$ = 10.992). Consequently, the sensor's temperature initially increased and then decreased. At the same time, the thermal convection stimulus caused the device to exhibit a $\Delta C/C_0$ of approximately 0.6% due to the pressure exerted by the airflow perpendicular to the sensor's surface. These findings distinguish thermal convection from a thermal radiation stimulus.

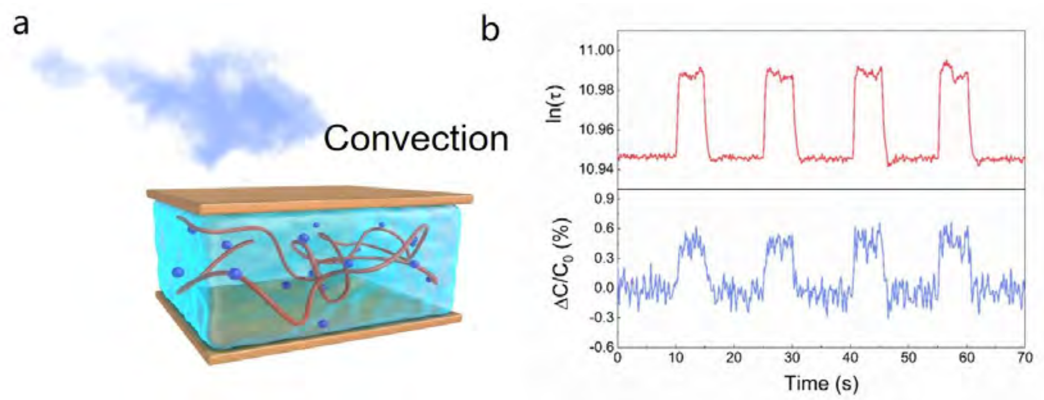

Figure 5.19 Multimodal temperature sensor stimulated by thermal convection. a) The schematic diagram when stimulated by thermal convection. b) $ln(\tau)$ and $\Delta C/C_0$ at a wind speed of 8 m/s.

In this study, a 5-second thermal stimulus was applied to the sensor using wind as the heat source in the thermal convection mode, as depicted in **Figure 5.20**. The main objective was to investigate the relationship between the wind stimulus and the variations in the normalized capacitance of the sensor at different wind speeds. Notably, the experimental results reveal a positive correlation between the magnitude of the capacitance change and the wind speed. Specifically, during thermal convective stimulation with a wind speed of 5 m/s, the change in $\Delta C/C_0$ was measured to be 0.38%. In comparison, it increased to 1.08% when the wind speed was raised to 14 m/s.

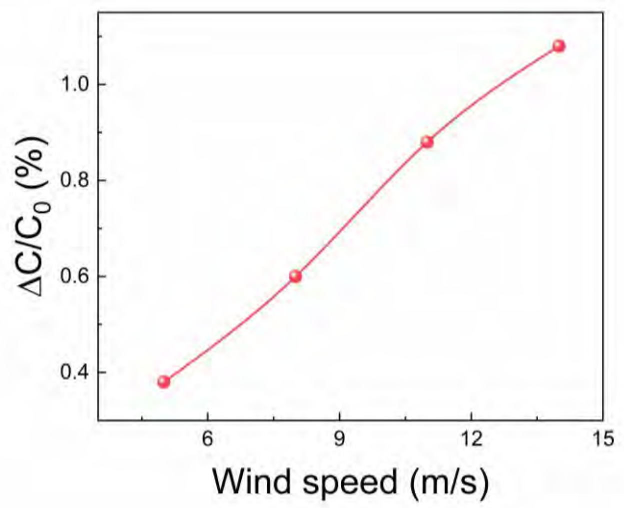

Figure 5.20 $\Delta C/C_0$ of multimodal temperature sensor stimulated by different wind speeds.

5.6.3 Identification of thermal conduction

Thermal conduction, a common method of heat transfer in natural systems, involves the interaction between an object and a heat source, resulting in heat transfer. To study this process, a multimodal temperature sensor can be used, which incorporates temperature, pressure, and proximity mechanisms. **Figure 5.21** illustrates the response of the multimodal temperature sensor to a thermally conductive stimulus. In this experiment, a finger was used as the heat source, applying a thermal stimulus to the device by continuously touching it for 5 seconds each time. Upon contact with the finger, the sensor shown a rapid increase in $ln(\tau)$ and $\Delta C/C_0$, indicating a rise in temperature and pressure. This resulted in a spike of approximately 6.4 °C ($ln(\tau)$ ranging from 10.966 to 11.298) and a 7% increase in $\Delta C/C_0$. Once the finger was removed, these values quickly returned to their initial levels. Interestingly, the capacitance signal exhibited a different behavior compared to the thermal convection stimulus, showing a negative spike of -1% before rising. This distinct behavior helps differentiate the negative capacitance change from the thermal convection mode. Before the finger makes contact with the sensor, the proximity process induces an inductive charge, affecting the surface electric field and generating a capacitance signal related to proximity sensing. This capacitance change opposes the pressure-sensing effect, making it easy to distinguish between the two heat source modes.

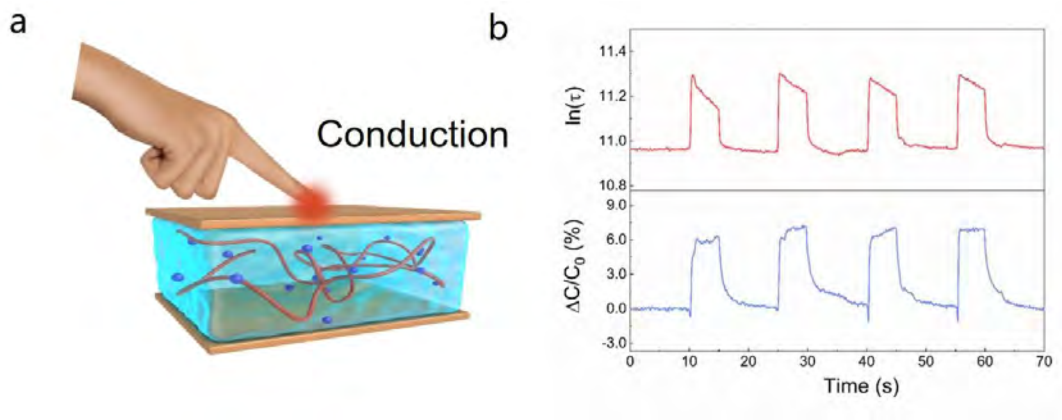

Figure 5.21 Multimodal temperature sensor stimulated by thermal conduction. a) The schematic diagram when stimulated by thermal conduction. b) $ln(\tau)$ and $\Delta C/C_0$ at a pressure stimulation of finger.

Figure 5.22 displays the change in $\Delta C/C_0$ of the multimodal temperature sensor when subjected to varying levels of finger-applied pressure. The findings demonstrated that the flexible ionic gel composition of the sensor allowed for deformation under different pressure intensities, resulting in an increase in capacitance. Specifically, under higher pressure conditions, the capacitance of the sensor was observed to change by more than 10%.

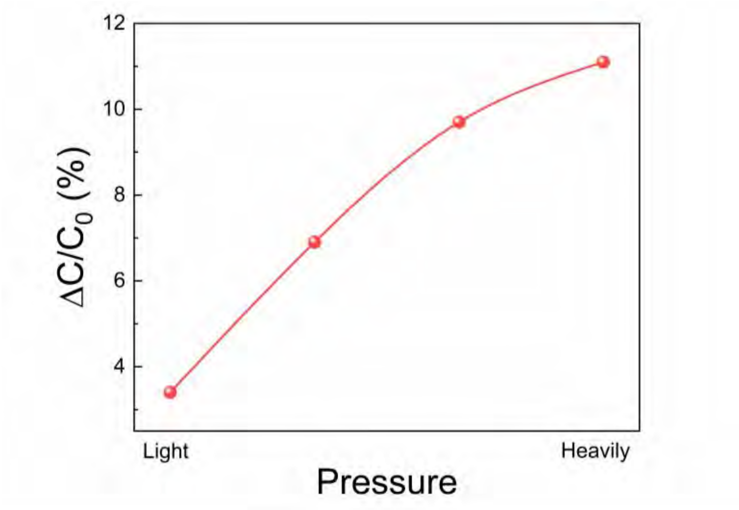

Figure 5.22 $\Delta C/C_0$ of multimodal temperature sensor stimulated by different pressures.

5.7 Outlook of sensor sensitivity

The multimodal temperature sensor, as a capacitive type of sensor, induces a change in capacitance in response to external pressure stimuli. However, during the recognition of the multimodal temperature sensor to the convective type of heat source, the thermal convective stimulus with a wind speed of 5 m/s caused only 0.38% change in $\Delta C/C_0$. This is due to the small relative deformation of the ionic gel and its inherent viscoelasticity resulting in a lower pressure sensitivity of the sensor. This is insufficient for the multimodal temperature sensor to sense small thermal convective responses.

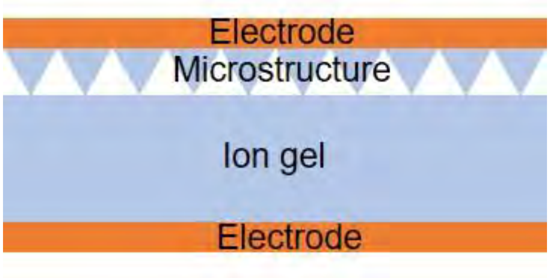

Figure 5.23 Microstructures improve the sensitivity of the pressure sensor.

The induction of different microstructures in the sensor aims to enhance the elastomeric strain, thereby improving the sensing range. This increase in sensitivity can be attributed to two main factors. Firstly, the presence of numerous voids in the microstructure film enables a lower elastic modulus, resulting in a greater deformation space when pressure is applied.[163-165] As a result, the distance between the electrodes can change more significantly under the same pressure stimulus, resulting in enhanced sensitivity. Secondly, the nodal constant of the polymer matrix surpasses the dielectric constant of air.[166-168] Consequently, when pressure is exerted, the polymer matrix fills the air volume, leading to a proportional increase in relative capacitance. Additionally, the microstructure reduces the elastomer's modulus of elasticity and viscoelasticity, further contributing to sensor sensitivity.[169, 170]

Sensors with microstructures can produce significant large structural changes at small strains, resulting in large changes in capacitance. Therefore, this type of highly sensitive sensor is ideal in application scenarios where small stress changes need to be detected.

5.8 Summary

In this chapter, signals from different heat sources are characterized by modeling. Thermal conduction has a temperature response, a pressure response, and a proximity response. Thermal convection has a temperature response and a pressure response. While thermal radiation has only a temperature response. Then, by using MPEG-DA ionogel as the active material, we developed a capacitively structured multimodal temperature sensor. The sensor responds to temperature, pressure, and proximity at the same time, making it a perfect fit for heat-source-identification. The multimodal temperature sensor offers excellent temperature sensing capability, an ultra-wide temperature range (-20 °C to 180 °C), a linear response to temperature (accuracy better than 0.005 °C), and outstanding stability. Meanwhile, based on the capacitive structure, the multimodal temperature sensor has significant positive capacitance change due to external deformation caused by pressure stimulation and negative capacitance change due to surface charge caused by proximity stimulation. Through experimental validation, we have successfully demonstrated the sensor's ability to accurately differentiate and recognize heat sources in all three modes of heat exchange: thermal radiation, thermal convection, and thermal conduction. As a result, we have realized intelligent multidimensional thermal sensing.

CHAPTER 6 INTEGRATION OF THERMOREGULATION AND THERMOSENSATION

6.1 Introduction

The integration of thermoregulation and thermosensation mechanisms described above constitutes a comprehensive thermo-sensory system. This system plays a critical role in the human body's perception and adaptation to the environment. Through the processes of thermosensation and thermoregulation, the human body receives information regarding the presence of heat and cold within both internal and external surroundings. Relying on the thermoregulatory system, the body achieves a delicate equilibrium of heat generation and dissipation, enabling the maintenance of normal physiological functions and ensuring a state of comfort.

Building upon the studies mentioned above, we have successfully developed an S-thermo-e-skin integrating a TE device with a PCM heat sink and a D-thermo-e-skin combining a flexible TE device with a Li-PAAm hydrogel. By implementing a PID control system, we have achieved isothermal regulation of the e-skin in complex temperature environments. To address the limitations of conventional temperature sensors in resolving temperature, we have also fabricated a multimodal temperature sensor utilizing the ion relaxation time. This innovative sensor not only has the capability to identify heat sources but also replicates the multi-dimensional thermosensation experienced by the human body.

Within this chapter, the integration of thermo-e-skin and multimodal temperature sensor yields a simulation of the human body's thermo-sensory system. Specifically, the temperature sensor within the PID control system, along with the multimodal temperature sensor, achieves multi-dimensional thermosensation for the e-skin. Complementarily, the thermo-e-skin emulates the human body's thermoregulation mechanism, facilitating isothermal regulation. Through experimental evaluations conducted under various environmental conditions, the synthesized e-skin successfully establishes a human-like thermo-sensory system that effectively combines sensing, feedback, and regulation functions.

6.2 Integration

The thermo-sensory system is essential to ensure a healthy life for the human organism. As shown in **Figure 6.1 a**, when temperature receptors in the skin are stimulated by external temperature (cold, warm, or hot), bioelectrical signals are generated and feedbacked to the nerve center for integration.[29] The nerve center then sends command signals to the temperature stimulus, changing the body's ability to generate or dissipate heat, and maintaining the body temperature in a comfortable state.

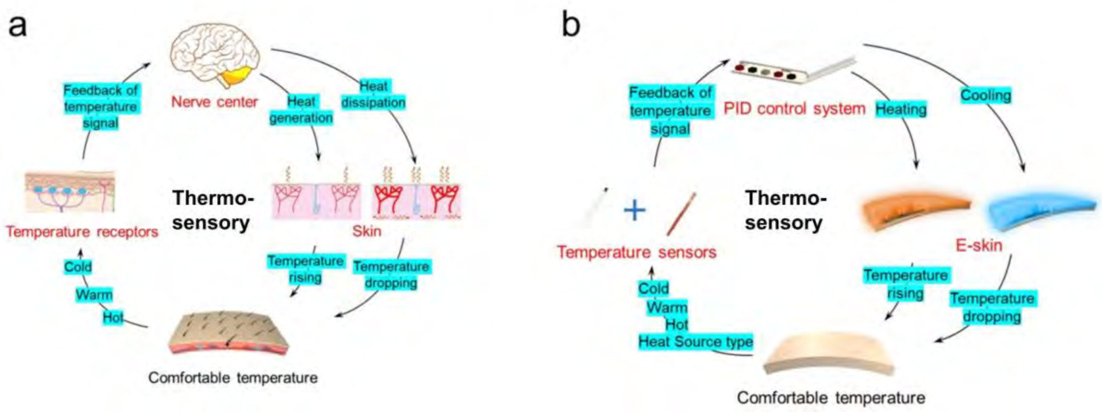

Figure 6.1 Thermo-sensory system of human and e-skin. a) The body's thermo-sensory system. b) The e-skin's thermo-sensory system.

This chapter presents a novel approach of integrating the multimodal temperature sensor and thermo-e-skin, inspired by the temperature sensory system in the human body. The system is controlled by a PID control system, which creates a thermo-sensory system that closely resembles that of a human body. As shown in **Figure 6.1 b**, both the PID's temperature sensor and the multimodal temperature sensor generate electrical signals in response to external temperature stimuli and heat sources. These signals are then sent back to the PID control system for analysis. The PID control system adjusts the temperature by regulating the electric current flowing through the thermoregulating e-skin, ensuring that the surface temperature of the e-skin remains within the desired range. In this setup, the temperature sensor of the PID system serves a dual role, acting as both the thermosensation for the thermo-sensory system and as a feedback circuit, reflecting the actual surface temperature of the e-skin. Furthermore, the multimodal temperature sensor enhances the system's capabilities by analyzing information related to the heat source.

As shown in **Figure 6.2 a-c**, a thermo-e-skin and a multimodal temperature sensor were integrated in a prosthesis and then were combined with a signal processing system to form a thermo-sensory system for a prosthesis that maintains a constant surface temperature (35 °C) while providing information on the temperature value of the thermal stimulus, the comfort level, and the type of heat source. The signal processing system can directly convert the temperature value through the correspondence between

$ln(\tau)$ and temperature. Meanwhile, it has been shown that the human body has different sensations to different temperature stimuli, feeling cold when it is lower than 30 °C, mild between 30 and 35 °C, and hot when it is higher than 35 °C. Therefore, the prosthesis can determine the comfort level of the heat source based on the temperature values. Finally, the multimodal temperature sensor has different signal responses to different heat source stimuli, which can be used as a basis for the prosthesis to recognize the type of heat source. Due to the fluctuating nature of the ambient thermal stimuli, $|\Delta C/C_0| \leqslant 0.2$, $\Delta C/C_0 > 0.2$, $\Delta C/C_0 < 0.2$ & $\Delta C/C_0 > 0.2$ are used as the signal characteristics of thermal radiation, thermal convection, and thermal conduction, respectively (**Figure 6.2 d**).

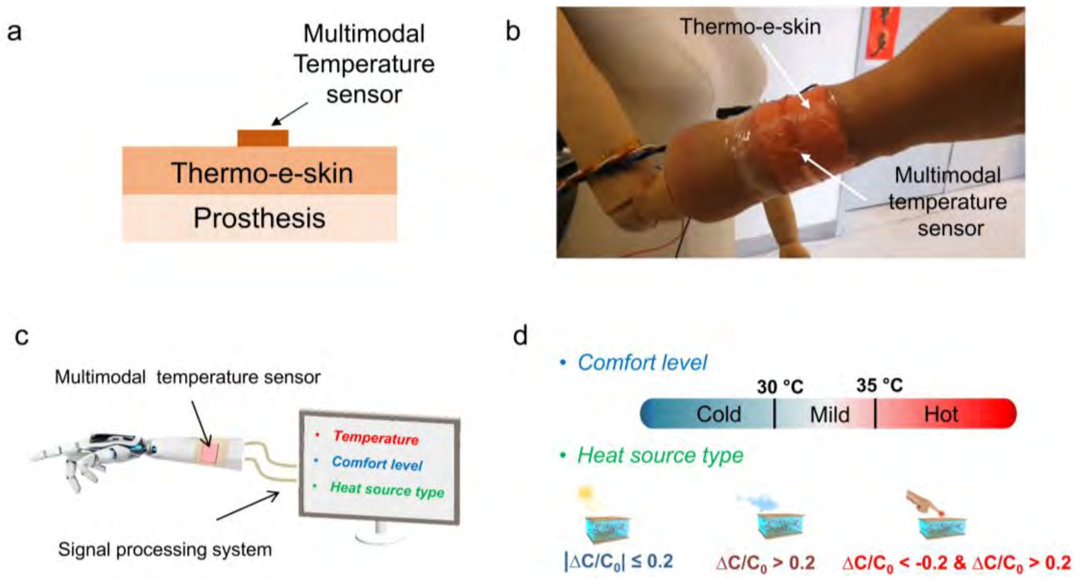

Figure 6.2 Establishment of the thermo-sensory system for e-skin. Schematic a) and photo b) of the e-skin thermo-sensory system. c) Multidimensional thermo-sensory systems for prosthesis. d) Recognition basis for a multi-dimensional thermo-sensory system.

6.3 Environment response performance

The body's thermo-sensory system is able to regulate internal and external temperature stimuli accordingly, thus keeping the body within a comfortable temperature range. Here, the thermo-sensory system of the e-skin demonstrates its ability to perform both internal and external regulation.

6.3.1 Internal regulation within the prosthesis

The thermo-sensory system of the human body is instrumental in regulating internal temperature. Similarly, the e-skin's thermo-sensory system enables the monitoring and regulation of internal temperature, allowing it to maintain a consistent surface temperature in different environments. This concept is illustrated in **Figure 6.2**, which depicts the e-skin transitioning from a lower temperature to a comfortable temperature when exposed to a room temperature environment. The temperature sensor of the PID system detected the lower temperature (25 °C) and provided feedback to the control system. Subsequently, the control system adjusted the current level, resulting in heating of the e-skin's surface. Consequently, the surface temperature rapidly rose from room temperature to 35 °C and remained stable for an extended period. During this thermoregulation process, changes in the ion relaxation time of the multimodal temperature sensor reflected the adjustments made to maintain the desired temperature. With a constant temperature of 35 °C, the prosthesis possessed temperature properties akin to those of the human body, facilitating emotional interaction with the external environment.

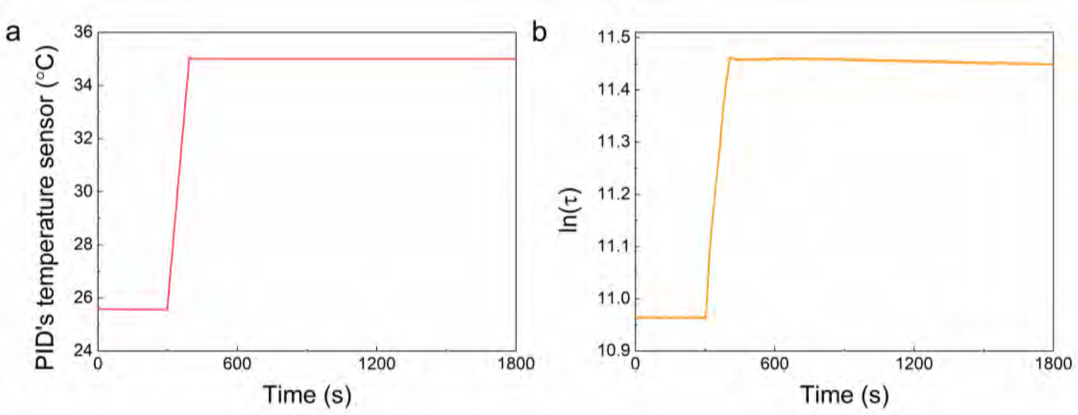

Figure 6.3 Internal regulation within the prosthesis. a) The temperature of the e-skin detected by the temperature sensor of the PID. b) The temperature of the e-skin detected by the multimodal temperature sensor.

The e-skin underwent a temperature elevation process from ambient conditions to achieve a comfortable temperature, mirroring the metabolic process of the human body's thermo-sensory system. This transition necessitates a corresponding expenditure of energy, as depicted in **Figure 6.3**. During the thermoregulation of the e-skin, the energy cost experienced a swift ascent from 0 to 56 mW/cm^2. This electrical energy was promptly converted into thermal energy, leading to an increase in the e-skin's surface temperature. Subsequently, as the surface temperature stabilized at 35°C, the energy cost gradually diminished and settles at approximately 38 mW/cm^2.

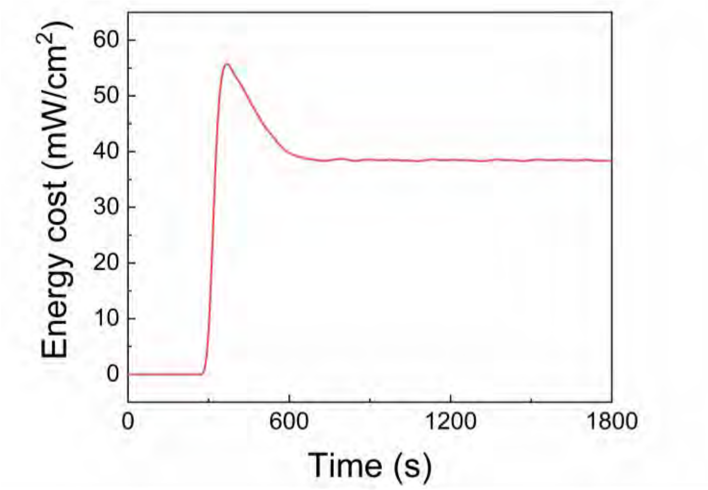

Figure 6.4 Energy cost of the e-skin to maintain a constant temperature.

6.3.2 External regulation of the outside environment

After the e-skin's thermo-sensory system maintains the surface temperature at 35°C, we simulated an experiment in which a prosthesis receives different temperature stimuli in an external environment as a way to verify the effectiveness of the thermo-sensory system. The experimental scenario consisted of the prosthesis being exposed to sunlight outside (Scenario I), moving from outside to inside to receive convective winds (Scenario II), and finally indoors to shake hands with other people (Scenario III) (**Figure 6.4**).

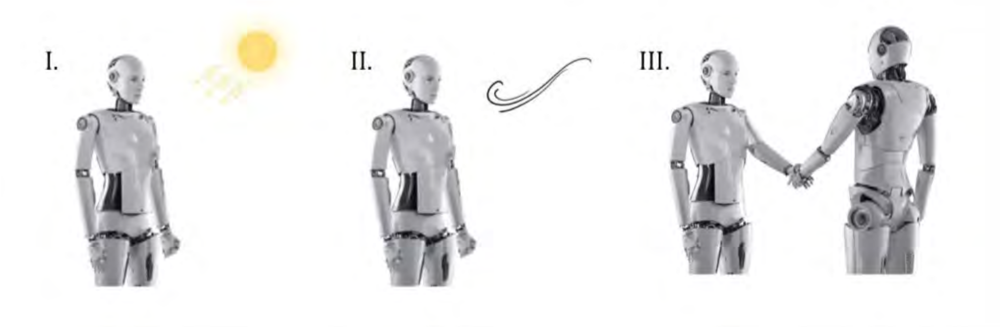

Figure 6.5 The thermo-sensory system of e-skin in different scenarios.

In Scenario I, the prosthesis was exposed to the sun and the heat from the sun affects the surface temperature of the prosthesis by means of radiation. At this time, the multimodal temperature sensor detects the temperature stimulus and transmits the signal to the signal processing system. The prosthesis can then determine a temperature value of 35.42 °C, with a body sensation of hot, and the heat source type of thermal radiation. At the same time, the e-skin would cause the surface temperature to oscillate because of the heat, and this oscillation would be quickly corrected by the thermo-sensory system to maintain a constant temperature (**Figure 6.5**).

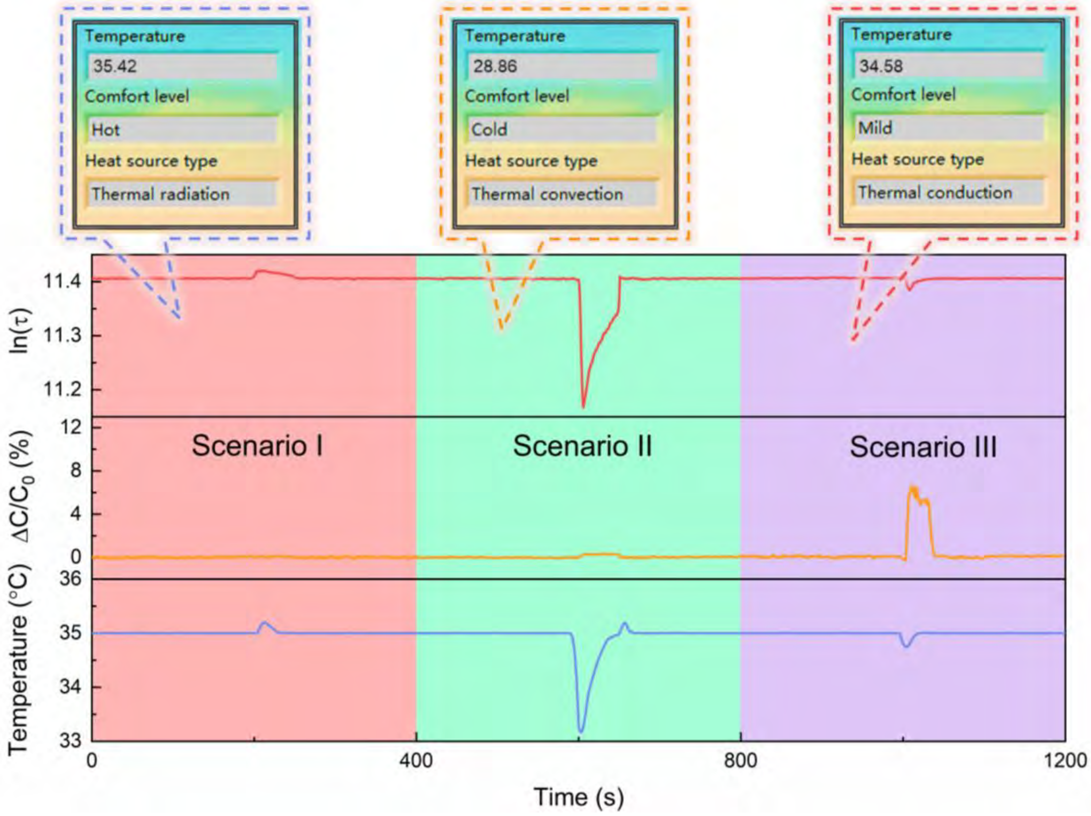

Figure 6.6 The thermo-sensory of prosthesis in different scenarios.

In Scenario II, the prosthesis was in a convective environment where the e-skin was able to utilize its thermo-sensory system for sensation and regulation purposes. The prosthesis relied on the multimodal temperature sensor and the signal processing system to determine that the temperature value was 28.86 °C, with the body sensation of cold, and the heat source type of thermal convection. When the electronic skin is exposed to cold air, the surface temperature decreases. In order to quickly restore the surface temperature to 35 °C, the control system initiates the heating process.

In Scenario III, the prosthesis shaked hands with other people, a process that involved direct heat transfer. According to the $ln(\tau)$ and $\Delta C/C_0$ values of the multimodal temperature sensor, the prosthesis was simultaneously subjected to temperature stimulus, proximity stimulus, and pressure stimulus, and determined that the temperature at this time was 34.58 °C, with a mild body sensation, and the type of heat source was thermal conduction. At the moment of contact, heat was rapidly conducted, resulting in a decrease in the surface temperature of the e-skin. In response, the control system swiftly initiated heat generation to elevate the surface temperature to 35 °C.

Simultaneously, it was observed that there is a discernible alteration in the energy cost of the e-skin required to sustain a consistent surface temperature of 35 °C (**Figure 6.7**). In response to Scenario I, the e-skin exhibited an isothermal regulation mechanism by decreasing its internal heat generation to achieve temperature stability. This resulted in a reduction in energy cost from 38.1 mW/cm^2 to 37.35 mW/cm^2. In Scenario II, the e-skin similarly exhibits a self-regulating thermal behavior that allows it to produce large amounts of heat when exposed to low temperatures. Thus, this adaptive mechanism enables the e-skin to maintain a stable temperature while reducing the energy cost from 38 mW/cm^2 to 42.9 mW/cm^2. In Scenario III, rapid heat exchange caused temperature fluctuations on the surface of the e-skin. To maintain the isothermal regulation of the e-skin, it increased its heat production to keep thermal balance. Consequently, the energy cost of the e-skin escalated from 38 mW/cm^2 to 39.3 mW/cm^2.

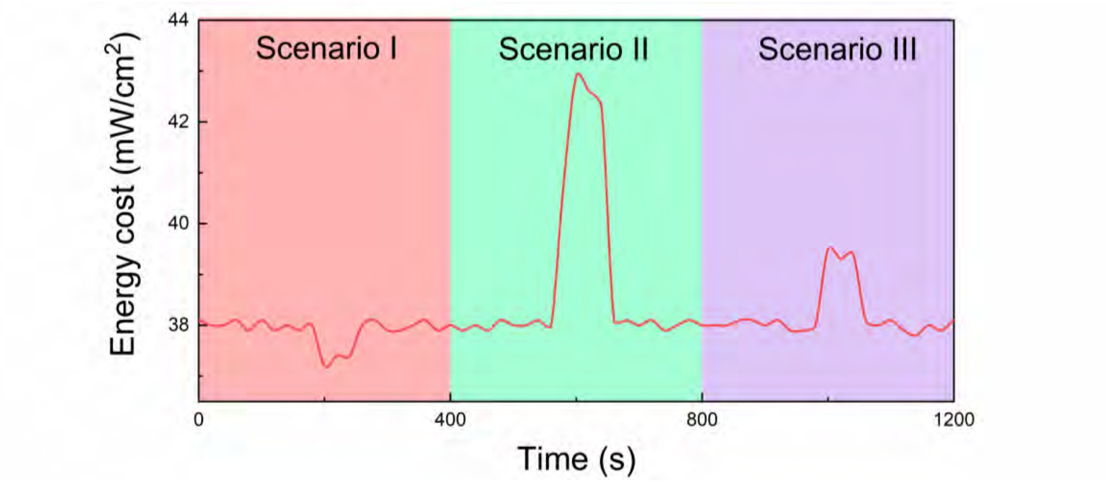

Figure 6.7 Energy cost of the e-skin to maintain a constant temperature in different scenarios.

6.5 Challenge in thinner thermo-e-skin

Thermo-e-skin has good bending properties and has been demonstrated for use in prosthesis. However, thermo-e-skin with flexible TE device structures based on bulk thermoelectric materials possesses a large thickness (about 4 mm), which results in only limited flexibility. As a result, the thermo-e-skin can only be applied on large curved surfaces with small curvature, while it is still challenging to apply it on fine areas with small curvature, such as fingers or joints (**Figure 6.8**).

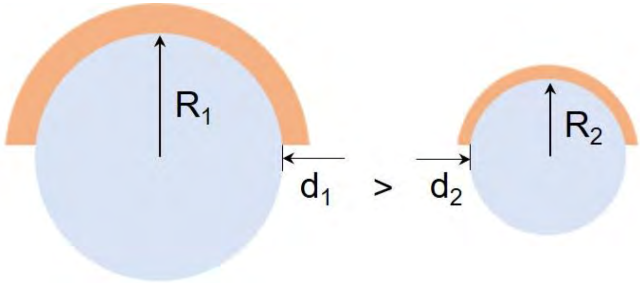

Figure 6.8 Excessive thickness affects the flexibility of the thermo-e-skin.

Reducing the thickness of thermo-e-skin components has been identified as the most effective method to enhance flexibility. Thin-film TE materials, in particular, have garnered significant attention due to their remarkable flexibility.[171] Of these materials, two-dimensional substances like graphene exhibit exceptional flexibility alongside favorable electrical and thermal transport properties, thus presenting immense potential for flexible Peltier cooling.[172-174] However, the high thermal conductivity of graphene limits the overall ZT values achieved. On the other hand, organic TE materials offer excellent flexibility, low thermal conductivity, and the added benefit of solution processability.[175, 176] Nonetheless, the low electrical conductivity of organic TE materials often leads to a notable Joule heating effect, thus hindering their successful implementation for flexible cooling applications.

The current level of flexibility exhibited by TE cooling devices is not yet satisfactory. To enhance the mechanical and TE properties of inorganic TE materials, the utilization of ultrathin, low-dimensional, and amorphous materials is deemed beneficial. However, further research is required to explore the potential of organic TE materials with good flexibility for application in flexible cooling systems.

6.5 Summary

In this chapter, the integration of a thermo-e-skin, multimodal temperature sensor, and PID control system within a prosthesis enables the development of a thermo-sensory system for e-skin. This constructed system replicates the thermoregulation mechanism found in the human body, encompassing thermosensation, heat-source-identification, signal feedback, and thermoregulation. Consequently, it achieves the resolution of diverse temperature stimulation signals in complex environments while ensuring the e-skin surface temperature remains within the comfort zone. The design enables the e-skin to have a human-like thermo-sensory system, which is important for the development of next-generation prosthetic limbs and intelligent robots.

CHAPTER 7 CONCLUSIONS AND SUGGESTIONS FOR FUTURE RESEARCH

7.1 Conclusions

The objective of this research is to develop an e-skin system that mimics human thermoregulation, thereby enhancing comfort and maintaining isothermal regulation in complex temperature environments. This involves modifying the temperature properties of conventional e-skin. To achieve this, two key components are integrated into the bionic thermo-sensory design. Firstly, flexible thermoelectric (TE) devices and other thermal management methods are incorporated to achieve human-like thermoregulation. Secondly, the properties of ion relaxation time are utilized for thermosensation, enabling the detection of heat sources. The subsequent section of this paper presents the significant findings of the study.

(a) The S-thermo-e-skin, a combination of a TE device and a PCM heat sink, has the capability to generate heat in low-temperature environments and dissipate heat in high-temperature environments. Experimental results have shown that this S-thermo-e-skin can maintain a constant surface temperature of 35 °C over a wide temperature range of 10-45 °C. This functionality is similar to the isothermal regulation of the human body, where it can maintain a stable temperature of 35 °C for extended periods even in colder environments. However, the heat storage capacity of the PCM limits its performance when exposed to temperatures above 35 °C. Remarkably, even at a temperature of 40 °C, the S-thermo-e-skin can sustain a surface temperature of 35 °C for approximately 1.5 hours, and for 0.75 hours even at 45 °C. The S-thermo-e-skin requires energy consumption to maintain a constant temperature similar to the metabolic processes of the human body. The amount of energy consumed depends on the ambient temperature, with the lowest energy cost occurring in the thermoneutral zone (14.22 mW/cm^2 at an ambient temperature of 35 °C) and significantly higher energy costs outside of the thermoneutral zone (71.32 mW/cm^2 at an ambient temperature of 10 °C).

(b) The D-thermo-e-skin comprises a flexible TE device and a Li-PAAm hydrogel composite, enabling both active TE thermoregulation and passive water evaporation. This novel combination facilitates the integration of heat generation and heat dissipation, ensuring the surface temperature of the D-thermo-e-skin remains at 35 °C within a wide temperature range of 10-45 °C. The inclusion of active and passive regulation layers significantly enhances the effective time of the D-thermo-e-skin in diverse environmental conditions. Specifically, at an ambient temperature of 25 °C, the D-thermo-e-skin demonstrates an effective time of 4.5 hours, while at an ambient temperature of 40 °C, it maintains thermoregulation for 4.2 hours. Furthermore, the hygroscopic properties of the hydrogel enable the D-thermo-e-skin to be rehydrated and reused after isothermal regulation, with a swift recovery time of just four hours under 90% humidity conditions. Additionally, the D-thermo-e-skin showcases rapid thermoregulation capabilities surpassing those of human skin. It rapidly achieves a surface temperature of approximately 32 °C within seconds of contact with various objects, utilizing the cooling or heating function of the flexible TE device.

(c) We propose a multimodal heat sensing signal model based on the signal differences of different heat sources. The model can accurately distinguish and identify heat sources in three modes of heat exchange: thermal radiation, thermal convection and thermal conduction, thus realizing multi-dimensional intelligent heat sensing. We then designed a capacitive multimodal temperature sensor based on ion relaxation dynamics to enable it to respond to temperature, proximity, and pressure stimuli simultaneously. The sensor shows a highly linear response (R^2 = 0.993) over the temperature range of -20 °C to 180 °C, making it ideal for thermal sensing. It also exhibits impressive accuracy with a temperature measurement precision of less than 0.005 °C and excellent stability, further confirming its superior temperature measurement capabilities. The multimodal temperature sensor demonstrates its potential for multitasking thermal sensing by efficiently separating temperature and pressure signals using temperature-sensitive ion relaxation times and pressure-sensitive normalized capacitance. Finally, we experimentally verified the response of the multimodal temperature sensor under different heat sources, demonstrating its effectiveness in the field of heat source identification.

(d) The prosthesis was outfitted with an integrated thermo-sensory system consisting of the thermo-e-skin, multimodal temperature sensor, and PID control system. This integration enabled the realization of an e-skin thermo-sensory system. Replicating the thermoregulation mechanism found in the human body, a thermo-sensory system of e-skin encompasses thermosensation, heat-source-identification, signal feedback, and thermoregulation capabilities. The system excels in resolving various temperature stimulation signals even in complex environments while ensuring that the surface temperature of the e-skin remains within the comfort zone.

7.2 Suggestions for future research

This thesis concentrates on achieving thermoregulation and thermosensation capabilities in e-skin, ultimately constructing a bionic thermosensation system akin to human skin. Nonetheless, certain limitations persist, necessitating future endeavors for further advancements. We assert that several pivotal aspects must be considered for the future progress of this field:

1. Thermo-e-skin demonstrates commendable thermoregulation capabilities. However, its composite structure imposes restrictions on its flexibility. As previously mentioned, the TE device, composed of bulk TE material, achieves bi-directional bending through circuit design. Nevertheless, the e-skin thickness exceeds 4 mm after encapsulation with PCM heat sink or hydrogel composite material, resulting in limited flexibility. To achieve a unified thermoregulation e-skin that excels in both flexibility and regulation performance, future endeavors should focus on developing superior flexible, high-performance TE materials, along with advanced encapsulation strategies.

2. The D-thermo-e-skin comprising a TE device and a Li-PAAm hydrogel demonstrated effective thermoregulation capabilities at 40 °C for a duration of 4.2 hours. However, when subjected to water evaporation, simulating human sweat, only a modest reduction of 11.54 wt.% was observed. This can be attributed to the sluggish transfer of excess heat generated at the hot side of the flexible TE device to the

hydrogel. As a result, water evaporation failed to reach its maximum potential before the TE device became incapable of regulating temperature. Moving forward, it is necessary to address the issue by reducing the thermal resistance between the flexible TE device and the hydrogel. This can be achieved through the design of a foam structure that facilitates efficient heat transfer or by employing encapsulation materials with higher thermal conductivity.

3. The bulk capacitance of the multimodal temperature sensor is constrained by the geometry of the parallel plate capacitor, though it successfully identifies heat sources. This restriction limits the sensor's capacitive response solely to the lower pressure range, rendering it insensitive to certain minute, low-pressure stimuli. This inadequacy hinders the measurement of subtle thermal convection stimuli. Incorporating microstructures into ionic conductors or electrodes presents a viable solution for optimizing performance to enhance the sensitivity and detection limit of pressure sensing in multimodal sensing applications.

4. The integration of a thermo-e-skin, a multimodal temperature sensor, and a PID control system, has successfully achieved biomimetic thermo-sensation. However, the current multimodal temperature sensor faces challenges in directly providing temperature signal feedback to the PID control system, thereby limiting the supplementation of the PID temperature sensor. To enhance the intelligent temperature feedback capabilities of the electronic skin, it is recommended to design corresponding circuit hardware and software that utilize the response of the multimodal temperature sensor as the signal input for the PID control system.

Reference

1. Chortos A, Liu J, Bao Z. Pursuing prosthetic electronic skin. Nature materials. 2016; 15(9):937-950.

2. Abraira VE, Ginty DD. The sensory neurons of touch. Neuron. 2013; 79(4):618-639.

3. Hammock ML, Chortos A, Tee BCK, Tok JBH, Bao Z. 25th anniversary article: The evolution of electronic skin (e-skin): A brief history, design considerations, and recent progress. Advanced Materials. 2013; 25(42):5997-6037.

4. Lee Y, Park J, Choe A, Cho S, Kim J, Ko H. Mimicking human and biological skins for multifunctional skin electronics. Advanced Functional Materials. 2020; 30(20) : 1904523.

5. Oh JY, Bao Z. Second skin enabled by advanced electronics. Advanced Science. 2019; 6(11) : 1900186.

6. Wang M, Luo Y, Wang Tet al. Artificial skin perception. Advanced Materials. 2021; 33(19) : 2003014.

7. Kim JJ, Wang Y, Wang H, Lee S, Yokota T, Someya T. Skin electronics: Next-generation device platform for virtual and augmented reality. Advanced Functional Materials. 2021; 31(39) : 2009602.

8. Liu Y, Pharr M, Salvatore GA. Lab-on-skin: A review of flexible and stretchable electronics for wearable health monitoring. Acs Nano. 2017; 11(10):9614-9635.

9. Wang S, Oh JY, Xu J, Tran H, Bao Z. Skin-inspired electronics: An emerging paradigm. Accounts of Chemical Research. 2018; 51(5):1033-1045.

10. Costa JC, Spina F, Lugoda P, Garcia-Garcia L, Roggen D, Munzenrieder N. Flexible sensors-from materials to applications. Technologies. 2019; 7(2) : 35.

11. Yuan Y, Liu B, Li Het al. Flexible wearable sensors in medical monitoring. Biosensors-Basel. 2022; 12(12) : 1069.

12. Liu M, Pu X, Jiang Cet al. Large-area all-textile pressure sensors for monitoring human motion and physiological signals. Advanced materials. 2017; 29(41):1703700.

13. Zhang X, Chen J, He J, Bai Y, Zeng H. Mussel-inspired adhesive and conductive hydrogel with tunable mechanical properties for wearable strain sensors. Journal of Colloid and Interface Science. 2021; 585:420-432.

14. Joh H, Lee SW, Seong M, Lee WS, Oh SJ. Engineering the charge transport of ag nanocrystals for highly accurate, wearable temperature sensors through all-solution processes. Small. 2017; 13(24):1700247.

15. Chen H, Song Y, Guo Het al. Hybrid porous micro structured finger skin inspired self-powered electronic skin system for pressure sensing and sliding detection. Nano Energy. 2018; 51:496-503.

16. Lee H, Choi TK, Lee YBet al. A graphene-based electrochemical device with thermoresponsive microneedles for diabetes monitoring and therapy. Nature nanotechnology. 2016; 11(6):566-572.

17. Bandodkar AJ, Jia W, Yardımcı C, Wang X, Ramirez J, Wang J. Tattoo-based noninvasive glucose monitoring: A proof-of-concept study. Analytical chemistry. 2015; 87(1):394-398.

18. Pang Y, Jian J, Tu Tet al. Wearable humidity sensor based on porous graphene network for respiration monitoring. Biosensors and Bioelectronics. 2018; 116:123-129.

19. Zhao J, Guo H, Pang YKet al. Flexible organic tribotronic transistor for pressure and magnetic sensing. ACS nano. 2017; 11(11):11566-11573.

20. Craig AD. Pain mechanisms: Labeled lines versus convergence in central processing. Annual Review of Neuroscience. 2003; 26:1-30.

21. Hall JE, Hall ME. Guyton and hall textbook of medical physiology e-book. Elsevier Health Sciences. 2020.

22. Lillywhite HB. Behavioral temperature regulation in the bullfrog, rana catesbeiana. Copeia. 1970:158-168.

23. Hong SY, Lee YH, Park Het al. Stretchable active matrix temperature sensor array of polyaniline nanofibers for electronic skin. Advanced materials. 2016; 28(5):930-935.

24. Li Q, Zhang LN, Tao XM, Ding X. Review of flexible temperature sensing networks for wearable physiological monitoring. Advanced healthcare materials. 2017; 6(12):1601371.

25. Su Y, Ma C, Chen Jet al. Printable, highly sensitive flexible temperature sensors for human body temperature monitoring: A review. Nanoscale Research Letters. 2020; 15:1-34.

26. Barmpakos D, Kaltsas G. A review on humidity, temperature and strain printed sensors-current trends and future perspectives. Sensors. 2021; 21(3) : 739.

27. Li M-Z, Han S-T, Zhou Y. Recent advances in flexible field-effect transistors toward wearable sensors. Advanced Intelligent Systems. 2020; 2(11) : 2000113.

28. Li W-D, Ke K, Jia Jet al. Recent advances in multiresponsive flexible sensors towards e-skin: A delicate design for versatile sensing. Small. 2022; 18(7) : 2103734.

29. Nakamura K. Central circuitries for body temperature regulation and fever. American journal of Physiology-Regulatory, integrative and comparative Physiology. 2011; 301(5):1207-1228.

30. Jessen C. Temperature regulation in humans and other mammals. Springer Science & Business Media. 2012.

31. Stolwijk JA, Hardy J. Temperature regulation in man—a theoretical study. Pflüger's Archiv für die gesamte Physiologie des Menschen und der Tiere. 1966; 291(2):129-162.

32. Lumpkin EA, Caterina MJ. Mechanisms of sensory transduction in the skin. Nature. 2007; 445(7130):858-865.

33. Patapoutian A, Peier AM, Story GM, Viswanath V. Thermotrp channels and beyond: Mechanisms of temperature sensation. Nature Reviews Neuroscience. 2003; 4(7):529-539.

34. Venkatachalam K, Montell C. Trp channels. Annual Review of Biochemistry. 2007; 76:387-417.

35. Gordon CJ. Temperature and toxicology: An integrative, comparative, and environmental approach. CRC press. 2005.

36. Cabanac M. Temperature regulation. Annual review of physiology. 1975; 37(1):415-439.

37. Robergs RA, Roberts S. Exercise physiology. Exercise, performance, andclinical applications. St. Louis: Mosby-Year Book. 1997; 840.

38. Hardy JD. Physiology of temperature regulation. Physiological reviews. 1961; 41(3):521-606.

39. Arens EA, Zhang H. The skin's role in human thermoregulation and comfort. 2006.

40. Hardy JD. The radiation of heat from the human body. Journal of Clinical Investigation. 1934; 13(4):593-604.

41. Anderson GS. Human morphology and temperature regulation. International Journal of Biometeorology. 1999; 43:99-109.

42. Gagge AP, Gonzalez RR. Mechanisms of heat exchange: Biophysics and physiology. Comprehensive physiology. 2010:45-84.

43. Baker LB. Physiology of sweat gland function: The roles of sweating and sweat composition in human health. Temperature. 2019; 6(3):211-259.

44. Hanna JM, Brown DE. Human heat tolerance: An anthropological perspective. Annual Review of Anthropology. 1983; 12(1):259-284.

45. Terrien J, Perret M, Aujard F. Behavioral thermoregulation in mammals: A review. Frontiers in Bioscience-Landmark. 2011; 16(4):1428-1444.

46. Cai J, Du M, Li Z. Flexible temperature sensors constructed with fiber materials. Advanced Materials Technologies. 2022; 7(7) : 2101182.

47. Feng Y, Liu H, Zhu Wet al. Muscle-inspired mxene conductive hydrogels with anisotropy and low-temperature tolerance for wearable flexible sensors and arrays. Advanced Functional Materials. 2021; 31(46) : 2105264.

48. Gu Y, Zhang T, Chen Het al. Mini review on flexible and wearable electronics for monitoring human health information. Nanoscale Research Letters. 2019; 14: 1-15.

49. Nakata S, Arie T, Akita S, Takei K. Wearable, flexible, and multifunctional healthcare device with an isfet chemical sensor for simultaneous sweat ph and skin temperature monitoring. Acs Sensors. 2017; 2(3):443-448.

50. Tran Quang T, Lee N-E. Flexible and stretchable physical sensor integrated platforms for wearable human-activity monitoring and personal healthcare. Advanced Materials. 2016; 28(22):4338-4372.

51. Chen J, Zhu Y, Chang Xet al. Recent progress in essential functions of soft electronic skin. Advanced Functional Materials. 2021; 31(42) : 2104686.

52. Khan Y, Ostfeld AE, Lochner CM, Pierre A, Arias AC. Monitoring of vital signs with flexible and wearable medical devices. Advanced Materials. 2016; 28(22):4373-4395.

53. Hua Q, Sun J, Liu Het al. Skin-inspired highly stretchable and conformable matrix networks for multifunctional sensing. Nature communications. 2018; 9(1):244.

54. Shih W-P, Tsao L-C, Lee C-Wet al. Flexible temperature sensor array based on a

graphite-polydimethylsiloxane composite. Sensors. 2010; 10(4):3597-3610.

55. Webb RC, Bonifas AP, Behnaz Aet al. Ultrathin conformal devices for precise and continuous thermal characterization of human skin. Nature Materials. 2013; 12(10):938-944.

56. Choi H, Li X. Fabrication and application of micro thin film thermocouples for transient temperature measurement in nanosecond pulsed laser micromachining of nickel. Sensors and Actuators A: Physical. 2007; 136(1):118-124.

57. Assumpcao D, Kumar S, Narasimhan V, Lee J, Choo H. High-performance flexible metal-on-silicon thermocouple. Scientific reports. 2018; 8(1):13725.

58. Shiran Chaharsoughi M, Zhao D, Crispin X, Fabiano S, Jonsson MP. Thermodiffusion‐assisted pyroelectrics—enabling rapid and stable heat and radiation sensing. Advanced Functional Materials. 2019; 29(28):1900572.

59. Root W, Bechtold T, Pham T. Textile-integrated thermocouples for temperature measurement. Materials. 2020; 13(3) : 626.

60. Wu P, He Z, Yang Met al. A review on flexible thermoelectric technology: Material, device, and applications. International Journal of Thermophysics. 2021; 42(8) : 111.

61. Zhang F, Zang Y, Huang D, Di C-a, Zhu D. Flexible and self-powered temperature–pressure dual-parameter sensors using microstructure-frame-supported organic thermoelectric materials. Nature communications. 2015; 6(1):8356.

62. Lee J, Kim HJ, Ko YJet al. Enhanced pyroelectric conversion of thermal radiation energy: Energy harvesting and non-contact proximity sensor. Nano Energy. 2022; 97:107178.

63. Albrecht A, Rivadeneyra A, Bobinger Met al. Scalable deposition of nanomaterial-based temperature sensors for transparent and pervasive electronics. Journal of Sensors. 2018; 7102069.

64. Ma Z, Zhang J, Li J, Shi Y, Pan L. Frequency-enabled decouplable dual-modal flexible pressure and temperature sensor. Ieee Electron Device Letters. 2020; 41(10):1568-1571.

65. Othayq MM, Giganti N, Shavezipur M. Development of capacitive temperature sensors with high sensitivity using a multiuser polycrystalline silicon process. Microelectronic Engineering. 2020; 226

66. Rao L, Ding J. Capacitive sensor for testing railroad's temperature stress. Journal of Transducer Technology. 2005; 24(2):60-65.

67. Othayq MM, Giganti N, Shavezipur M. Development of capacitive temperature sensors with high sensitivity using a multiuser polycrystalline silicon process. Microelectronic Engineering. 2020; 226:111287.

68. Khan N, Omran H, Yao Y, et al. Flexible PVDF ferroelectric capacitive temperature sensor. 2015 IEEE 58th International Midwest Symposium on Circuits and Systems (MWSCAS). IEEE, 2015: 1-4.

69. Lei Z, Wang Q, Wu P. A multifunctional skin-like sensor based on a 3d printed thermo-responsive hydrogel. Materials Horizons. 2017; 4(4):694-700.

70. Fan J, Newell B, Garcia J, Voyles RM, Nawrocki RA. Effect of additive manufacturing on β-phase poly (vinylidene fluoride)-based capacitive temperature sensors. Advanced Engineering Materials. 2022; 24(11):2200485.

71. Choi S, Park J, Hyun Wet al. Stretchable heater using ligand-exchanged silver nanowire nanocomposite for wearable articular thermotherapy. ACS nano. 2015; 9(6):6626-6633.

72. Hong S, Lee H, Lee Jet al. Highly stretchable and transparent metal nanowire heater for wearable electronics applications. Advanced materials. 2015; 27(32):4744-4751.

73. Yang C, Chang C, Song CYet al. Fabrication and performance evaluation of flexible heat pipes for potential thermal control of foldable electronics. Applied Thermal

Engineering. 2016; 95:445-453.

74. Bae SH, Shabani R, Lee JB, Baeck SJ, Cho HJ, Ahn JH. Graphene-based heat spreader for flexible electronic devices. IEEE Trans. Electron Devices. 2014; 61(12):4171-4175.

75. Luo XC, Chugh R, Biller BC, Hoi YM, Chung DDL. Electronic applications of flexible graphite. Journal of Electronic Materials. 2002; 31(5):535-544.

76. Im K, Cho K, Kwak K, Kim J, Kim S. Flexible transparent heaters with heating films made of indium tin oxide nanoparticles. J. Nanosci. Nanotechnol. 2013; 13(5):3519-3521.

77. Hsu P-C, Liu X, Liu Cet al. Personal thermal management by metallic nanowire-coated textile. Nano letters. 2015; 15(1):365-371.

78. Yang C, Song CY, Shang W, Tao P, Deng T. Flexible heat pipes with integrated bioinspired design. Progress in Natural Science. 2015; 25(1):51-57.

79. Guo Y, Dun C, Xu Jet al. Ultrathin, washable, and large-area graphene papers for personal thermal management. Small. 2017; 13(44):1702645.

80. Lal S, Gautam D, Razeeb KM. Fabrication of micro-thermoelectric devices for power generation and the thermal management of photonic devices. Journal of Micromechanics and Microengineering. 2019; 29(6) : 065015.

81. Ren ZQ, Kim JC, Lee J. Transient cooling and heating effects in holey silicon-based lateral thermoelectric devices for hot spot thermal management. IEEE Transactions on Components, Packaging, and Manufacturing Technology. 2021; 11(8):1214-1222.

82. Song WJ, Bai FF, Chen MB, Lin SL, Feng ZP, Li YL. Thermal management of standby battery for outdoor base station based on the semiconductor thermoelectric device and phase change materials. Applied Thermal Engineering. 2018; 137:203-217.

83. Wang K Y. Thermal management of a medical device using thermoelectric

coolers.Twentieth Annual IEEE Semiconductor Thermal Measurement and Management Symposium (IEEE Cat. No. 04CH37545). IEEE, 2004: 122-124.

84. Solbrekken G L, Yazawa K, Bar-Cohen A. Experimental demonstration of thermal management using thermoelectric generation.The Ninth Intersociety Conference on Thermal and Thermomechanical Phenomena In Electronic Systems (IEEE Cat. No. 04CH37543). IEEE, 2004, 1: 284-290.

85. Chen W-Y, Shi X-L, Zou J, Chen Z-G. Thermoelectric coolers: Progress, challenges, and opportunities. Small Methods. 2022; 6(2) : 2101235.

86. Mao J, Chen G, Ren Z. Thermoelectric cooling materials. Nature Materials. 2021; 20(4):454-461.

87. Pourkiaei SM, Ahmadi MH, Sadeghzadeh Met al. Thermoelectric cooler and thermoelectric generator devices: A review of present and potential applications, modeling and materials. Energy. 2019; 186: 115849.

88. Zhao D, Tan G. A review of thermoelectric cooling: Materials, modeling and applications. Applied Thermal Engineering. 2014; 66(1-2):15-24.

89. Li X, Mahmoud S, Al-Dadah R, Elsayed A. Thermoelectric cooling device integrated with pcm heat storage for ms patients. Energy Procedia. 2014; 61:2399-2402.

90. Hong S, Gu Y, Seo JKet al. Wearable thermoelectrics for personalized thermoregulation. Science advances. 2019; 5(5):eaaw0536.

91. Choi J, Dun C, Forsythe C, Gordon MP, Urban JJ. Lightweight wearable thermoelectric cooler with rationally designed flexible heatsink consisting of phase-change material/graphite/silicone elastomer. Journal of Materials Chemistry A. 2021; 9(28):15696-15703.

92. Kishore RA, Nozariasbmarz A, Poudel B, Sanghadasa M, Priya S. Ultra-high performance wearable thermoelectric coolers with less materials. Nature communications. 2019; 10(1):1765.

93. Bartlett MD, Kazem N, Powell-Palm MJet al. High thermal conductivity in soft elastomers with elongated liquid metal inclusions. Proceedings of the National Academy of Sciences. 2017; 114(9):2143-2148.

94. Fu Y, Nabiollahi N, Wang Tet al. A complete carbon-nanotube-based on-chip cooling solution with very high heat dissipation capacity. Nanotechnology. 2012; 23(4):045304.

95. Kordas K, Tóth G, Moilanen Pet al. Chip cooling with integrated carbon nanotube microfin architectures. Applied Physics Letters. 2007; 90(12):123105.

96. Zhang K, Tao P, Zhang Y, Liao X, Nie S. Highly thermal conductivity of cnf/aln hybrid films for thermal management of flexible energy storage devices. Carbohydrate polymers. 2019; 213:228-235.

97. Kou Y, Sun KY, Luo JPet al. An intrinsically flexible phase change film for wearable thermal managements. Energy Storage Mater. 2021; 34:508-514.

98. Li W, Wang F, Cheng W, Chen X, Zhao Q. Study of using enhanced heat-transfer flexible phase change material film in thermal management of compact electronic device. Energy Conversion and Management. 2020; 210:112680.

99. Liu Z, Qin S, Chen X, Chen D, Wang F. Pdms-pdms micro channels filled with phase-change material for chip cooling. Micromachines. 2018; 9(4):165.

100. Shi YL, Wang CJ, Yin YF, Li YH, Xing YF, Song JZ. Functional soft composites as thermal protecting substrates for wearable electronics. Advanced Functional Materials. 2019; 29(45) : 1905470.

101. Umair MM, Zhang Y, Iqbal K, Zhang SF, Tang BT. Novel strategies and supporting materials applied to shape-stabilize organic phase change materials for thermal energy storage-a review. Applied Energy. 2019; 235:846-873.

102. Ferber S, Behrens AM, McHugh KJet al. Evaporative cooling hydrogel packaging for storing biologics outside of the cold chain. Advanced healthcare materials. 2018;

7(14):1800220.

103. Kim J, Im S, Kim JHet al. Artificial perspiration membrane by programmed deformation of thermoresponsive hydrogels. Advanced materials. 2020; 32(6):1905901.

104. Lee C, Kang S, Seo J, Lee J. Temperature-responsive on–off control over water evaporation achieved via sweat-gland-mimetic composites. ACS Applied Materials & Interfaces. 2021; 13(3):4442-4449.

105. Lu Z, Strobach E, Chen N, Ferralis N, Grossman JC. Passive sub-ambient cooling from a transparent evaporation-insulation bilayer. Joule. 2020; 4(12):2693-2701.

106. Wang C, Hua L, Yan H, Li B, Tu Y, Wang R. A thermal management strategy for electronic devices based on moisture sorption-desorption processes. Joule. 2020; 4(2):435-447.

107. Fraivillig J. Flexible thermal management circuits bonded directly to aluminum heat sinks.PROCEEDINGS-SPIE THE INTERNATIONAL SOCIETY FOR OPTICAL ENGINEERING. International Society for Optical Engineering; 1999, 2003: 797-800.

108. Li YH, Chen JY, Zhao S, Song JZ. Recent advances on thermal management of flexible inorganic electronics. Micromachines. 2020; 11(4) : 390.

109. Xu KC, Lu YY, Yamaguchi T, Arie T, Akita S, Takei K. Highly precise multifunctional thermal management-based flexible sensing sheets. Acs Nano. 2019; 13(12):14348-14356.

110. Yin YF, Cui Y, Li YH, Xing YF, Li M. Thermal management of flexible wearable electronic devices integrated with human skin considering clothing effect. Applied Thermal Engineering. 2018; 144:504-511.

111. Fu Y, Hansson J, Liu Yet al. Graphene related materials for thermal management. 2D Materials. 2020; 7(1):012001.

112. Balandin AA. Thermal properties of graphene and nanostructured carbon materials.

Nature materials. 2011; 10(8):569-581.

113. Umair MM, Zhang Y, Iqbal K, Zhang S, Tang B. Novel strategies and supporting materials applied to shape-stabilize organic phase change materials for thermal energy storage–a review. Applied Energy. 2019; 235:846-873.

114. Tong JK, Huang X, Boriskina SV, Loomis J, Xu Y, Chen G. Infrared-transparent visible-opaque fabrics for wearable personal thermal management. Acs Photonics. 2015; 2(6):769-778.

115. Kim Y, Lee HR, Saito T, Nishi Y. Ultra-thin and high-response transparent and flexible heater based on carbon nanotube film. Applied Physics Letters. 2017; 110(15) : 153301.

116. Lim W, Khadka A, Kim BYet al. Wearable heater composites comprising traditional hanji cellulose fib ers coate d with graphene, silver nanowires, and pedot: Pss via scalable supersonic spraying. Journal of Materials Science & Technology. 2023; 164:27-36.

117. Zhang JH, Xu R, Feng J, Xie Y, Zhou T. Laser direct writing of flexible heaters on polymer substrates. Industrial & Engineering Chemistry Research. 2021; 60(30):11161-11170.

118. Sivarenjini TM, Panbude A, Sathiyamoorthy Set al. Design and optimization of flexible thermoelectric coolers for wearable applications. Ecs Journal of Solid State Science and Technology. 2021; 10(8) : 081006.

119. Varghese T, Hollar C, Richardson Jet al. High-performance and flexible thermoelectric films by screen printing solution-processed nanoplate crystals. Scientific Reports. 2016; 6

120. Xu S, Li M, Dai Yet al. Realizing a 10 degrees c cooling effect in a flexible thermoelectric cooler using a vortex generator. Advanced Materials. 2022; 34(41) : 2204508.

121. Choi SJ, Kwon TH, Im Het al. A polydimethylsiloxane (pdms) sponge for the selective absorption of oil from water. Acs Applied Materials & Interfaces. 2011; 3(12):4552-4556.

122. Li HS, Ding Y, Ha Het al. An all-stretchable-component sodium-ion full battery. Advanced Materials. 2017; 29(23): 1700898.

123. Liu W, Chen Z, Zhou GMet al. 3d porous sponge-inspired electrode for stretchable lithium-ion batteries. Advanced Materials. 2016; 28(18):3578-3583.

124. Song Y, Chen HT, Su ZMet al. Highly compressible integrated supercapacitor-piezoresistance-sensor system with cnt-pdms sponge for health monitoring. Small. 2017; 13(39) : 1702091.

125. Kingma BR, Frijns AJ, Schellen L, van Marken Lichtenbelt WD. Beyond the classic thermoneutral zone: Including thermal comfort. Temperature. 2014; 1(2):142-149.

126. Gagge AP, Stolwijk J, Hardy J. Comfort and thermal sensations and associated physiological responses at various ambient temperatures. Environmental research. 1967; 1(1):1-20.

127. Cho H, Rho H, Kim JHet al. Graphene–carbon–metal composite film for a flexible heat sink. ACS applied materials & interfaces. 2017; 9(46):40801-40809.

128. Wang Q, Han X, Sommers A, Park Y, T'Joen C, Jacobi A. A review on application of carbonaceous materials and carbon matrix composites for heat exchangers and heat sinks. International journal of refrigeration. 2012; 35(1):7-26.

129. Moharram KA, Abd-Elhady M, Kandil H, El-Sherif H. Enhancing the performance of photovoltaic panels by water cooling. Ain Shams Engineering Journal. 2013; 4(4):869-877.

130. Huang H-S, Weng Y-C, Chang Y-W, Chen S-L, Ke M-T. Thermoelectric water-cooling device applied to electronic equipment. International Communications in Heat

and Mass Transfer. 2010; 37(2):140-146.

131. Lee G, Kim CS, Kim S, Kim YJ, Choi H, Cho BJ. Flexible heatsink based on a phase-change material for a wearable thermoelectric generator. Energy. 2019; 179:12-18.

132. Boon-in S, Theerasilp M, Crespy D. Temperature-responsive double-network cooling hydrogels. Acs Applied Polymer Materials. 2023; 5(4):2562-2574.

133. Cui S, Hu Y, Huang Z, Ma C, Yu L, Hu X. Cooling performance of bio-mimic perspiration by temperature-sensitive hydrogel. International Journal of Thermal Sciences. 2014; 79:276-282.

134. Xu L, Sun DW, Tian Y, Fan TH, Zhu ZW. Nanocomposite hydrogel for daytime passive cooling enabled by combined effects of radiative and evaporative cooling. Chemical Engineering Journal. 2023; 457:12-18.

135. Sato K, Kang W, Saga K, Sato K. Biology of sweat glands and their disorders. I. Normal sweat gland function. Journal of the American Academy of Dermatology. 1989; 20(4):537-563.

136. Adrian R, Helmreich E, Holzer Het al. The physiology, pharmacology, and biochemistry of the eccrine sweat gland. Reviews of Physiology, Biochemistry and Pharmacology, 1977; 79:51-131.

137. Wilke K, Martin A, Terstegen L, Biel S. A short history of sweat gland biology. International journal of cosmetic science. 2007; 29(3):169-179.

138. Mishra AK, Wallin TJ, Pan Wet al. Autonomic perspiration in 3d-printed hydrogel actuators. Science Robotics. 2020; 5(38):eaaz3918.

139. Peng Y, Zhou J, Yang Y, Lai JC, Ye Y, Cui Y. An integrated 3d hydrophilicity/hydrophobicity design for artificial sweating skin (i-trans) mimicking human body perspiration. Advanced Materials. 2022; 34(44):2204168.

140. Pu S, Su J, Li L, Wang H, Chen C, Hu X. Bioinspired sweating with temperature sensitive hydrogel to passively dissipate heat from high-end wearable electronics. Energy Conversion and Management. 2019; 180:747-756.

141. Pu S, Fu J, Liao Yet al. Promoting energy efficiency via a self - adaptive evaporative cooling hydrogel. Advanced Materials. 2020; 32(17):1907307.

142. Yang P, Feng C, Liu Yet al. Thermal self-protection of zinc-ion batteries enabled by smart hygroscopic hydrogel electrolytes. Advanced Energy Materials. 2020; 10(48):2002898.

143. Nandakumar DK, Ravi SK, Zhang YX, Guo N, Zhang C, Tan SC. A super hygroscopic hydrogel for harnessing ambient humidity for energy conservation and harvesting. Energy & Environmental Science. 2018; 11(8):2179-2187.

144. Pu SR, Fu J, Liao YTet al. Promoting energy efficiency via a self-adaptive evaporative cooling hydrogel. Advanced Materials. 2020; 32(17) :1907307.

145. Pu SR, Liao YT, Chen KLet al. Thermogalvanic hydrogel for synchronous evaporative cooling and low-grade heat energy harvesting. Nano Letters. 2020; 20(5):3791-3797.

146. Yang PH, Feng CZ, Liu YPet al. Thermal self-protection of zinc-ion batteries enabled by smart hygroscopic hydrogel electrolytes. Advanced Energy Materials. 2020; 10(48) :2002898.

147. Gomez CR. Disorders of body temperature. Handbook of clinical neurology. 2014; 120:947-957.

148. Lao L, Shou D, Wu Y, Fan J. “Skin-like” fabric for personal moisture management. Science advances. 2020; 6(14):eaaz0013.

149. Wang X, Huang Z, Miao D, Zhao J, Yu J, Ding B. Biomimetic fibrous murray membranes with ultrafast water transport and evaporation for smart moisture-wicking fabrics. Acs Nano. 2018; 13(2):1060-1070.

150. Shou D, Fan J. An all hydrophilic fluid diode for unidirectional flow in porous systems. Advanced Functional Materials. 2018; 28(36):1800269.

151. Liu Z, Wang W, Xie R, Ju X-J, Chu L-Y. Stimuli-responsive smart gating membranes. Chemical Society Reviews. 2016; 45(3):460-475.

152. Liu J, Wang N, Yu L-Jet al. Bioinspired graphene membrane with temperature tunable channels for water gating and molecular separation. Nature communications. 2017; 8(1):2011.

153. Kuroki H, Ohashi H, Ito T, Tamaki T, Yamaguchi T. Isolation and analysis of a grafted polymer onto a straight cylindrical pore in a thermal-responsive gating membrane and elucidation of its permeation behavior. Journal of Membrane Science. 2010; 352(1-2):22-31.

154. Li Q, Zhang L-N, Tao X-M, Ding X. Review of flexible temperature sensing networks for wearable physiological monitoring. Advanced Healthcare Materials. 2017; 6(12)

155. Su Y, Ma C, Chen Jet al. Printable, highly sensitive flexible temperature sensors for human body temperature monitoring: A review. Nanoscale Research Letters. 2020; 15(1) : 1-34.

156. Cai JY, Du MJ, Li ZL. Flexible temperature sensors constructed with fiber materials. Advanced Materials Technologies. 2022; 7(7) : 2101182.

157. Chen HR, Lou Z, Shen GZ. An integrated flexible multifunctional sensing system for simultaneous monitoring of environment signals. Science China-Materials. 2020; 63(12):2560-2569.

158. Hao L, Ding JN, Yuan NYet al. Visual and flexible temperature sensor based on a pectin-xanthan gum blend film. Organic Electronics. 2018; 59:243-246.

159. Lee C Y, Lee S J, Wu G W. Fabrication of micro temperature sensor on the flexible substrate. 2007 7th IEEE Conference on Nanotechnology (IEEE NANO). IEEE, 2007:

1050-1053.

160. Park JS, Lee DS, Nho HW, Kim DS, Hwang TH, Lee NK. Flexible platinum temperature sensor embedded in polyimide films for curved surface temperature monitoring applications: Skin temperature of human body. Sensors and Materials. 2017; 29(9):1275-1283.

161. Zhao XL, Long Y, Yang TT, Li J, Zhu HW. Simultaneous high sensitivity sensing of temperature and humidity with graphene woven fabrics. Acs Applied Materials & Interfaces. 2017; 9(35):30171-30176.

162. You I, Mackanic DG, Matsuhisa Net al. Artificial multimodal receptors based on ion relaxation dynamics. Science. 2020; 370(6519):961-965.

163. Madsen FB, Daugaard AE, Hvilsted S, Skov AL. The current state of silicone-based dielectric elastomer transducers. Macromolecular rapid communications. 2016; 37(5):378-413.

164. Mannsfeld SC, Tee BC, Stoltenberg RMet al. Highly sensitive flexible pressure sensors with microstructured rubber dielectric layers. Nature materials. 2010; 9(10):859-864.

165. Park S, Kim H, Vosgueritchian Met al. Stretchable energy-harvesting tactile electronic skin capable of differentiating multiple mechanical stimuli modes. Advanced Materials. 2014; 26(43):7324-7332.

166. Zhang H, Tang Q, Chan Y. Development of a versatile capacitive tactile sensor based on transparent flexible materials integrating an excellent sensitivity and a high resolution. AIP Advances. 2012; 2(2) : 022112.

167. Gao Y, Yu G, Shu Tet al. 3d-printed coaxial fibers for integrated wearable sensor skin. Advanced Materials Technologies. 2019; 4(10):1900504.

168. Nie B, Li R, Cao J, Brandt JD, Pan T. Flexible transparent iontronic film for interfacial capacitive pressure sensing. Advanced Materials. 2015; 27(39):6055-6062.

169. Kim H, Kim G, Kim Tet al. Transparent, flexible, conformal capacitive pressure sensors with nanoparticles. Small. 2018; 14(8):1703432.

170. Tee BCK, Chortos A, Dunn RR, Schwartz G, Eason E, Bao Z. Tunable flexible pressure sensors using microstructured elastomer geometries for intuitive electronics. Advanced Functional Materials. 2014; 24(34):5427-5434.

171. Ding J, Zhao W, Jin W, Di Ca, Zhu D. Advanced thermoelectric materials for flexible cooling application. Advanced Functional Materials. 2021; 31(20):2010695.

172. Anno Y, Imakita Y, Takei K, Akita S, Arie T. Enhancement of graphene thermoelectric performance through defect engineering. 2D Materials. 2017; 4(2):025019.

173. Xu Y, Li Z, Duan W. Thermal and thermoelectric properties of graphene. Small. 2014; 10(11):2182-2199.

174. Amollo TA, Mola GT, Kirui M, Nyamori VO. Graphene for thermoelectric applications: Prospects and challenges. Critical Reviews in Solid State and Materials Sciences. 2018; 43(2):133-157.

175. Russ B, Glaudell A, Urban JJ, Chabinyc ML, Segalman RA. Organic thermoelectric materials for energy harvesting and temperature control. Nature Reviews Materials. 2016; 1(10):1-14.

176. Zhang Q, Sun Y, Xu W, Zhu D. Organic thermoelectric materials: Emerging green energy materials converting heat to electricity directly and efficiently. Advanced Materials. 2014; 26(40):6829-6851.